University of Chinese Academy of Sciences

博士学位论文

基于 Gaia 和 LAMOST 巡天数据通过流体力学模型区分厚盘和恒星晕的界面

作者姓名：　　　João Antônio Silveira do Amarante

指导教师：　　　Martin C. Smith 研究员

　　　　　　　中国科学院上海天文台

学位类别：　　　理学博士

学科专业：　　　天体物理

培养单位：　　　中国科学院上海天文台

2020年 **12** 月

The interface of the thick disc and stellar halo as seen by

Gaia, LAMOST and hydrodynamical simulations

A dissertation submitted to

University of Chinese Academy of Sciences

in partial fulfillment of the requirement

for the degree of

Doctor of Philosophy

in Astrophysics

By

João Antônio Silveira do Amarante
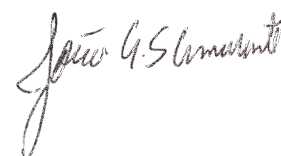
Supervisor : Prof. Martin C. Smith

Shanghai Astronomical Observatory

Chinese Academy of Sciences

December 2020

中国科学院大学

研究生学位论文原创性声明

本人郑重声明：所呈交的学位论文是本人在导师的指导下独立进行研究工作所取得的成果。尽我所知，除文中已经注明引用的内容外，本论文不包含任何其他个人或集体已经发表或撰写过的研究成果。对论文所涉及的研究工作做出贡献的其他个人和集体，均已在文中以明确方式标明或致谢。
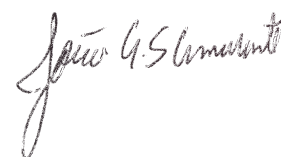
Author: João Antônio Silveira do Amarante

October, 2020

中国科学院大学

学位论文授权使用声明

本人完全了解并同意遵守中国科学院有关保存和使用学位论文的规定，即中国科学院有权保留送交学位论文的副本，允许该论文被查阅，可以按照学术研究公开原则和保护知识产权的原则公布该论文的全部或部分内容，可以采用影印、缩印或其他复制手段保存、汇编本学位论文。涉密及延迟公开的学位论文在解密或延迟期后适用本声明。
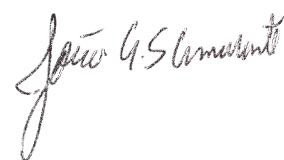
Author: João Antônio Silveira do Amarante

Supervisor: Martin C. Smith

October, 2020

University of Chinese Academy of Sciences
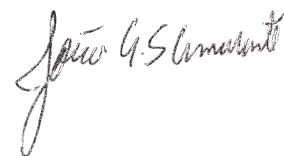## Originality Statement of Graduate Dissertation

I solemnly declare that the dissertation submitted is the result of my independent research work under the guidance of my supervisor. To the best of my knowledge, this paper does not contain any other research results that have been published or written by individuals or collectives, except for the content cited in the article. Other individuals and groups who have contributed to the research work involved in the thesis have been clearly marked or acknowledged in the article.

Author: João Antônio Silveira do Amarante

October, 2020

University of Chinese Academy of Sciences
Statement of Authorised Use of Dissertation

I fully understand and agree to abide by the provisions of the Chinese Academy of Sciences regarding the preservation and use of dissertations, that is, the Chinese Academy of Sciences has the right to retain a copy of the dissertation, allow the dissertation to be consulted, and publish the dissertation in accordance with the principles of open academic research and protection of intellectual property rights. All or part of the content of the thesis can be preserved and compiled by photocopying, reduction printing or other reproduction methods. This statement shall apply to the dissertations involving secrets and delayed publication after the decryption or delay period.

Author: João Antônio Silveira do Amarante

Supervisor: Martin C. Smith

October, 2020

Dedicated to my mom, Regina.

Loloano, in memoriam...

Acknowledgements

I am who I am, thanks to all the experiences I had and people I've met during my life (Yes, I know that's cliche, but it's true). The following is a tentative list of those who were extremely important during the 4 years period of my PhD. I hope I can remember everyone. I thank my family:

- Special thanks to my parents, Regina and João, for all the support, care and love they gave me during my life. They always incentivized me to keep the head up and follow my dreams. I specially thanks to my mom, for being a strong person and, despite the difficulties, always being kind and caregiving to me.

- My sister, Joana, for all her support. Her smile during our weekend conversations always brought joy to me.

- Tia Carminha, Tio Cassinho, Tio Dode, Tia Idalina and Márcio for being such lovely family members.

- Prima Carol for her long audio messages that entertained me, especially during the pandemic situation.

- My carioca families that "adopted" me since my undergrad in Rio, and still demonstrate such care and love towards me:

  - Ribeiro's Family – Robson, Cristina, Pedro, Lívia and Marcela.
  - Almeida's Family – José, Ana and Victor.

I thank all my friends and colleagues for all the good and bad moments we faced together during my PhD. Special thanks to:

- Simone de Novaes and her family for their care and incentive to pursuit this PhD in China.

- Emerson for the awesome beers and snacks during football matches;

- Office mates Vera, Timur and Daniel. Special thanks to Vera for being so nice to me and having many funny conversations about life. I am very glad to have met her daughter Wanda and husband Spiegel.

- Silvia for all the conversations during lunchtime and for inviting me for New Year's eve together with Wim.

Thanks to all SHAO staff. I am very grateful to ChuYi, Wang Hui, Ma Jin and Cai Li for all their administrative support in SHAO. All the cookers, cleaning ladies and security guards, who always smiled to me and replied to my "你好/早上好".

During my academic life, I have always had the luck to meet supervisors, who were not only my "bosses" but very good friends. Thank you:

- Helio Rocha-Pinto listened to my fears in 2014 with care and attention and still strongly encouraged me to return to Astronomy career. Thanks to him I had the motivation to look for a PhD outside Brazil.

- Martin Smith who kept pushing me and opened the doors that enable me to improve my scientific and writing skills. The lunch and dinners that he offered were a relief to the research. Thanks to him, I also pushed myself and ran three times a half-marathon! I also thank his parents and wife for having me together during Christmas in the UK.

- Professor Ralph Schoenrich for hosting me in Oxford and having fruitful discussions about my work.Jeff Carlin for teaching me the basics to observe at Palomar Observatory and having a pleasant time there.

- Victor P. Debattista who gave me the liberty to do my own research in Preston and always pushed for good scientific results. Victor was extremely important for the development of this thesis and co-supervised me during my last year.

A special thanks to Rong Jia Yue who showed me that love can be light and simple but still make us feel complete. Her smile gives me the strength to keep going...

Abstract

Although the stellar halo accounts for just $\sim 1\%$ of the total stellar mass of the Milky Way, its kinematics can tell us a lot about the origins and evolution of our Galaxy. For instance, it is known that the Milky Way experienced several merger events which left their imprints on the stellar halo. In particular, with the European Space Agency's *Gaia* satellite mission, we now know that when our Galaxy was still young, in its first Gyrs, a major merger happened and, likely, perturbed its disc-shaped structure. One imprint of this merger, the *Gaia*-Enceladus-Sausage event, has been revealed by the double sequence in the Hertzsprung-Russell diagram of high transverse velocity stars in *Gaia* DR2. However, in the solar neighbourhood, selecting a pure stellar halo sample is non-trivial due to its significant overlap with the thick disk's velocity and metallicity distributions. It is then crucial to disentangle these two populations in order to study the effects of the merger better. Firstly, I will present a new methodology for finding the local fractions of the stellar halo and thick disc stars by fitting the distribution of the high transverse velocity stars. I fit these stars by updating the popular Besancon/Galaxia model, incorporating the latest observational results for the stellar halo. I am able to obtain a good match to the *Gaia* data and provide new constraints on the properties of the disc and halo. In particular, I show that the thick disc contribution to this high-velocity tail is small, but not negligible, and likely has an influence on the red sequence of the HR diagram. I look in greater detail using chemistry from LAMOST DR5, finding again that the red sequence contains a fraction of thick-disc stars. I also investigate the proposed dynamical substructures in this sample, concluding that they are probably due to resonant orbits rather than accreted populations. Secondly, I will study the formation of a metal rich ([Fe/H] > -1 dex), low angular momentum ($v_\phi < 100$ km/s) stellar population, called "the Splash". The Splash's formation has been attributed to the *Gaia*-Enceladus-Sausage merger event, but in order to fully understand the effects of such an event, we need to know the chemical and dynamical characteristics of the young Milky Way, i.e., before the major merger event. For this purpose, I use the SPH + N-body tree-code GASOLINE to explore formation scenarios of Milky Way-like galaxies. I explore the evolution of an isolated simulation galaxy and find evidence which supports a clumpy phase of star formation in the young Galaxy. This

scenario is supported by observations of high redshift ($z > 1$) galaxies with high dense clumpy regions. I will show that kinematical and chemical properties of the stars associated with the Splash can be explained by the clumpy formation scenario. This population forms in the first Gyrs of the simulation, suggesting that its formation could be independent from the *Gaia*-Enceladus-Sausage merger.

Keywords: Milky Way dynamics, Milky Way formation, Hydrodynamical simulations

摘要

恒星晕的质量仅是银河系恒星总质量的~1%，但在它们的运动学中暗藏着很多我们星系的起源和演化过程信息。例如，已知银河系经历了多次的并合，这就在恒星晕中留下了印记。尤其，随着欧洲航天局的Gaia卫星的发射，我们发现了在银河系年轻的时候，也就是在最初几亿年，它经历了一次主并合，可能扰动了它的类盘形状结构。这次并合的其中之一的印记就是Gaia-Enceladus-Sausage事件，Gaia DR2数据中的高切向速度恒星在赫罗图中呈现双序现象。然而，恒星晕和厚盘恒星的速度和金属丰度存在明显的重叠，因此在近邻区域难以获得纯恒星晕样本。因此，至关重要的是区分这两个星族，以便更好地研究合并的影响。首先，我将提出一种新的方法，通过拟合高切向速度恒星的分布来计算恒星晕和厚盘恒星的比例。我采用更新后的普及Besancon / Galaxia模型，并结合恒星晕最新观测结果来拟合这些恒星。我能够很好与Gaia数据匹配，并对银盘和银晕的属性提供新的约束。尤其，我的工作显示厚盘对高速尾的贡献很小，但不可忽略，并且可能会影响赫罗图的红序。我对LAMOST DR5数据的化学成分进行了更详细的研究，再次发现红序中包含小部分的厚盘星。我还研究了此样本中拟议的动力子结构，相对于不是吸积星族，认为它们更可能是共振轨道其次，我研究了富金属（[Fe/H] > −1),低角动量（v_ϕ >100 km/s）的星族，简称为"斑点"。斑点是否又Gaia-Enceladus-Sausage并合事件产生的，但为了充分了解此类事件的影响，我们需要知道年轻银河系（即主并合事件之前）的化学和动力学特征。为此，我通过SPH + N-body tree-code GASOLINE模型帮我们探索类银河星系的形成场景。探索孤立模型星系的演化，发现年轻星系的恒星形成过程中存在成块阶段。这种现象得到高红移（z > 1）星系的观测支持，显示它具有更致密的成团区域。我将证明，类似于斑点的恒星运动学和化学性质都可以由结块形成情况来解释。模型显示这类星族早在前几亿年就形成了，与Gaia-Enceladus-Sausage并合事件没有关系。其次，我研究了富金属（[Fe/H] > −1 ）、低角动量（v_ϕ >100 km/s)的星族，简称为"斑点"。斑点是否又Gaia-Enceladus-Sausage并合事件产生的，但为了充分了解此类事件的影响，我们需要知道年轻银河系（即主并合事件之前）的化学和动力学特征。为此，我通过SPH + N-body tree-code GASOLINE模型帮我们探索类银河星系的形成场景。探索孤立模型星系的演化，发现年轻星系的恒星形成过程中存在成块阶段。这种现象得到高红移（z > 1）星系的观测支持，显示它具有更致密的成团区域。我将证明，类似于斑点的恒星运动学和化学性质都可以由结块形成情况来解释。模型显示这类星族早在前几亿年就形成了，与Gaia-Enceladus-Sausage并合事件没有关系。

关键词： 银河系动力学；银河系形成；流体动力学模拟

Table of contents

List of figures

List of tables

Chapter 1

Introduction

Our unique observation point in space and time, i.e. inside view at a single snapshot in time, of our own Galaxy challenges ourselves in the study of its structure and evolution. Firstly, as we are located at the disc plane of the Galaxy, we model its geometrical structure through, for example, star counts (Herschel 1785, Kapteyn and van Rhijn 1920, Jurić et al. 2008) with complementary radio observations to find the Galactic centre and the spiral arms (e.g. Oort and Rougoor 1960, Lockman 2002). Despite the development of observational technology, there are limitations in observing the opposite symmetrical side of our Galaxy due to strong light absorption towards the Galactic Centre.

Secondly, the study of the dynamical evolution of our Galaxy, either backwards or forward in time, requires not only velocity measurements of the stars, and/or the gas, but also the knowledge of the potential of the Galaxy. Nonetheless, observations of disc-like galaxies over a large range of redshifts (e.g. Fathi et al. 2012, Krywult et al. 2017) allow us to "look-back in time" at the evolution of disc-like galaxies. This provides important constraints on simulations that model the formation of the Milky Way.

The Milky Way is known to be a star-forming galaxy and is characterised by a central bulge, an axisymmetric radially extended disc, a diffuse stellar halo and all of these structures are embedded in a dark matter halo (Bland-Hawthorn and Gerhard, 2016). Our Galaxy also features non-axisymmetric structures, e.g., spiral arms and giant molecular clouds located in the disc, and a bar-structure in the bulge. Besides that, we observe several satellite dwarf galaxies and stellar streams currently in the stellar halo, which itself is composed of disrupted stellar systems hinting at past accretion events. A schematic representation of our current understanding of the Milky Way structure is shown in Figure 1.1. The Sun is located in the Galactic disc at a distance of 8.18 kpc (Gravity Collaboration et al., 2019) from the Galactic centre and at $z \approx 0.017$ kpc (Yao et al. 2017, Bennett and Bovy 2019) above the mean disc
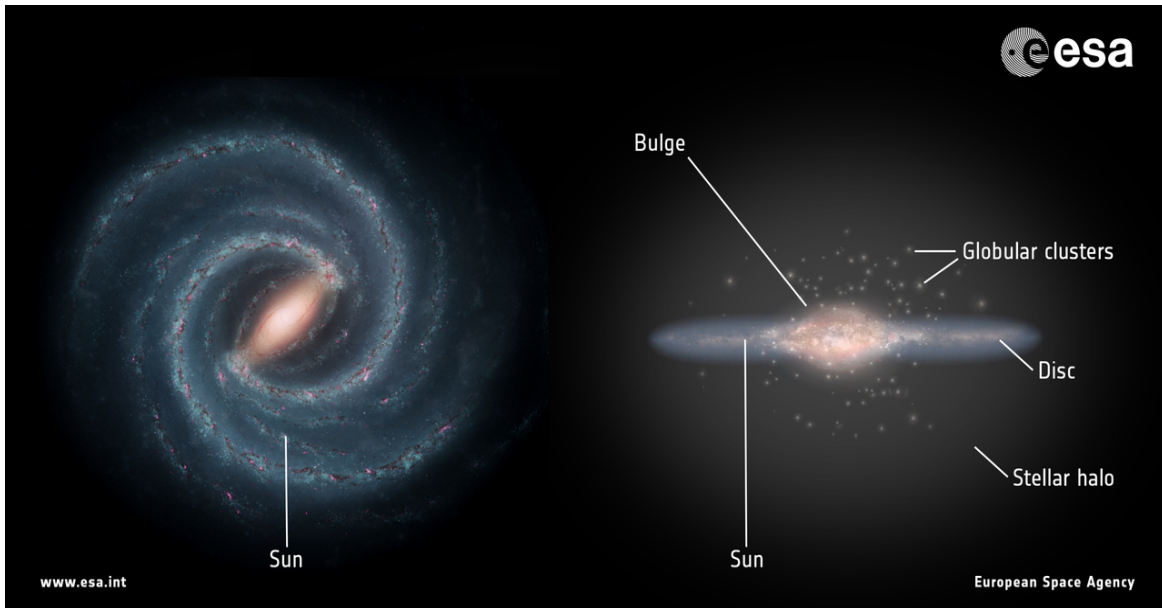
Fig. 1.1 Artistic impression of the Milky Way Galaxy. **Left panel:** the face-on view shows the spiral arms in the disc, the central barred-bulge region and the place where the Sun is located. **Right panel:** the edge-on view shows the discy shape of the Galaxy and the diffuse stellar halo distributed around the Galaxy. *Copyright: Left: NASA/JPL-Caltech; right: ESA; layout: ESA/ATG medialab*

plane. All the aforementioned characteristics make our own Galaxy a data-rich laboratory for studying dynamics and chemical evolution of disc-like galaxies.

To understand our Galaxy's structure and formation, precise measurement of stellar positions, velocities and chemical abundances are necessary. Until recently, these studies were restricted to nearby stellar samples – stars within 100 pc from the Sun – with velocities and distances determined, mostly, by the Hipparcos mission (Perryman et al., 1997). But now the European Space Agency's *Gaia* satellite (Gaia Collaboration et al., 2016), which was launched in mid-2016, has increased the spatial range of accurate measurements – up to 3-5 kpc from the Sun – without compromising the quality of the measurements. By the end of its mission, in 2023, *Gaia* will have measured parallax and proper motions for 1 billion stars, with parallax precision up to 7-25 μas at $V = 15$. In comparison, Hipparcos measurements had a precision up to 2 mas and observed only ~ 120 thousand stars. Combined with ground-based large spectroscopic surveys, such as APOGEE (Zasowski et al., 2013) and LAMOST (Luo et al., 2015), which provide abundance and line-of-sight velocity measurements, *Gaia* will be a milestone in characterising the structure and evolution of our Galaxy.

With the exquisite data from *Gaia*, this thesis is focused on the study of two of the oldest components of the Milky Way: the thick-disc and the (inner) stellar halo. Although initially

thought as distinct and unrelated populations, recent studies, including two papers of this thesis' author, revealed an inter-connection and a common origin between them during the Galaxy's first Gyrs.

1.1   The stellar halo

The stellar halo of the Milky Way is the most extended baryonic component of the Galaxy, reaching up to ≈ 200kpc. Despite that, its relative paucity of stars, compared with the dominant population of disc stars, makes its study relatively difficult. Its total mass, $\approx 10^8 M_\odot$, only contributes around 1% to the total stellar mass of the Galaxy, while the disc contributes approximately $\approx 90\%$ (Binney and Tremaine, 2008). Closer to the Solar Neighbourhood, e.g. within 1 kpc from the Sun, the stellar halo fraction is even lower, with values ranging from 0.1 to 1%. We will explore more about the total local fraction in Chapter 2.

The study of the stellar halo provides valuable information about our Galaxy's formation, since it contains most of the metal-poor, $[\mathrm{Fe/H}] < -1$ dex , and oldest stars, age > 10 Gyrs, in the Galaxy (e.g. Das et al., 2020). It is important to note that not all stars are located sparsely in the spherical halo, as it also comprises the majority of known ancient globular clusters and dwarf galaxies (Helmi, 2020).

The stellar halo started being identified as a distinct population from the disc stars in the early 1950s due to its higher velocities in respect to the Sun. For example, Perek (1951) noticed that RR Lyrae variable stars (age $> \sim 10$ Gyr) have a net higher velocities compared to classical Cepheids (age ≈ 1 Gyr). Later, Roman (1954), studying high-velocity F-type stars, found a negative correlation between the star metallicity and velocity and settled the link between Galactic populations associated with kinematics and chemistry/age. Moreover, Roman (1954) also found the spatial distribution of the high-velocity F stars resembled those from RR-Lyrae and globular clusters.

With the known correlations between kinematics, abundances, age and spatial distribution of stars, it was still lacking a clear picture of the processes that formed the Milky Way and created distinct populations. The first proposed scenario of the stellar halo origin by Eggen et al. (1962) describes the formation of the oldest stars during the radial collapse of a primordial gas cloud towards the galactic centre. In this scenario, known as the "monolithic-collapse" scenario, the collapse is rather rapid and it would attain equilibrium in a time-scale of 10^8 years. Old stars form before the collapse, whereas young stars form afterwards during the formation of a rotating disc. Nonetheless, the stellar halo and disc would have originated from the same population. But, this simple model was unable to account for the large spread

in the globular clusters age (Searle and Zinn, 1978) and the presence of retrograde stars (Yoshii and Saio, 1979). Moreover, selection effects on the sample used by Eggen et al. (1962) may have induced an underestimate in the timescales involved in the process (e.g. Isobe, 1974; Saio and Yoshii, 1979).

Searle and Zinn (1978) proposed a second formation scenario where the outermost globular clusters in the stellar halo have an extragalactic origin. In this scenario, the globular clusters form in extremely metal poor dwarf galaxies and then merge into the Galactic outer halo through tidal disruption. This model is known as the "hierarchical/fragmented" picture of halo formation. The fragmented and monolithic scenarios predict a slightly different rotation profile (Deason et al., 2018): in the latter the rotational signature of the outer halo should be aligned with the angular momentum of the disc, whereas in the former the presence of a rotational feature can constrain the accretion history of the halo. Interestingly enough, most of the kinematics and chemical studies show that the stellar halo may have gone through both of the formation scenarios (as already argued by Sandage 1990).

1.1.1   The inner halo and its kinematic-chemical correlation

The discussion above stresses the importance of characterising the stellar halo kinematics to constrain the Galaxy's formation models. However, as we will see, one must compare different studies taking in consideration the strong dependence of the stellar halo kinematics with the star's metallicity. Moreover, as summarised, e.g., in Battaglia et al. (2017), the spatial variations in the kinematic, metallicity and age properties of the stellar halo is consistently described by two overlapping components that shift their dominance at Galactocentric distances of ≈ 15 kpc:

  i. A slightly flattened inner population, with a mild prograde sense of rotation velocities and metallicity distribution peaking at [Fe/H] $\approx$ -1.6;

  ii. A relatively more spheroidal outer halo component, with no (or little retrograde) rotation and a metallicity distribution peaking at [Fe/H] $\approx$ -2.3.

The distinction between inner and outer halo is also observed in the radial spatial distribution as it is described by a double-power law distribution (Cohen et al., 2017; Deason et al., 2011). The break/separation between the two components appear to be at $r \approx 15 - 20$ kpc (Deason et al., 2018). The inner component is consistent with the early assembly scenario (Eggen et al., 1962) and experienced a faster chemical enrichment compared to the outer halo. Das et al. (2016) support this scenario as they found that BHB stars are older as you go further out

in the Galaxy. Historically, the innermost stellar component of the halo was often labelled as the "*in-situ*" halo, but, as we will see, it might actually be composed of both an accreted population (from a massive merger) as well as in-site stars.

On the other hand, the outer halo is dominated exclusively by stars with an extra-galactic origin, originally from low mass satellites accreted onto the Galaxy, thus consistent with the hierarchical formation scenario (Searle and Zinn, 1978). Although extremely important to the assembly history and mass measurements of our Galaxy (Li et al., 2020) and chemical evolution of dwarf galaxies (e.g., Kirby et al. 2010,Aoki et al. 2020), among other studies, the outer halo will not be explored in the present work (interested readers should see, for example, the review of Helmi, 2008a).

To rule out the inner halo formation models, it is extremely important to have a reliable estimation of its kinematics. This used to rely on small sample sizes and there was a lack of complete space-velocity information for candidate stellar halo stars. As can be seen in Table 1.1 there is a disagreement in the literature regarding the value of the moments for the velocity distribution and the stellar halo fraction. The latter will be discussed in detail in Chapter 2. Interestingly, until recently, there was no strong consensus whether the inner halo had a sense of positive, negative or zero rotation. For instance, measurements of the mean and dispersion in the rotational velocity component were found to vary from $\approx$ (-20,20) and $\approx$ (80, 110) $\mathrm{km\,s^{-1}}$, respectively.

More recently, taking advantage of the crossmatch between *Gaia* DR1 and the SDSS survey, Belokurov et al. (2018) studied the velocity distribution of stars within 10 kpc from the Sun. With the full 7-D information (phase-space + [Fe/H]) for 190 thousand stars, they were able to study the velocity-chemistry relation, at different spatial ranges, for the stellar halo. Figure 1.2 shows the radial and azimuthal spherical velocities plane, $v_r - v_\theta$, for their sample. The top and bottom rows show stars at $1 < |z|/\mathrm{kpc} < 3$ and $3 < |z|/\mathrm{kpc} < 5$, respectively. Each column has a different metallicity range going from the most metal-poor to metal-rich from left to right. At the most metal-poor end, a single Gaussian component is sufficient to fit the data for each velocity component. Moreover, the velocity dispersion of each component is equivalent, reflecting the relatively spherical shape of the distribution. However, towards the more metal-rich end ([Fe/H]> -1.66) an extra component is required to fit the stellar disc and, furthermore, the velocity component associated with the stellar halo ($< v_\phi > \approx 20$) is stretched towards the radial velocity component.

Their result shows that the anisotropy of the stellar halo, which is given by $\beta = 1 - \frac{\sigma_\theta^2 + \sigma_\phi^2}{2\sigma_r^2}$, is strongly dependent on the metallicity and is radially anisotropic ($\beta > 0.7$) for the metal-rich stellar halo. Moreover, they also find a statistically significant sign of rotation for the

Reference	System	Component	$\langle v \rangle$ $(\mathrm{km\,s^{-1}})$	σ_v $(\mathrm{km\,s^{-1}})$	$f_h[\%]$
Woolley (1978)	Spherical	v_r	–	148	
		v_ϕ	–	122	
		v_θ	–	82	
Norris (1986)	Cartesian	v_x	–	131 ± 6	
		v_y	–	106 ± 6	
		v_z	–	85 ± 4	
Gould and Popowski (1998)	Cartesian	v_x	-5 ± 15	171 ± 11	0.07
(Kinematically selected sample)		v_y	-2 ± 13	99 ± 8	
		v_z	1 ± 8	90 ± 7	
Gould and Popowski (1998)	Cartesian	v_x	-3 ± 9	160 ± 7	0.2
(Non-kinematically selected sample)		v_y	-21 ± 9	109 ± 9	
		v_z	2 ± 5	94 ± 5	
Chiba and Beers (2000)	Cartesian	v_x	-16 ± 16	141 ± 11	
		v_y	-19 ± 12	106 ± 9	
		v_z	-5 ± 11	94 ± 8	
Gould (2003)	Cartesian	v_x	-1 ± 3	171 ± 10	
		v_y	-2 (fixed)	99 ± 8	
		v_z	2 ± 3	90 ± 7	
Robin et al. (2003)	Cartesian	v_x	–	131	$0.06^* - 0.11^{**}$
($*$ for stars at $M_V < 8$		v_y	–	106	
$**$ within 1 kpc from the Sun extrapolation)		v_z	–	226	
Kepley et al. (2007)	Cylindrical	v_R	-2 ± 11	157 ± 8	
		v_ϕ	23 ± 8	110 ± 6	
		v_z	-1 ± 6	84 ± 4	
Jurić et al. (2008)	–	–	–	–	0.4
Kordopatis et al. (2013)	Cylindrical	v_R	7 ± 4	30 ± 1	$0.5^* - 0.6^{**}$
($*$ Solar cylinder; chemical decomposition		v_ϕ	15 ± 9	119 ± 19	
$**$ Solar cylinder; kinematic decomposition)		v_z	-7 ± 3	110 ± 12	
Robin et al. (2014)	–	–	–	–	0.04
Posti et al. (2018)	Cylindrical	v_R	-10 ± 9	141 ± 6	0.46
		v_ϕ	9 ± 7	78 ± 4	
		v_z	-8 ± 9	94 ± 4	
Belokurov et al. (2018)	Cylindrical	v_R	0	140	
(avareged over all [Fe/H])		v_ϕ	30	78	
		v_z	0	80	
Amarante et al. (2020b)	–	–	–	–	0.47

Table 1.1 Stellar halo velocity parameters compiled by Smith et al. (2009). The table was updated including more recent studies and the stellar halo fraction, f_h. For a nearby sample, $v_y = v_\phi$. A value of $v_\phi > 0$ indicates prograde rotation. The estimates for the bulk motion have been standardised using the value of the solar motion from Schönrich et al. (2010).
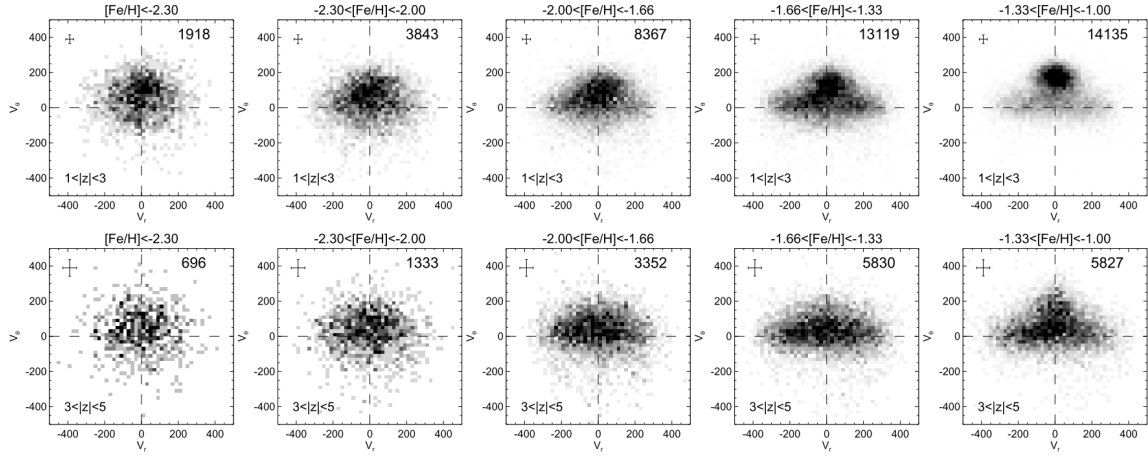
Fig. 1.2 The radial v_r and azimuthal v_θ spherical velocities for stars in the SDSS-*Gaia* DR1 sample. Each panel contains stars in different metallicity bins (increasing from left to right) and altitude |z| (increasing from bottom to top, in kpc). The lower metallicity bins show the presence of an isotropic halo population, therefore consistent with the known canonical halo. Intriguingly, closer to the plane and at higher metallicities (i.e. the last two panels in the top row) the distribution is consistent with a rotating disc population ($v_\theta > 150 \, \mathrm{km\,s}^{-1}$) and a mildly rotating and radially anisotropic population, which is distinct from the disc. They named this structure the *"Gaia-Sausage"* and concluded it is the product of a major merger event (see Section 1.1.1 for details). [*Reproduced from Belokurov et al. (2018), figure 2.*]

stellar halo, which decreases from $<v_\phi> \approx 50 \, \mathrm{km\,s}^{-1}$ to $<v_\phi> \approx 20 \, \mathrm{km\,s}^{-1}$ as [Fe/H] increases. Based on cosmological hydrodynamical simulations, the authors suggest that the accretion of several low-mass satellites would not form a highly radially anisotropic stellar halo, instead a major merger would be able to reproduce the observations. Thus, they suggest the Milky Way went through a major merger event during its first Gyrs and labelled it the *Gaia*-Sausage event.

Simultaneously, but with a different approach, Helmi et al. (2018) also concluded that the Milky Way had a major merger event that built its inner-halo and called it the *Gaia*-Enceladus event. This merger event that might have built the inner halo is now commonly called *Gaia*-Enceladus-Sausage (GES). The detailed analysis of this merger is beyond the scope of this thesis, but we refer to Evans (2020) for an overview.

Nonetheless, we will discuss the possible imprints of this merger in the early disc of the Milky Way. Before we do this, we first need to describe another old population of the Milky Way that might have been largely influenced by it: the thick disc.

1.2   The thick disc

The Milky Way disc has a total mass of $\approx 10^{10} M_\odot$ (Rix and Bovy, 2013) and is radially extended: the ratio between its scale-length and scale-height is ≈ 3.6. It is in the (thin) disc that the stellar formation regions are located (e.g. Kennicutt and Evans 2012), therefore the youngest and more metal-rich stars are closer to the plane. However, not all stars are young and metal-rich: the oldest stars in the disc are as old as ≈ 10 Gyrs and its metallicity reaches down to $\approx$ -1.2 dex (see, e.g., Haywood et al. 2013, Hayden et al. 2017). Initially thought of as a smooth population, in the early 1980s the stellar disc started to be depicted as having two components.

Yoshii (1982) found that the stellar density distribution of the disc could be modelled using two exponential distributions with distinct scale-heights. Gilmore and Reid (1983) independently, but intriguingly more famously[1], found similar results with a different stellar sample. It is important to note that both studies rely on stellar counts covering different regions of the sky. Later, Yoshii et al. (1987) confirmed the previous results and the scenario of a duality in the Milky disc was established.

More than a decade later, the thick disc started to be seen, rather than a purely geometrical component, as a distinct chemical population of the disc. Bensby et al. (2003) used a sample of 66 F and G dwarfs stars in the solar vicinity, classifying stars as thin and thick disc based on their kinematics. They found a clear distinction between the two populations: the thick disc stars have [α/Fe] larger compared to the thin disc stars. α elements are mainly produced by supernovae explosions of massive young stars (e.g., oxygen and magnesium) and thus identify stars born in rapid bursts of star formation. Therefore this difference in the [α/Fe] abundance reflects different timescales for the thin and thick disc formation. Afterwards, [α/Fe] was commonly used to distinguish stellar populations in the thin and thick discs.

The association of $\alpha-$rich stars with the thick disc became clearer with larger sample sizes. With a sample of 23 thousand stars from SDSS/SEGUE (Abazajian et al., 2009), Bovy et al. (2012) fit number density models for mono-abundance populations and concluded that each population is associated with a scale height and scale length. Figure 1.3 shows that α-rich stars have large scale heights, ≈ 0.8 kpc, and are radially concentrated with scale length ≈ 1.8 kpc. On the other hand, α-poor stars have low scale height, ≈ 0.2 kpc, and are radially extended, with scale length ≈ 3 kpc. The notion of the geometric aspect of the thin and thick disc, as found in the early 1980s, reflects the superposition of single

---

[1]As observed in Gilmore et al. (1989): *"Similar results to those of Gilmore and Reid (1983) were earlier derived from the Basel surveys by Yoshii (1982), though not widely appreciated at that time."*
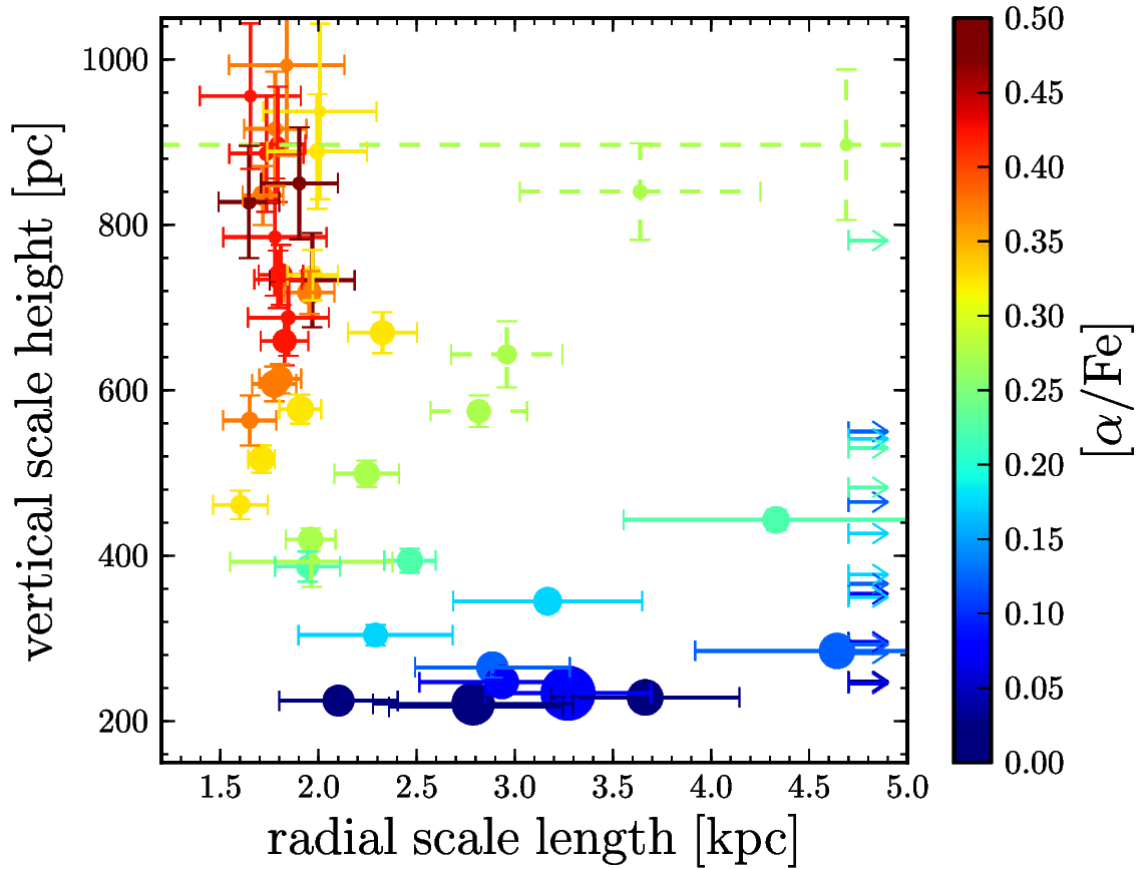
Fig. 1.3 The radial scale length vs the vertical scale height, colour coded by [α/Fe], of mono-abundance population stars. There is a clear segregation between α-rich, yellow/red points, and α-poor, green/blue points. The former have smaller scale length and larger scale height compared to the latter. It indicates that the geometrical thin and thick discs can be disentangled chemically. [*Reproduced from Bovy et al. (2012), figure 5.*]

mono-abundance populations with different scale heights (as advocated also by, e.g. Minchev et al. 2015, Kawata et al. 2018).

The distinct scale height and scale length for the α-rich and α-poor populations is reflected in the [Fe/H]-[Mg/Fe] plane at different spatial ranges (see, e.g., Hayden et al. 2017). Using a crossmatch between *Gaia* DR2 and APOGEE DR15 (Zasowski et al., 2013), we select stars with good parallax (i.e. relative error lower than 20%) and show in Figure 1.4 how the abundance plane varies with galactocentric radius (R) and altitude (z). The z range increases from bottom to top, while the R range increases from left to right. The clump associated with the thick disc population is located at [Mg/Fe] ≈ 0.3 and dominates the abundance plane at smaller R and larger z. On the other hand, the thin disc population ([Mg/Fe] ≈ 0) dominates for larger R and lower z.
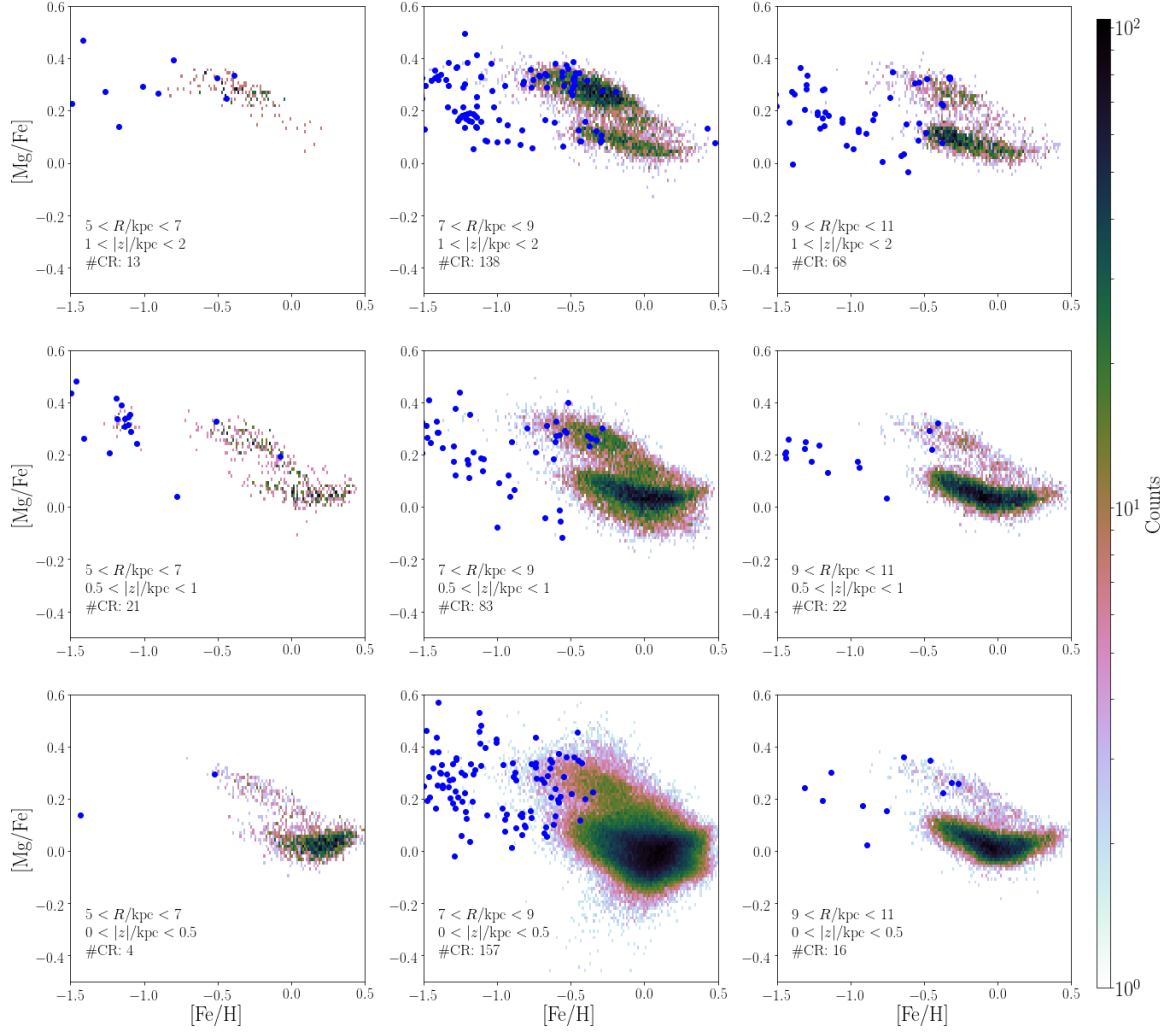
Fig. 1.4 The [Fe-H]-[Mg/Fe] distribution for APOGEE-*Gaia* stars at different locations in the Galaxy. The cylindrical galactocentric radius increases from left to right and the distance from the plane increases from bottom to top. The upper-middle panel shows stars closest to the Sun - here it is possible to see two separate α-rich ([Mg/Fe] $\approx$ 0.3) and α-poor ([Mg/Fe] $\approx$ 0.0) populations. As the altitude from the plane increases, the α-rich stars dominate over the α-poor. Therefore, α-rich stars are associated with the thick-disc and the α-poor with the thin-disc. Moreover, for fixed altitudes, there is a noticeable reduction in the prominence of the α-rich population at larger radii. Finally, the blue points show counter-rotating stars in the sample. Notice that a number of these are located in the same region of the diagram as the thick-disc population (see Section 1.2 for discussion).

We also show counter-rotating stars, $v_\phi < 0$ km s^{-1}, in Figure 1.4 as blue circles. The vast majority of these stars are located outside the clumps associated with the disc and are likely to be accreted stars (e.g. Mackereth et al., 2019). However, it is interesting to note that a non-negligible number of them have thick disc chemistry. Typically, it is not expected that disc stars should have retrograde motion and yet these stars are in general too metal rich ([Fe/H] ≈ -0.7) to be associated with the canonical stellar halo. The observation of metal-rich low angular momentum stars raises questions about the formation mechanisms of the thick disc, in particular its overlap/connection with the in-situ stellar halo. We will explore these themes in the following section.

1.3   The inner stellar halo – thick disc overlap

Metal-rich stars ([Fe/H]>-1), with halo-like kinematics has been in evidence for about a decade (as in, e.g. Nissen and Schuster 2010, Schuster et al. 2012). Nonetheless, a clear picture of how these stars are characterised in the velocity-chemical space was yet to come. Di Matteo et al. (2019) took a step forward, exploring the overlap in the chemical-velocity space between the inner stellar halo and the thick disc for 60 thousand stars in a crossmatch between *Gaia* DR2 and APOGEE DR14 (Majewski et al., 2017).

Figure 1.5 shows several [Fe/H]-v_ϕ planes at different [Mg/Fe] intervals. In this Figure, negative (positive) v_ϕ corresponds to prograde (retrograde) rotation. At low [Mg/Fe] abundances (top row panels) the stars associated with the thin disc are located at $v_\phi \approx -220$ km s^{-1} and have [Fe/H] ≈ 0. A few retrograde stars ($v_\phi > 0$ km s^{-1}) are also observed at lower [Fe/H], but their chemical-velocity properties are detached from the disc stars due to their accreted nature. As [Mg/Fe] increases, the mean rotational velocity and metallicity decreases as more stars associated to the thick disc are included in the sample. Moreover, the low angular momentum stars populate a larger [Fe/H] range, with several retrograde stars in the range $-0.7 <$[Fe/H]< -0.2. As these stars seem to be connected to the thick disc population, Di Matteo et al. (2019) suggested that they could be heated thick disc stars. In fact, they argued the Milky Way in-situ halo is solely composed of heated thick disc stars.

The picture that emerges is of a disc formed in the first Gyrs of the Milky Way, which was then heated and puffed up by the GES merger. This process created a population of metal-rich low-angular momentum stars, including the counter-rotating ones, which built up the inner stellar halo. This scenario is supported by the discovery of ultra-metal poor stars on disc-like circular orbits (Sestito et al., 2019), indicating that the young Galaxy could already have formed a proto-disc prior to the GES merger event. It also strengthens the formation
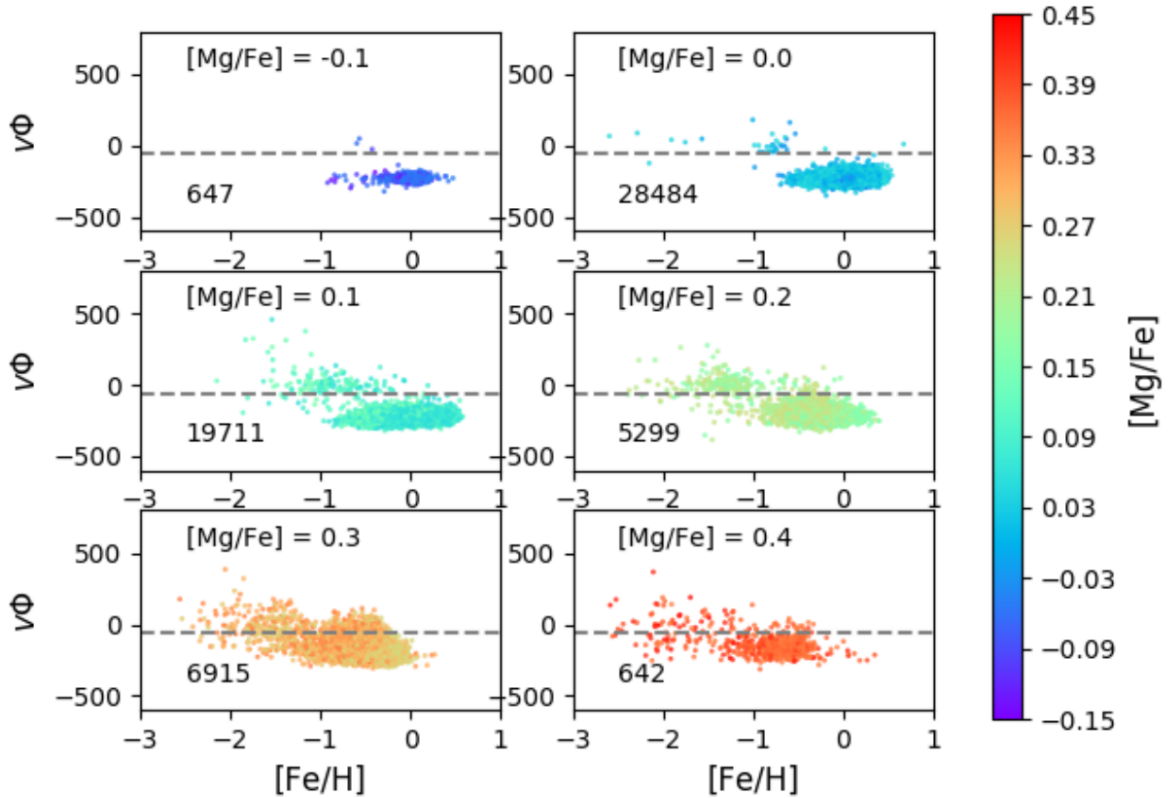
Fig. 1.5 The distribution of [Fe/H]-v_ϕ, in $\mathrm{km\,s^{-1}}$, for stars in APOGEE-*Gaia* grouped by [Mg/Fe]. In this panel, $v_\phi < 0\,\mathrm{km\,s^{-1}}$ indicates prograde rotation. For higher [Mg/Fe] values, a population of retrograde stars becomes apparent. Intriguingly this includes not only canonical stellar halo stars ([Fe/H] $\lesssim -1.2$), but also relatively metal-rich stars ([Fe/H] ≈ -0.7) which would typically be associated with the chemical thick disc. [*Reproduced from Di Matteo et al. (2019), figure 12.*]

mechanism of the thick disc via a major merger (e.g. Quinn et al. 1993, Villalobos and Helmi 2008, Grand et al. 2020).

The major merger scenario is not the only proposed mechanism for the thick disc formation. For example, Brook et al. (2004) proposed that the thick disc stars are formed from the accreted gas at high redshift. This would explain the large velocity dispersion of the thick disc in contrast to the thin disc.

There are other mechanisms that can explain the formation of the thick disc solely by in-situ secular processes, without requiring any ex-situ processes. Stellar radial migration (Schönrich and Binney 2009, Loebman et al. 2011) causes stars from the inner parts of the Galaxy to migrate outwards. During this process they feel a decreased restoring force in the vertical direction and thus can reach larger $|z|$. Kawata et al. (2017) also suggests that mono-age stellar populations form in a disc where the scale-height increases with radius.

This scenario, the flared star-forming disc, explains for example the presence of $\alpha-$poor stars at larger $|z|$ in the outer regions of the Galaxy, Figure 1.4 top right panel. Another mechanism is scattering by massive clumps during the Galaxy's first Gyrs(Bournaud et al. 2009, Clarke et al. 2019, Beraldo e Silva et al. 2020). In this scenario the α-rich (i.e. thick disc) stars are produced quickly in the clumps and subsequently scattered by them. This scattering increases the vertical velocity dispersion of the stars and gives rise to the geometrical and chemical thick disc. It is important to stress that in this scenario the thin- and thick-disc dichotomy arises early in the Galaxy and would already be present before and during the GES merger event.

In the following Chapters we will explore with greater detail the heated thick disc population. In Chapter 2 we explicitly quantify the amount of thick disc stars with stellar halo kinematics, using a new approach to model the local thick and halo fractions. We will also find evidence for a significant metal-rich counter-rotating population, taking advantage of chemistry information from LAMOST DR5. In Chapter 3. we explore the formation of the metal-rich, low angular momentum population via the clumpy formation scenario. This has a major implication in the consequences of the GES merger event. Finally, in Chapter 4 we address our conclusions and future prospects.

Chapter 2

The stellar halo in the Solar Neighbourhood

As discussed in the previous Chapter, the inner stellar halo and thick disc populations have a significant overlap in metallicity and velocity space. We will explore a new methodology to disentangle both populations using a kinematically biased sample that enables us to quantify the amount of heated thick disc stars in the Solar Neighbourhood. Most of the following content was originally published in *Amarante et al. 2020, MNRAS, 492,3816*.

2.1 Introduction

Gaia Collaboration et al. (2018a) have demonstrated the amount of detail it's possible to obtain from the analysis of the HR diagrams drawn from *Gaia* data (Gaia Collaboration et al., 2018b, 2016). For instance, for those interested in the stellar halo and thick disc, their figure 21 is especially relevant (reproduced here in Section 2.4). By selecting stars with transverse velocity greater than 200 $\mathrm{km\,s^{-1}}$, two distinct sequences are clearly distinguishable in the colour-magnitude diagram. This kinematic selection cut is likely to produce a sample dominated by halo stars and so the fact that two sequences are observed could be an indication that the local halo is composed of two different stellar populations. However, one might wonder whether this cut produces a pure halo sample. Could there be contamination from the thick disc and, if so, how does this affect our interpretation of the data? For that matter, the relative fractions of the stellar halo and the thick disc at the Solar Neighbourhood, turn out to be a very important constraint, nonetheless not trivial to obtain.

In the last decade, several studies have provided clues to the local stellar halo fraction, f_h, using different methods and volumes[1], see 1.1. For example, Gould et al. (1998) used deep HST star counts to constrain $f_{h,\odot}$, finding it to be in the range 0.07 to 0.2%. Later, Jurić et al. (2008), using the large photometric Sloan Digital Sky Survey (SDSS), modelled the number density of stars in the Milky Way and found that, at the Solar position, $f_{h,\odot} = 0.4\%$. Large spectroscopic surveys, such as the Radial Velocity Experiment (RAVE), also reinvigorated studies of the Milky Way's structure. Kordopatis et al. (2013), using RAVE DR4 data, found that the local f_h varies from 0.5% to 0.6% depending on whether they use a chemical or kinematic selection, respectively. More recently, Posti et al. (2018) used the cross-match between *Gaia* DR1 and RAVE to select, through Action Angle distributions (Binney and Tremaine, 2008), the local stellar halo. From their study they conclude that $f_h \approx 0.45\%$. Even though these studies all use different selection criteria and could be subject to various selection effects, it seems that the value of f_h within 1 kpc seems to be converging on $\approx 0.5\%$.

The value of f_h is an important ingredient for models of the distribution of stars in our Galaxy. The most influential model in the past two decades has been the Besançon model. In their original model, which was the standard model for most of this time, Robin et al. (2003) adopted a value for the halo normalisation based on star counts at high and medium latitudes. They estimated $f_{h,\odot} = 0.06\%$ for $M_V < 8$, which corresponds to $f_h \approx 0.06\%$. This was subsequently updated in Robin et al. (2014) to incorporate a new multi-component thick disc, but still a low value for the halo normalisation was adopted ($f_h = 0.04$). Therefore it is worth emphasising that the halo normalisation in the Besançon model is significantly less than the above consensus. This means that models and data products which are based on the Besançon model, such as the Galaxia model (Sharma et al., 2011) or Rybizski mock *Gaia* catalogue (Rybizki et al., 2018), will significantly underestimate the halo contribution.

Since the thick disc was first proposed as a distinct component of the Milky Way (see Chapter 1), its local fraction, f_{TD}, is still an open question: due to the degeneracy with its scale length, f_{TD} ranges from 2% (Gilmore and Reid, 1983) to 12% (Jurić et al., 2008). We refer to Bland-Hawthorn and Gerhard (2016) review where they found a mean value of $f_{TD} = 4\% \pm 2\%$, after compiling 25 results from photometric surveys without any detailed stellar abundance information. Nonetheless, it's worth mentioning a few specific studies, e.g., Kordopatis et al. (2013) found that the local f_{TD} was either 15.2% or 18.3%, depending on whether a kinematic or chemical selection was used, respectively. The caveat with these

---

[1]Throughout this Chapter, we take f_h and f_{TD} to refer to the fraction of halo and thick disc stars, respectively, within 1 kpc of the Sun, e.g. f_h is the number of halo stars divided by the total number of halo, thick and thin disc stars. In the rare instances that we refer to the fraction at the Solar position (i.e. the in-plane normalisation at the Solar radius), we denote this as $f_{h,\odot}$ or $f_{TD,\odot}$.

values is the assumption of a Gaussian distribution for both azimuthal velocity, v_ϕ, and metallicity distributions. As will be discussed later, the asymmetric drift in the disc makes the v_ϕ distribution skew towards lower velocities, thus a Gaussian may not be physically meaningful to describe it. Moreover, it may underestimate (*overestimate*) the contribution of the thin (*thick*) disc stars. Finally, if high resolution spectroscopic data are included and the thin and thick discs are defined as [α/Fe] poor and rich, respectively, the scale length and scale heights are clearly different for both populations (Bensby et al., 2003). For example, Bovy et al. (2012), find that the [α/Fe] rich stars have a larger scale height and smaller scale length than the [α/Fe] poor stars. This helps to break the aforementioned degeneracy with f_{TD} and favour lower values for the thick disc normalisation.

Another challenge is to correctly distinguish stellar halo and thick disc stars when dealing with a local sample. There is a non-negligible overlap between the former's metal rich end and the latter's metal poor end, with both co-existing at around [Fe/H]≈ -0.8, which means that some cuts in [Fe/H] could lead to contaminated samples. Nevertheless, α peak elements, especially magnesium, can help distinguishing both populations. For example, using data from APOGEE Hawkins et al. (2015) and Hayes et al. (2018) have shown that for [Fe/H] $\lesssim -0.7$ there are two distinct populations: an [α/Fe] poor sequence with zero net rotation, which is consistent with stars being mainly accreted from small dwarf satellites whose stellar populations were formed in the first few Gyr of the universe; and an [α/Fe] rich sequence, which has some net rotation and is kinematically colder than the [α/Fe] poor sequence. Hawkins et al. (2015) point out that these [α/Fe] rich stars could come from either the thick disc or from some form of in-situ (in their words "canonical") halo population. They conclude that these two populations are not chemically distinct and that this may suggest a common origin.

In this Chapter, we present a different approach to estimate f_h and f_{TD} in order to quantify the amount of thick disc contamination in the *Gaia* high transverse velocity sample. As discussed above, this could potentially change the interpretation of a dual stellar halo population in the solar neighbourhood, as suggested by Haywood et al. (2018) and Gallart et al. (2019). This Chapter is organised as follows: Section 2.2 describes the data we will use in our analysis; Section 2.3 models the tail of the high transverse velocity distribution, in order to obtain f_h and f_{TD}; Section 2.4 dissects the chemistry of these stars, using spectroscopic data from LAMOST; Section 2.5 explores the dynamical properties of the sample; Section 2.6 brings together our findings and presents our take on the nature of the stars in this sample; finally in Section 2.7 we provide some brief conclusions.

2.2   Data selection

The sample was extracted from the GDR2 catalogue using the same ADQL query as described in Gaia Collaboration et al. (2018a), which we reproduce in Appendix A. The query selects all stars within 1 kpc that have G < 17 and with transverse velocity $v_t = 4.74/\varpi \sqrt{\mu_{\alpha^*}^2 + \mu_\delta^2} >$ 200 $\mathrm{km\,s^{-1}}$. The total sample size is 77,107. In addition to this sample, since in Section 2.3 we also wish to compare to the entire v_t distribution, we randomly selected a sample of 672,138 stars that satisfy the same constraints as the high v_t main sample except without the v_t cut.

Throughout this Chapter, we use the Galactocentric cylindrical velocities v_R, v_ϕ and v_z, where they are positive in the direction to the Galactic centre, Galactic rotation and North Galactic pole, respectively. We adopt from Schönrich (2012) the values for the solar Galactocentric distance $R_\odot = 8.27$ kpc and local circular velocity $v_c = 238$ $\mathrm{km\,s^{-1}}$. We assume the Solar motion with respect to the Local Standard of Rest to be $(U_\odot, V_\odot, W_\odot) = (11.1, 12.24, 7.25)$ $\mathrm{km\,s^{-1}}$ (Schönrich et al., 2010).

2.3   Transverse velocity modelling

2.3.1   Galaxia: a synthetic population model

The Galaxia code[2] (Sharma et al., 2011) is a population synthesis model based on the Besançon Galaxy model (Robin et al., 2003), which is itself constrained using a variety of observational results. Galaxia is a convenient tool for understanding large observational surveys, such as *Gaia*, and is especially useful for modelling selection effects in all-sky surveys. In Galaxia, both the stellar halo and thick disc have their 3D velocities described by a Gaussian distribution. We summarise the parameters of each population in Table 2.1, where these parameters are the same as Robin et al. (2003). It is important to note that the Besançon model used in Galaxia is the original model, as described in Robin et al. (2003), and not the updated model presented in Robin et al. (2014) and available online[3]. This newer model, which incorporates a multi-component thick disc, does not significantly improve the match to the v_t distribution, as we will discuss later in this section. In order to understand the properties of our observed *Gaia* sample, a good starting point is to compare what would be the expected transverse velocity distribution from a canonical model of the Milky Way. For this purpose, we use the mock catalogue created by Rybizki et al. (2018), available at

---

[2]http://galaxia.sourceforge.net/
[3]http://model2016.obs-besancon.fr/

	Galaxia		Model	
	TD	Halo	TD	Halo
$\langle v_R \rangle ; \sigma_{v_R} \, [\mathrm{km\,s^{-1}}]$	$[0;66]$	$[0,135]$	$[0;58]$	$[0,140]$
$\langle v_\phi \rangle ; \sigma_{v_\phi} \, [\mathrm{km\,s^{-1}}]$	$[195;51]$	$[11;85]$	$[196,48]^*$	$[30,78]$
$\langle v_z \rangle ; \sigma_{v_z} \, [\mathrm{km\,s^{-1}}]$	$[0;42]$	$[0,84]$	$[0;42]$	$[0,80]$
$f_{pop}(\varpi > 1) \, [\%]$	10.95	0.11	6.52	0.47

Table 2.1 Parameters for the canonical Galaxia model and our updated model. The stellar halo model parameters are averaged over the whole range of [Fe/H].
* We do not use a Gaussian distribution to model v_ϕ for the thick disc and so these numbers are just included to give an indication of the mean and spread of our distribution. See text for details.

GAVO[4] as *gdr2mock.main*, which is based on the Galaxia canonical model. Using the same ADQL query as for the observational sample, a total of 42,128 mock stars with $v_t > 200$ $\mathrm{km\,s^{-1}}$ were obtained.

Although the full mock catalogue has the same number of stars as the *Gaia* DR2 catalogue, it is not expected to precisely match the number of stars in either a specific stellar population (e.g. thick disc or halo) nor a selected sample (e.g. $v_t > 200$ $\mathrm{km\,s^{-1}}$). For example, even though the total number of stars in the mock and observed samples are similar for the same magnitude and spatial cuts, namely 25 and 29 million stars, respectively, if we look at the stars with $v_t > 200$ $\mathrm{km\,s^{-1}}$ we find that the numbers are 42 and 80 thousand stars, respectively. The factor of two difference already indicates that there may be a deficiency in the underlying model from which the mock sample is drawn. This is shown more clearly in Fig 2.1, where we have normalised both distributions by the total number of stars that satisfy the original ADQL query without the v_t cut, i.e. over the whole range of transverse velocities. Clearly, the canonical model of the Galaxy is unable to reproduce the observed data as there is a significant lack of stars for $vt \gtrsim 200$ $\mathrm{km\,s^{-1}}$. For completeness we also include the distribution from the updated Besançon model Robin et al. (2014). Although this marginally improves the fit for moderate values of v_t, it still significantly underestimates the number of stars in the tail beyond $v_t \approx 250$ $\mathrm{km\,s^{-1}}$. The fact that these distributions don't agree could be due to either (a) how the velocities are assigned to each population within a given model, or (b) the assumed normalisation fraction of each population. In the high v_t tail the two dominant populations are the stellar halo and thick disc. For the rest of this

---

[4]http://dc.g-vo.org/tap
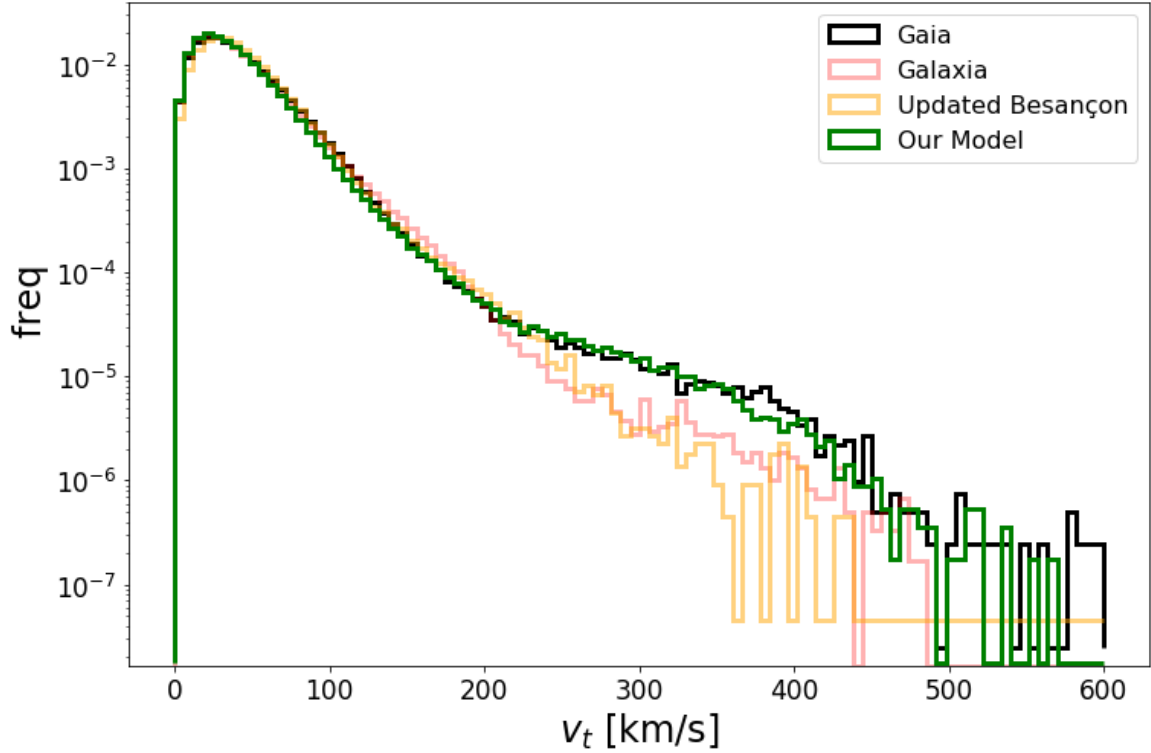
Fig. 2.1 The normalised histogram of v_t for *Gaia* data and our model, in black and green respectively. The canonical Galaxia model, in red, is unable to describe the observed data for $v_t > 200$ km s^{-1} mainly due to the adopted normalisation factors for the thick disc and stellar halo populations. The updated Besançon model (Robin et al., 2014), in yellow, is also unable to fit the tail of the v_t distribution.

section we will focus on these two populations, describing our prescription for obtaining an improved parameterisation of the thick disc and halo.

2.3.2   Thick disc

It is well known that the asymmetric drift affects the v_ϕ distribution of disc stars, meaning that a single Gaussian cannot provide a good match to the skewed observed distribution (e.g. Binney and Tremaine 2008). One common approach is to model this with two Gaussians, each with different mean (μ), standard deviation (σ) and weight (w). For example, Kordopatis et al. (2013), while studying stars between 1 and 2 kpc above the Galactic plane, decomposed the observed v_ϕ distribution using three Gaussians, each one representing the thin disc, the thick disc and the halo. Although the results are consistent with the expected fractions for thin and thick disc, the real physical meaning of the Gaussian parameters, especially for the disc populations, is rather unclear.

The asymmetry in the azimuthal velocity distribution for the disc, also known as asymmetric drift, can be understood by the following three reasons:

i. Due to conservation of angular momentum, stars have slower rotational velocity as they approach apocentre, so their guiding-centre radii, R_g, are smaller than the solar radius, R_0;

ii. There is an increase in the density of stars towards the inner parts of the disc and also in the random velocities of the stars. This latter property means that there are a greater fraction of stars on eccentric orbits, which can lead them far from their R_g;

iii. Populations of stars become kinematically hotter over time and the deviations from axi-symmetry in the Galactic potential[5] cause such populations to expand spatially. Consequently, due to the conservation of angular momentum, their mean rotation rate decreases.

In order to better depict the asymmetry in the azimuthal velocity distribution, Schönrich and Binney (2012) presented a new formula to describe the disc kinematics using physically meaningful parameters. It is constructed within a dynamical framework that connects the skewness of the v_ϕ distribution to the standard deviations of v_R and v_z. Their model shows how the distribution of v_ϕ changes for slices in distance from the plane (z) and Galactocentric radius (R). The final distribution, given in equation 29 of Schönrich and Binney (2012), is:

$$n(v_\phi | R, z) = \frac{\mathcal{N}}{g(c)} \exp\left[\frac{-(R_g - R_0)}{R_d}\right] \exp\left[\frac{-\Delta\Phi_{\text{eff}}}{\sigma_0^2}\right] f(z, R_g - R), \qquad (2.1)$$

where:

$$c(R_g) = \frac{v_c^2}{2\sigma(R_g)},$$

$$g(c) = \frac{e^c (c - 1.5)!}{2c^{(c-0.5)}},$$

$$f(z, R_g - R) = \exp\left(\frac{R_g - R}{(2 + \alpha)R_d}\right) \exp\left\{\frac{|z|}{h_0}\left(1 - \exp\left(\frac{R_g - R}{(2 + \alpha)R_d}\right)\right)\right\}$$

---

[5]Although the Galactic potential is usually modelled as axi-symmetric, which holds to a first approximation, the spiral arms and the central bar creates an asymmetry.

and α is the exponent of the relation between the scale height and surface density of a given stellar population, which is assumed to decrease with height as:

$$\alpha(z) = \begin{cases} 2 - 1.5z/1.5\text{kpc} & \text{for } z \leq 1.5\text{kpc} \\ 0.5 & \text{otherwise.} \end{cases}$$

The dependence on v_ϕ is implicit in the definition of the guiding radius $R_g = Rv_\phi/v_c$, where v_c is the circular velocity speed. Therefore, Equation 2.1 is a function of: the Galactocentric radius of the measurement (R_0), the scale length of the observed population (R_d), the local radial velocity dispersion (σ_0), the scale length on which the radial velocity dispersion varies (R_σ) and the scale height of the vertical density profile (h_0). All the parameters reflect the characteristics of the dominant population, e.g. thin or thick disc stars, in a given sample. Finally, it can be noted that this equation also depends on the assumed Galactic potential, $\Delta\Phi_{\text{eff}}$.

Our first update to the canonical Galaxia model is on the description of the thick disc kinematics. Instead of the canonical Gaussian distribution for the velocity components, we use the physically motivated Equation 2.1 to draw the three velocity components of the mock thick disc data. This requires us to adopt values for the aforementioned parameters for the thick disc (i.e. R_d, σ_0, R_σ and h_0). Since there is no firm consensus on the values of these parameters (see Bland-Hawthorn and Gerhard 2016 for a discussion), we obtain values using data from the APOGEE survey. We take our data from the publicly available APOGEE-*Gaia* DR12 catalogue[6], selecting all stars within 1 kpc of the Sun with relative errors in parallax lower than 20%, -1.1<[Fe/H]<-0.1 and 0.2<[Mg/Fe]<0.45. We note that our chemical selection is within the same range of the selected thick disc (alpha rich) stars from Mackereth et al. (2019). We fit the APOGEE v_ϕ distribution according to Schönrich and Binney (2012), using the Affine Invariant Markov Chain Monte Carlo *emcee* package[7] (Foreman-Mackey et al., 2013). In order to reduce degeneracies in the modelling we fix $R_d = 1.8$ kpc and $h_0 = 0.9$ kpc, leaving σ_0 and R_σ free. This procedure gives $\sigma_0 = 53.4$ $\text{km}\,\text{s}^{-1}$ and $R_\sigma = 12.3$ kpc. Although this is a simplistic approach, we are only concerned with obtaining a qualitatively good fit and have found that our results are not especially sensitive to the choice of parameters. Fig. 2.2 shows the resulting v_ϕ distribution from our model, compared to the observed APOGEE-*Gaia* thick disc sample. Our model provides a reasonable fit and one that is statistically superior to the canonical Gaussian model. Since the

---

[6]https://www.sdss.org/dr12/irspec/spectro_data/
[7]http://dfm.io/emcee/current/
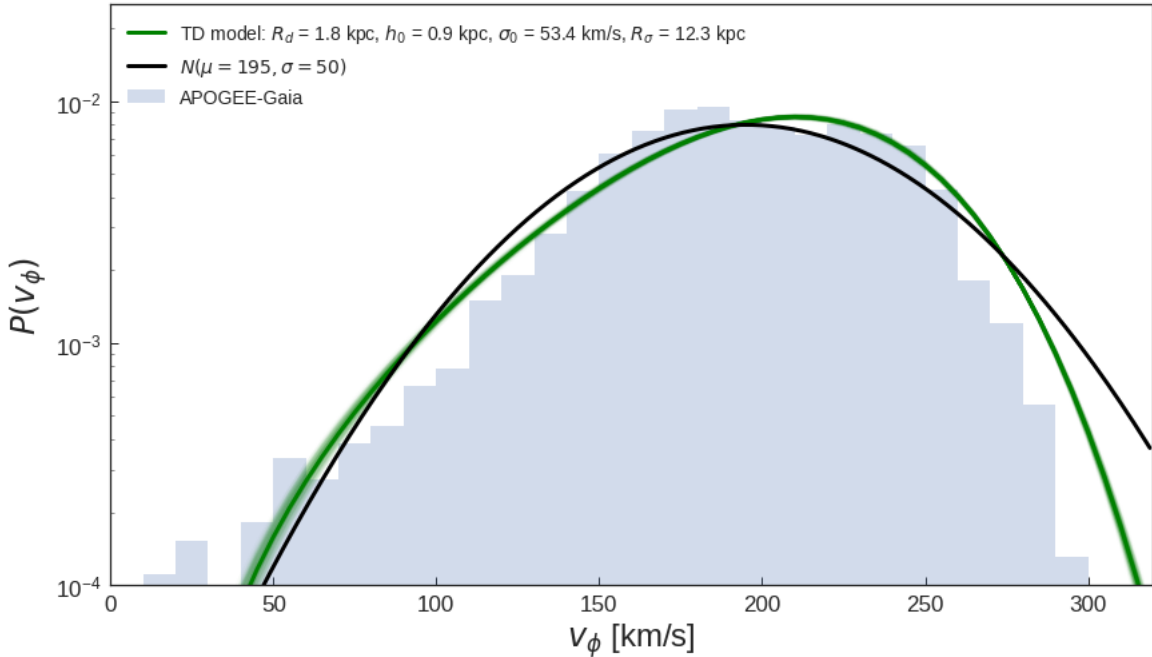
Fig. 2.2 The distribution of v_ϕ for the thick disc. The solid histogram shows an APOGEE-*Gaia* sample (see text for details), while the green line shows our adopted model based on the work of Schönrich and Binney (2012). In grey we show the canonical Gaussian distribution adopted by the Galaxia model ($\mu = 195$ km s^{-1} and $\sigma = 51$ km s^{-1}).

goal of this Chapter is not to find the best fit for the local thick disc, we defer more detailed modelling to future work.

2.3.3   Stellar halo

Belokurov et al. (2018) showed that, within 10 kpc, the stellar halo's velocity ellipsoid has a strong dependence on metallicity. As the metallicity increases, the anisotropy (β) of the halo also increases, indicating a radially biased population. Moreover, not only does the stellar halo have a mild rotation, the rotation signature is stronger for more metal poor stars. None of these features are incorporated into the original Galaxia stellar halo model, thus we updated the stellar halo model incorporating the rotation and anisotropy dependency on [Fe/H]. Since Belokurov et al. (2018) only explored the halo for $|z| > 1$ kpc, we extrapolated their results and assumed that the features observed for $1 < |z| < 3$ kpc are the same for $|z| < 1$ kpc. Table 2.1 shows the features of the updated stellar halo model, averaged over all [Fe/H]. Fig. 2.3 shows the first two moments of the spherical velocity distribution for the adopted stellar model (solid lines) and the canonical Galaxia model (dashed lines). The left panel shows how the radial/rotational velocity dispersion increases/decreases significantly
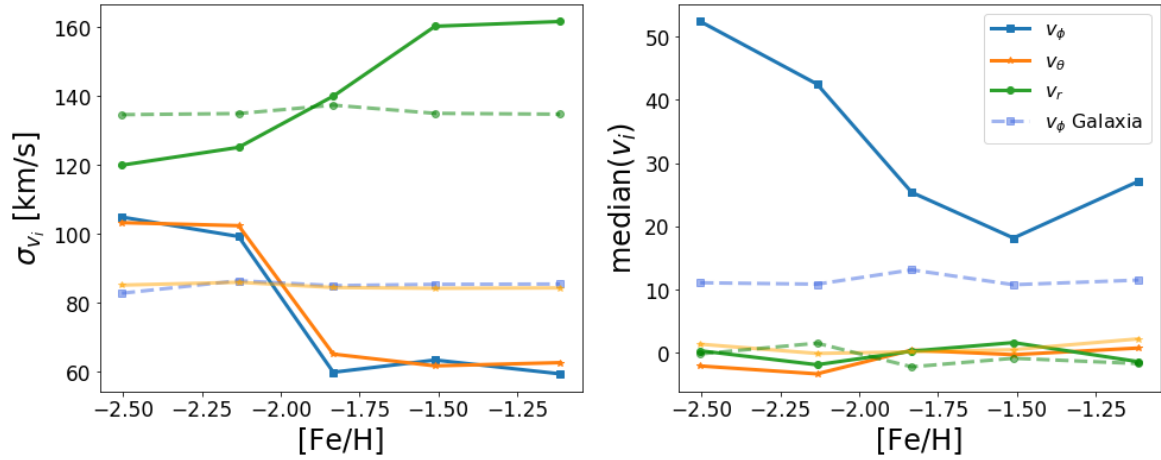
Fig. 2.3 The dispersion and median of the stellar halo velocity ellipsoid, within 1 kpc of the Sun, for our model (solid lines) and Galaxia's canonical model (dashed lines). The radial, azimuthal and tangential velocities are represented by the green, orange and blue lines, respectively, in both panels. This is an extrapolation of Belokurov et al. (2018) results where we assume their observed features for $1 < |z| < 3$ kpc are the same for $|z| < 1$ kpc.

with [Fe/H], resulting in $\beta \approx 0.9$[8]. On the other hand, the Galaxia canonical model has a constant anisotropy of $\beta \approx 0.6$ representing a more spherically symmetric halo. The right panel also shows that the new halo model has more significant rotation. Finally, we note that the tilt of the halo ellipsoid is likely to be negligible for our sample (see, for example, Wegg et al. 2019) and so we are safe to neglect any correlations in the velocities.

2.3.4 Fitting procedure

Once the functions that describe the velocity distributions for our halo and thick disc populations are chosen, our modelling is very straightforward. We first select all the stars in the mock catalogue that follow the magnitude and distance criteria from the original ADQL query. For the thick disc and halo stars we re-sample their velocities using our updated velocity parameters and recalculate their v_t. We then compare the v_t distribution to the observed distribution over the range $v_t > 200$ km s^{-1}. To do this, we take bins of width 10 km s^{-1} and calculate the maximum likelihood using a standard χ^2 technique, where we have two free parameters corresponding to the re-weighting factors for the thick disc (c_{TD}) and halo (c_h). We do not re-weight the thin disc because the fraction of thin disc stars in this v_t range is negligible ($< 0.3\%$), as expected.

---

[8]The anisotropy is defined as s $\beta = 1 - \frac{\sigma_z^2 + \sigma_\phi^2}{2\sigma_r^2}$.

Our adapted Galaxia model is described by the following equation,

$$\mathrm{N}^i_{\mathrm{model}} = \mathcal{N}\left[c_h \cdot \mathrm{N}^i_h + c_{TD} \cdot \mathrm{N}^i_{TD} + \mathrm{N}^i_{td}\right] , \tag{2.2}$$

where, N^i_{model} is the total number of stars in the i-th bin, $N^i_h/N^i_{TD}/N^i_{td}$ are the number of halo/thick-disc/thin-disc stars in the original mock catalogue, c_h and c_{TD} are the aforementioned re-weighting parameters, and $\mathcal{N}$ is the normalisation. Note that, in order to maintain a good fit over the whole velocity range, we normalise over the entire range of v_t, not just $v_t > 200$ km s^{-1}, using the following normalising factor,

$$\mathcal{N} = \left(\mathrm{N}^{tot}_{td} + c_h \cdot \mathrm{N}^{tot}_h + c_{TD} \cdot \mathrm{N}^{tot}_{TD}\right)^{-1} , \tag{2.3}$$

where the superscript *tot* is the total number of mock stars for each component in the original Galaxia model (i.e. within the distance and magnitude range of the observed data and for all v_t).

We then compare N^i_{model} to the corresponding bin from the observed *Gaia* distribution, N^i_{Gaia}, using a standard χ^2 maximum likelihood technique, assuming Poisson uncertainties,

$$\mathcal{L} \propto \prod_i \exp\left(\frac{\mathrm{N}^i_{\mathrm{Gaia}} - \mathrm{N}^i_{\mathrm{model}}}{\sqrt{\mathrm{N}^i_{er,\mathrm{Gaia}}}}\right)^2 . \tag{2.4}$$

N^i_{Gaia} is also normalised by the total number of *Gaia* stars in the same selection criteria. $N^i_{er,\mathrm{Gaia}}$ is the Poison error in the i-th bin.

To identify the values of c_h and c_{TD} that maximise our Equation 2.4 we again use *emcee*, finding $c_h = 3.78 \pm 0.02$ and $c_{TD} = 0.52 \pm 0.01$. If we return to Fig. 2.1 we can now compare our model (green line) to the observed data, where it is clear that our re-weighting has produced a significant improvement in the tail of the distribution compared to the standard Galaxia model. Moreover, even though our fit used only the available data for the tail, we can see that the model is in good agreement with the v_t distribution as a whole.

2.3.5 Results

We can use these correction factors to calculate the local halo and thick disc fractions within 1 kpc and for $G < 17$, obtaining $f_h = 0.47\%$ and $f_{TD} = 6.52\%$. In comparison, the Galaxia values are 0.12% for the stellar halo and 10.95% for the thick disc.

The fact that our values differ from the Galaxia ones is not necessarily surprising, as can be seen from our discussion in Section 2.1. For the halo, recent studies seem to be converging on fractions of around 0.4 to 0.5% (e.g. Jurić et al. 2008, Kordopatis et al. 2013, Posti et al. 2018). For the thick disc fraction, there is no firm consensus. This is mainly due to the degeneracy with its scale height and the reliance on statistical methods to disentangle thin and thick disc samples. Low values of f_{TD} have been reported previously, e.g. Just and Jahreiß (2010) who claim that a massive thick disc is inconsistent with the kinematics of nearby K and M dwarfs.

With these updated fractions, our model predicts that $\approx 13\%$ of the high v_t *Gaia* sample has kinematics consistent with the thick disc. We note that this result is not sensitive to our assumed form for the thick disc velocity distribution. For example, if we take R_σ, σ_0 and R_d from the dynamical studies listed in Bland-Hawthorn and Gerhard (2016) table 5, or if we simply use the canonical Gaussian distribution from Galaxia, then the fraction stays within the range $12 - 14$ %. Nevertheless, we still favour our assumed thick-disc model due to the improved fit to the APOGEE data (Fig. 2.2).

Finally, we can take advantage of the better fit to the high v_t data and use our new model to produce an updated Toomre diagram. This diagram is generally used to kinematically select stellar halo and/or thick disc stars (e.g. Bensby et al. 2003; Helmi 2008b). Given assumptions on the properties of the stellar populations (namely their relative contributions and velocity dispersion), we can predict which regions of the v_ϕ vs $\sqrt{v_R^2 + v_z^2}$ plane will be dominated by which populations. To illustrate this, the left panel of Fig. 2.4 shows the Toomre diagram for our updated model. The thin disc, thick disc and stellar halo are represented by the orange, grey and green shaded regions, respectively. The darkness in the shading corresponds to regions where a given population has a fraction greater than 75%, 85% or 95% overall. For comparison, the dashed lines show the regions where Galaxia predicts that the stellar halo (green) or the thick disc (black) has a fraction greater than 85%. The right panel uses the same colour scheme to show the Toomre diagram for a kinematically biased sample with $v_t > 200$ km s^{-1}. While the thin-disc stars are not present anymore, due to the v_t cut, there is still a region dominated by the thick-disc population. Over-plotted in this panel we show the *Gaia* DR2 high v_t stars, colour-coded according to their position in the HRD (see Section 2.4.2).
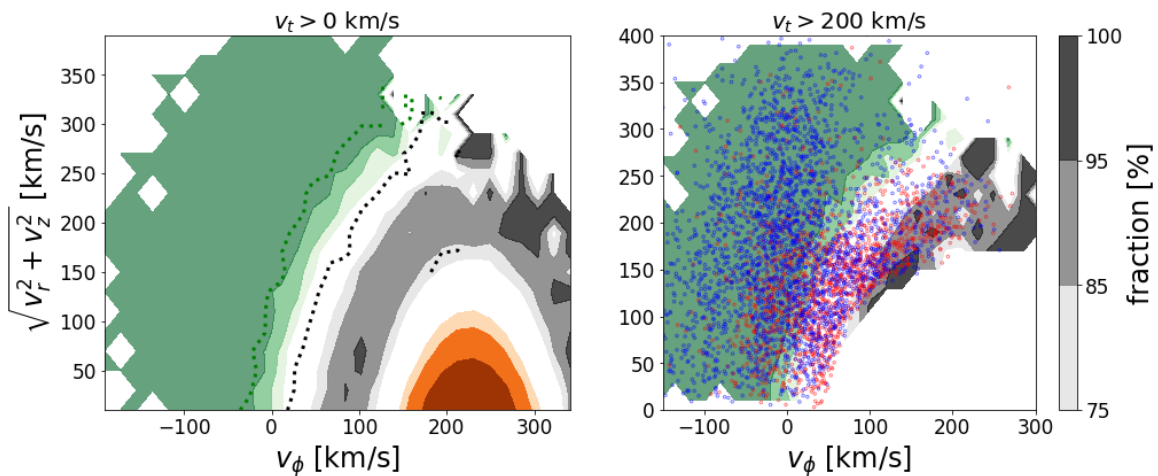
Fig. 2.4 The Toomre diagram for our updated model. The thin disc, thick disc and stellar halo are represented by the orange, grey and green colours, respectively. The darkness in shading corresponds to the fraction of a given population at that location of the diagram (75%, 85% or 95%). **Left panel:** no kinematic cut, i.e., $v_t > 0$ km s^{-1}. The dashed lines are the 85% dominance regions for the thick disc (black) and stellar halo (green) in the canonical Galaxia model. **Right panel:** $v_t > 200$ km s^{-1}. The *Gaia* DR2 high v_t sample is overplotted using blue and red symbols, where the colour denotes their position in the HRD.

2.4   Chemistry and HR diagram

In the previous section we have shown that a kinematic decomposition of the *Gaia* high v_t stars indicates that ~ 13 % have thick disc kinematics, while the remaining ~ 87 % have halo kinematics. This suggests that a dual population scenario is still plausible and so, to investigate this further, we will now explore the chemistry of these stars.

2.4.1   LAMOST-*Gaia* high v_t

The LAMOST spectroscopic survey telescope has been collecting low-resolution (R ~ 2000) data for millions stars since operations began in 2011 (Luo et al., 2015). This survey is ideal for our study, allowing us to analyse the chemistry of these high v_t stars. We take stellar parameters from the pipeline of Boeche et al. (2018), which has been updated to incorporate data from the fifth public data release[9]. After removing repeats, stars with signal-to-noise less than 40, and other artefacts, we cross-match with *Gaia* DR2 and obtain a final sample of 2982 stars with $v_t > 200$ km s^{-1}. For these stars we have full 6D phase-space, together with [Fe/H] and [α/Fe]. The median uncertainties on the chemistry are δ[Fe/H] ≈ 0.06 and

---

[9]dr5.lamost.org

$\delta[\alpha/\text{Fe}] \approx 0.13$. Although the uncertainties on $[\alpha/\text{Fe}]$ are too large to provide insights for individual stars, Boeche et al. (2018) show that the systematics are small and hence $[\alpha/\text{Fe}]$ can be used on a statistical basis.

In Fig. 2.5 we show the distribution of stars in the $[\alpha/\text{Fe}]$-$[\text{Fe/H}]$ plane, colour-coded by various properties. The density in this plane (Fig. 2.5a) shows that there is a wide spread in metallicities and a hint of bimodality, with peaks at $[\text{Fe/H}] \approx -1.2$ and ≈ -0.6 . Neither the spread, nor the bimodality, would be expected for a pure stellar halo population. For example, although dealing with slightly larger volumes (within a few kpc), the studies of Smith et al. (2009) and Ivezić et al. (2008) found that the halo $[\text{Fe/H}]$ distribution is well-fit by a single Gaussian with $\mu \approx -1.5$ and $\sigma \approx 0.3$ and, in both cases, does not extend to solar metallicity. Furthermore, the more metal-rich stars have a relatively narrow peak in their $[\alpha/\text{Fe}]$ distribution, unlike the more metal-poor stars. This peak is what we would expect for a thick disc population (Hayden et al., 2017).

Although a Gaussian distribution is unlikely to accurately represent the metallicity distribution for a complex system such as the halo or thick disc, for simplicity's sake we proceed to fit the distribution with two Gaussians. The blue and red lines in the top panel show the results of this fit, with parameters $(\mu_1 = -0.98; \sigma_1 = 0.41; w_1 = 0.71)$ and $(\mu_2 = -0.54; \sigma_2 = 0.17; w_2 = 0.29)$, where w_i is the normalisation factor for each Gaussian.

The more metal poor Gaussian is indicative of a halo population. It's broader than what is expected, extending to metallicities much higher than typical halo stars (e.g. Ivezić et al. 2012; Smith et al. 2009). The peak is also shifted slightly to higher metallicities. To check this further we have also analysed metallicities from the default LAMOST pipeline (LASP, Luo et al., 2015) and found that in this case the metal-poor stars peak around -1.22, which is in better agreement with literature results for the nearby stellar halo. We note that the overall shape of the distribution, and the resulting double-Gaussian fit, is essentially unchanged, apart from this small shift and a slightly more prominent bimodality.

The second Gaussian is consistent with the expected $[\text{Fe/H}]$ distribution for the canonical thick disc at low galactic latitudes (Cheng et al., 2012). Interestingly enough, it contributes about 30% of the total distribution, which is significantly larger than the fraction predicted from the kinematic analysis ($\sim 13\%$). One should not over-interpret this simple decomposition; issues such as the overly broad halo distribution or the reduced thick-disc fraction are likely due to the fact that a double-Gaussian model does not accurately represent the underlying distributions. Whether the stellar halo is more metal rich for lower altitudes is still unclear and investigating this is beyond the scope of this work. A more realistic decomposition would consist of a narrower halo distribution, with a peak around -1.2 and

spread extending to around -0.8. The remaining stars would then be attributed to population with thick-disc chemistry. We return to this issue in more detail in Section 2.6.

Panels b and c in Fig. 2.5 show the $[\alpha/\text{Fe}]$-$[\text{Fe/H}]$ plane colour-coded by the medians of v_t and v_ϕ, respectively. The differences between the metal rich and metal poor stars is clear, with a division around $[\text{Fe/H}] \approx -0.7$: the former have significant rotation (with $v_\phi \gtrsim 35$ km s^{-1}), and much smaller v_t (with $v_t \approx 200$ km s^{-1}); the latter have little rotation and larger values of v_t, typically $v_t > 260$ km s^{-1}. Thus, if one is interested in obtaining a clean sample of metal-poor stars with halo kinematics, a higher v_t cut is recommended (as advocated by, for example, Gould et al., 1998).

The value of net rotation for the metal rich stars is significantly slower than what we expect for the thick disc. This is because the cut of $v_t > 200$ km s^{-1} removes most of the co-rotating stars, leaving a kinematically biased subset of thick disc stars. The cut also biases the halo population, removing any net rotation and shifting the mean towards lower values. Therefore the stars in our sample with weakly pro-grade motion are most-likely unrelated to the halo and are simply the low angular momentum tail of the thick disc population.

Despite the strong gradients with $[\text{Fe/H}]$ in panels b and c, the trends with $[\alpha/\text{Fe}]$ are less clear. A weak trend can be found if one looks at fixed $[\text{Fe/H}]$. For example, for $[\text{Fe/H}] = -0.8$ it can be seen that median v_ϕ increases as $[\alpha/\text{Fe}]$ increases, as one would expect if the high $[\alpha/\text{Fe}]$ stars are dominated by thick-disc population. Similarly, at this $[\text{Fe/H}]$ v_t decreases as $[\alpha/\text{Fe}]$ increases, again reflecting the expected trend. These trends support the hypothesis that the accreted halo stars, as in (Hawkins et al., 2015), are expected to be α-poor compared to stars born in the Milky Way.

2.4.2   The Blue and Red Sequences

As mentioned in Section 2.1, the intriguing feature of the high v_t *Gaia* sample is the two distinct tracks in the HRD, which suggests the presence of two distinct populations. In order to better understand this, we now analyse the properties of the stars subdivided into two groups corresponding to the blue and red sequences (hereafter, BS and RS, respectively).

Fig. 2.6 left panel shows the HRD after correcting for extinction using the *MW.Combined15*[10] map from Bovy et al. (2016). The position of a star in the HRD can be determined by its chemistry, e.g., $[\text{Fe/H}]$ and $[\alpha/\text{Fe}]$ abundances, mass and age. However, for this particular HRD, where most of the objects are old main sequence stars, the age information is completely degenerate with the metallicity of the star. We illustrate this using isochrones from

---

[10]https://github.com/jobovy/mwdust
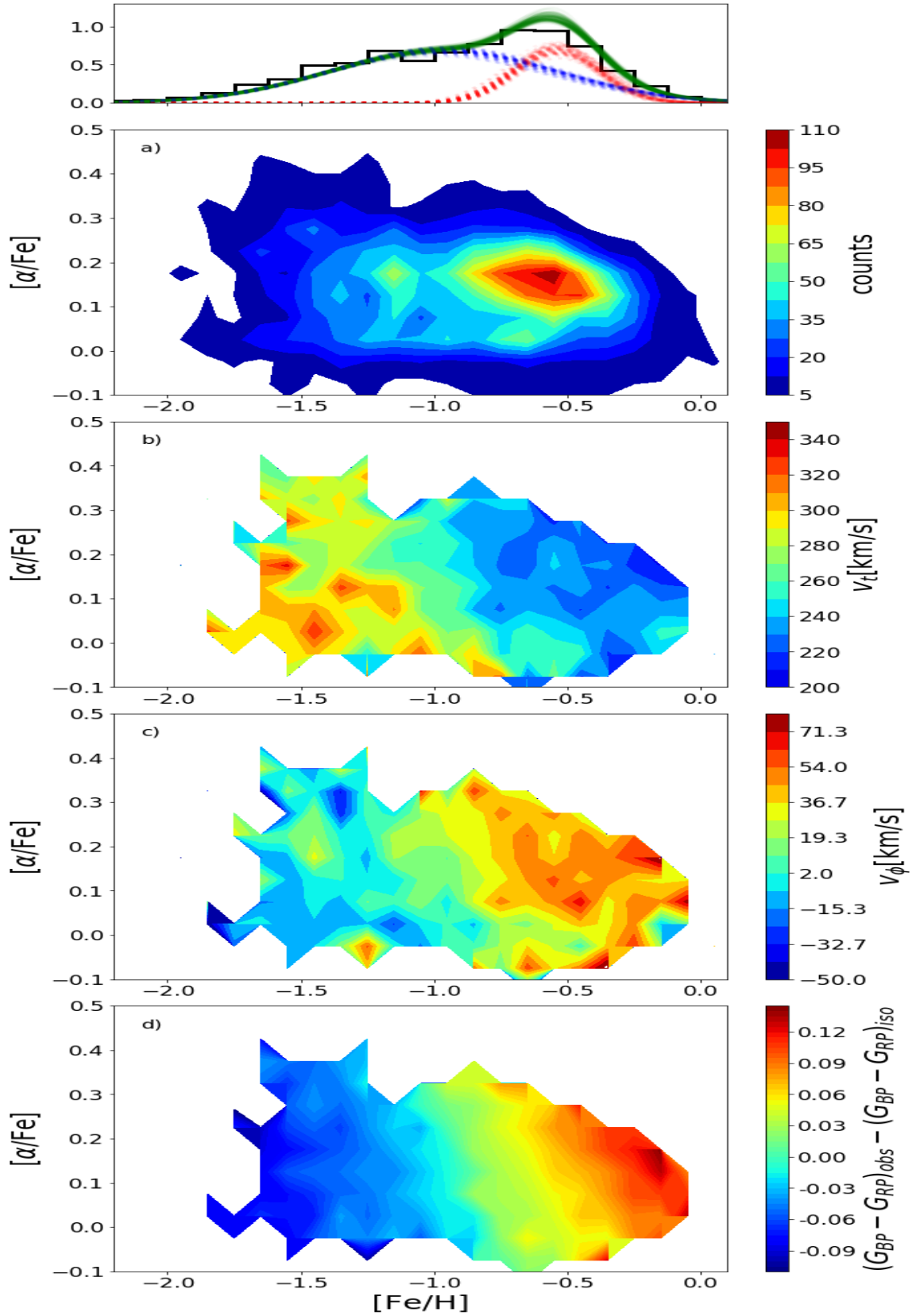
Fig. 2.5 [Fe/H]-[α/Fe] plane for the *Gaia* stars with $v_t > 200$ km s^{-1}. The contour curves in each panel are colour-coded by a specific quantity: *a)* number counts, *b)* median v_t, *c)* median v_ϕ and *d)* median distance from the bisecting isochrone. We only show regions with at least 5 stars in each pixel, with each pixel being 0.1x0.05 dex. The top histogram shows the marginalised distributions of [Fe/H] and its double-Gaussian fit.

Dartmouth Stellar Evolution Database[11] (Dotter et al., 2008) in the right panel of Fig. 2.6: for a fixed [Fe/H]= -0.5 (*-1.5*), represented by the red (*blue*) lines, the isochrones completely overlap for ages of 10 and 12 Gyr in the main sequence region. Moreover, variations in $[\alpha/\text{Fe}]$ have little effect on the main sequence tracks, as can be seen from the light blue/red lines, which are isochrones with $[\alpha/\text{Fe}]$=0.2. In contrast to the main sequence, the turn-off region of the HRD is where the differences between ages and $[\alpha/\text{Fe}]$, for a given metallicity, become more evident. Nonetheless, it requires high quality spectroscopic data to be able to discern precisely these differences. We conclude that between [Fe/H], $[\alpha/\text{Fe}]$, mass and age, the former is the most significant parameter in creating a discernible bifurcation in the isochrone tracks.

From Gallart et al. (2019) and Sahlholdt et al. (2019), we know that the two sequences can be represented by isochrones with metallicities $\sim$-1.5 and and $\sim$-0.7 for BS and RS, respectively. Although we do not pursue a systematic fit of the HRD as in Gallart et al. (2019), we stress [Fe/H] is the driving factor in producing the two clearly-separated sequences, as discussed in the previous paragraph. One might wonder whether unresolved binaries could play a role in this double sequence, as equal mass binaries would cause a shift in magnitude by a factor $2.5\log 2$, i.e. similar to the observed separation of the two sequences. However, the standard deviation of the epoch radial velocities[12] for both sequences are very similar, implying that unresolved binaries are unlikely to play an important role in creating the double sequence (see Appendix B). Finally, in Fig. 2.6 we show that the two sequences are bifurcated about an isochrone of [Fe/H]=-0.7, $[\alpha/\text{Fe}]$=0.2 and age=11.4 Gyrs.

Fig. 2.5*d* shows the $[\alpha/\text{Fe}]$-[Fe/H] plane colour-coded by the colour-offset from the bisecting isochrone, i.e. $(\text{BP}-\text{RP})_{\text{obs}} - (\text{BP}-\text{RP})_{\text{iso}}$. As expected, there is a direct correlation between colour and [Fe/H]. This means that a bimodality in [Fe/H], as we have seen in panel *a*, will naturally result in a bimodality in colour. For the rest of this section we define RS/BS stars as those with colours redder/bluer than the bisecting isochrone. We obtain 31752 and 45355 stars in the RS and BS, respectively.

The left panel of Fig. 2.7 shows the v_ϕ histogram for both sequences. The BS is consistent with a population with zero rotation, whereas RS has a mild sign of rotation. The rotation signature in the RS is likely reflecting the fact that most of the thick disc contamination belongs to the RS. This contamination introduces some net rotation to this group of stars. As pointed out in the Section 2.4.1, the fact that this sample is based on kinematic cut (i.e. $v_t > 200$ km s^{-1}) means that the inferred kinematic properties are going to be biased. For

---

[11]http://stellar.dartmouth.edu/models/index.html
[12]http://gea.esac.esa.int/archive/documentation/GDR2/Gaia_archive/chap_datamodel/sec_dm_main_tables/ssec_dm_gaia_source.html
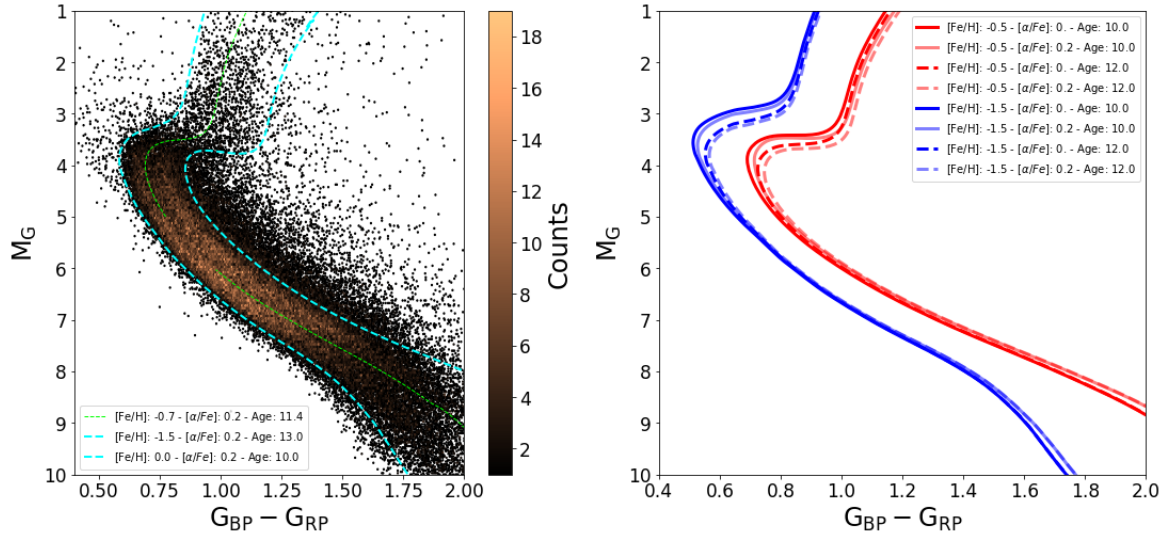
Fig. 2.6 **Left panel:** Dereddened *Gaia* HRD diagram for the high v_t stars within 1 kpc. The green dashed line is the bisecting isochrone used to delineate the blue and red sequences. The cyan line shows two "boundary" isochrones, illustrating the typical age and metallicity spread of the sample. **Right panel:** Isochrones from *Dartmouth Stellar Evolution Database* (Dotter et al., 2008). Blue and red lines have a fixed [Fe/H] of -1.5 and -0.5, respectively. The solid and dashed lines have fixed ages of 10 and 12 Gyrs, respectively. Finally, dark and light lines have fixed $[\alpha/\text{Fe}]$ of 0 and 0.2, respectively.

example, even though the BS stars have zero net rotation, we cannot infer that the stellar halo has zero net rotation because the prograde stars in this population are preferentially removed by the v_t cut.

In order to quantify the contribution of stars with thick disc kinematics in the RS, we have applied our kinematic modelling to it, as described in Section 2.3.4. We note that, as we normalise with the total number of stars in *Gaia* and in the mock catalogue, we do not need to know the number of RS/BS stars in the mock catalogue. Our fitting has only two free parameters, namely the re-weighting factors c_h and c_{TD}. We find that the best fit to the v_t distribution predicts that $\approx 36\%$ of the RS sample has thick disc kinematics. The BS is consistent with having no stars with thick disc kinematics, and so the total fraction is $\approx 16\%$, in agreement with Section 2.3.5. This fraction is enough to produce the rotation signal observed in the RS.

The middle panel of Fig. 2.7 shows the metallicity distribution for both sequences. Given the direct correlation between metallicity and colour (Fig. 2.5*d*), it is not surprising to find that the RS has more metal rich stars compared to the BS, although there is some overlap which is likely due to age effects or scatter from observational errors. The mean

metallicity of the RS ($\langle [\text{Fe/H}] \rangle = -0.63$) is higher than what we expect for the "canonical" halo, e.g. -1.55 (Smith et al., 2009) or -1.45 (Ivezić et al., 2012), supporting the conjecture that there is thick-disc contamination in this sequence. As expected, the blue sequence ($\langle [\text{Fe/H}] \rangle = -1.24$) is more consistent with a pure halo population.

One could argue that the overlap in metallicities is caused by a poor choice of bisecting isochrone. However, we have tested it using a range of different isochrones and found that the results are similar. This spread can also be understood by looking at the bottom panel of Fig. 2.5, where the distance from the bisecting isochrone is slightly slanted, i.e. for the same median value $(\text{BP}-\text{RP})_{\text{obs}} - (\text{BP}-\text{RP})_{\text{iso}}$ there is an [Fe/H] gradient of about 0.2 dex. Therefore, even if we adopt a more metal rich/poor cut by shifting the bisecting isochrone slightly to the right/left, the RS would still have a tail towards the metal poor end.

Finally the $[\alpha/\text{Fe}]$ histograms, shown in the right panel of Fig. 2.7, also provide clues to the differences between the two sequences. The RS distribution has a prominent peak, in contrast to the much broader BS distribution. Although the halo should span a large range of $[\alpha/\text{Fe}]$ (e.g. de Boer et al., 2014), the thick disc should have a much narrower distribution (e.g. Ishigaki et al., 2012). This can also be seen in figure 6 of Di Matteo et al. (2019). In this work they show that the canonical thick disc is located in the interval [Mg/Fe] = [0.25,0.35], whereas the stars consistent with the stellar halo have a broader interval in [Mg/Fe] = [0.1,0.35]. Therefore the $[\alpha/\text{Fe}]$ distributions for each sequence again suggest that the RS is a mix of stars with thick-disc and halo chemistry.

2.5 Dynamics

We now investigate the orbits of stars in the high v_t sample. We calculate orbits using the *Galpy* package[13] (Bovy, 2015) with the axisymmetric potential *MWPotential2014*. Even though observational uncertainties and limitations in the adopted potential can affect our ability to recover true dynamical properties (e.g. Coronado et al., 2018), deeper insights can still be obtained. An important orbital parameter to study is the eccentricity of a star. Each population of the Milky Way tends to have a different distribution in eccentricity, i.e., going from close to circular for the thin disc, to moderately eccentric for the thick disc and eccentric for halo stars.

Since the eccentricity distribution of the high v_t sample will be biased due to the fact that it is based on a kinematic selection, we need to compare to model predictions. Fig. 2.8 shows our observed eccentricity distribution (black), which is clearly not reproduced by the

---

[13]http://github.com/jobovy/galpy
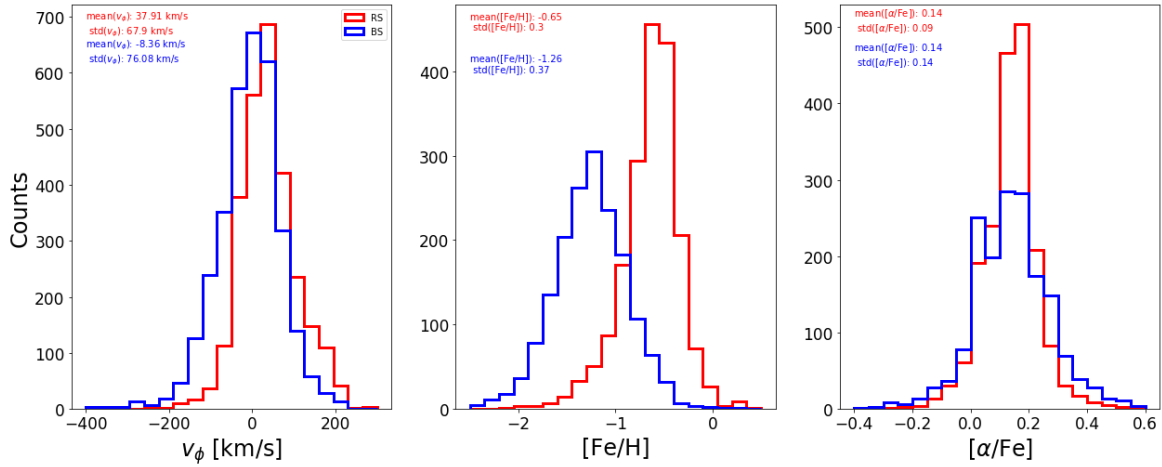
Fig. 2.7 **Left panel:** v_ϕ distribution for the blue and red sequences in the HR diagram. The BS is consistent with a non-rotating population whereas the RS shows a significant sign of rotation. **Middle panel:** [Fe/H] histograms for both sequences. As expected, the RS is mainly composed of metal-rich stars, in contrast to the more metal-poor BS. **Right panel:** [α/Fe] histograms. The strong peak observed in the RS indicates the presence of stars with thick-disc chemistry.

canonical Galaxia model (red). On the other hand, our updated model (solid green) provides a very good agreement. The two main reasons for this improvement are: *i.* the updated fractions of thick disc and halo stars in the sample and *ii.* the new stellar halo model, which is more anisotropic compared to the canonical Galaxia stellar halo as advocated by Belokurov et al. (2018). In the right panel of Fig. 2.8 we show the normalised histograms for the RS and BS eccentricity distribution. The RS has slightly fewer high eccentricity orbits compared to the BS. This is due to the thick disc contamination, which (as can be seen in the left panel) peaks at an eccentricity of around 0.7.

It has also been suggested that the orbital apocentre and maximum altitude can be used to infer the origin of these populations. In particular, Haywood et al. (2018) noticed that the distribution in this space is not smooth and hence attributed it to the effects of an accretion event that heated the early disc. Indeed there is evidence that a major accretion event happened in the early Galaxy (e.g. Belokurov et al., 2018; Brook et al., 2003; Chiba and Beers, 2000; Helmi et al., 2018), which is likely to have some effect on the pre-existing disc (e.g. Grand et al., 2016; Jean-Baptiste et al., 2017). However, these structures in the apocentre and maximum altitude plane are likely just a consequence of the different orbital families that exist in the sample.

For instance, we show the $R_{apo} - z_{max}$ plane for the *Gaia* DR2 high v_t sample in the top-right panel of Fig. 2.9. The stars are split into the blue and red sequences. The "lumpiness"
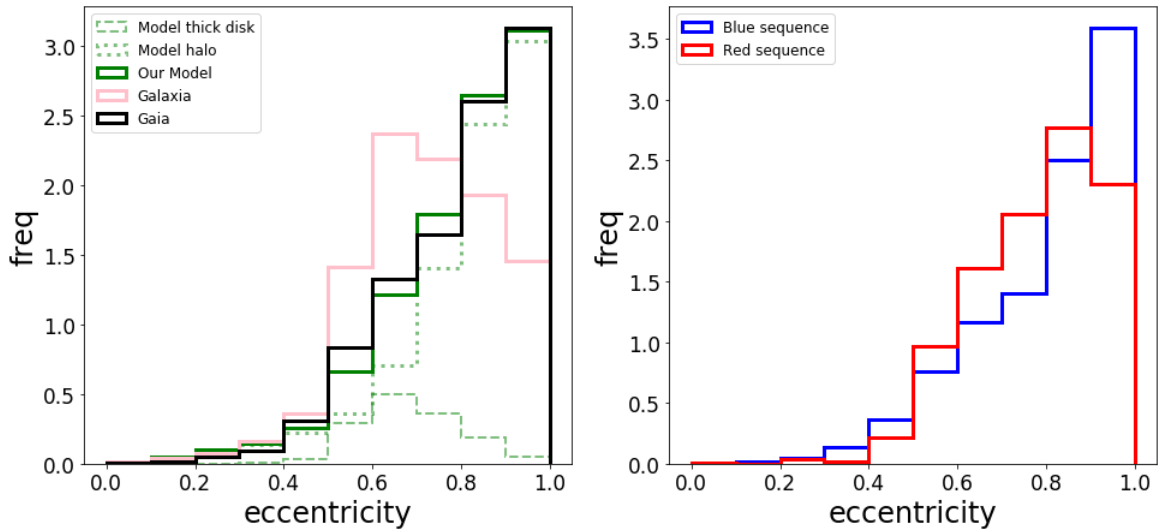
Fig. 2.8 **Left panel:** The eccentricity distribution of the *Gaia* sample (black), Galaxia model (red) and our updated model (green). In contrast to the Galaxia canonical model, our new model provides a good match to the observed distribution. We also show the individual distributions for the mock thick disc (dashed) and halo (dotted). **Right panel:** Eccentricity distribution for the blue and red sequences. The RS appears to have more stars with moderate eccentricities, reflecting the presence of thick disc stars.

is clear, i.e. the stars seem to prefer discrete "tracks" in this plane. Although the RS stars are concentrated towards lower z_{max} and shorter apocenter, we note that neither sequence seems to follow a preferred track. This is confirmed in the top right histogram of Fig. 2.9, where we can see that both sequences have extended distributions towards higher z_{max} and have peaks at the same values of z_{max}.

It is known that halo stars can be clustered in a characteristic energy-Jacobi diagram due to resonant trapping, e.g. as in Moreno et al. (2015). Inspired by this fact, we now perform a couple of simple tests to determine if the observed tracks can be explained by resonant effects with an axisymmetric Galactic potential.

Using our updated model with new values for f_{TD}, f_h and new stellar kinematics (see Section 2.3 for details), we draw a sample of mock stars within 1 kpc and with $v_t > 200\,\mathrm{km\,s^{-1}}$. We calculate their orbits and plot the resulting distribution in the $R_{apo} - z_{max}$ plane in the top left panel of Fig.2.9. This mock distribution shows the same tracks as the observed data. The fact that we observe these tracks in our mock data, despite the smooth underlying kinematics with no accretion, tells us that this is simply a natural consequence of resonant effects.

We illustrate this further in the bottom-left panel of Fig. 2.9. Here we show how z_{max} varies as a function of v_z for a star initially at the Sun's position. To simplify the situation,

we fix the values for the radial and azimuthal velocities. As expected, z_{max} increases with v_z, but this is not a 1:1 trend; there are both discontinuities and regions where the trend is reversed. For example, as v_z approaches ~ 80 km s^{-1} we can see z_{max} "jump" from ~ 2 kpc to ~ 3.5 kpc. This corresponds to the significant gap seen at ~ 2.5 kpc in the upper panels, both for the observed and mock data. The nature of this gap is illustrated in the bottom-right panel, where we have shown an example orbit from either side of this discontinuity. Both orbits have the same values for v_R and v_ϕ, but have $v_z = 72$ and 74 km s^{-1}. Even though the change in v_z is less than 3%, there is a dramatic change in z_{max} as the orbital family changes. Therefore it is clear that the tracks observed in the $R_{apo} - z_{max}$ plane are due to transitions from one orbital family to another. The locations of these gaps are determined by the adopted potential and cannot be used to learn about the physical origins of the stars.

2.6   Conclusion and discussion

In this Chapter we investigated the intriguing double-sequence in the HRD for high transverse velocity stars, as first shown in Gaia Collaboration et al. (2018a). We have taken a different approach from previous studies in accounting for the expected thick-disc contamination, leading to a slightly different interpretation of the two sequences. In this section we bring together our results and discuss their implications.

2.6.1   On kinematics

Our first step was to model the tail of the v_t distribution, i.e., $v_t > 200$ km s^{-1}. We have updated the description of the kinematics in the Galaxia stellar halo, using recent results from Belokurov et al. (2018). More importantly, we have also updated the thick disc kinematic model, adopting a physically meaningful azimuthal velocity distribution as described in Schönrich and Binney (2012). Our fitting procedure enables us to estimate the overall (i.e. for $v_t > 0$) stellar halo and thick disc fractions within 1 kpc from the Sun, f_h and f_{TD} respectively. We obtain a much better match to the tail (Fig. 2.1) and find that $f_h = 0.47\%$ and $f_{TD} = 6.52\%$. The strength of this new approach is that it is based solely on kinematics, avoiding any pre-selection based on chemistry which could bias the result.

The best-fit model predicts that around 13% of the high v_t sample have thick-disc kinematics. Therefore, if one is interested in selecting a pure halo sample based solely on a v_t cut, we recommend a higher cut than 200 km s^{-1}. For example, a cut of $v_t > 220$ km s^{-1} produces a sample where $\approx 94\%$ stars have stellar halo kinematics, while a cut of 250 km s^{-1}
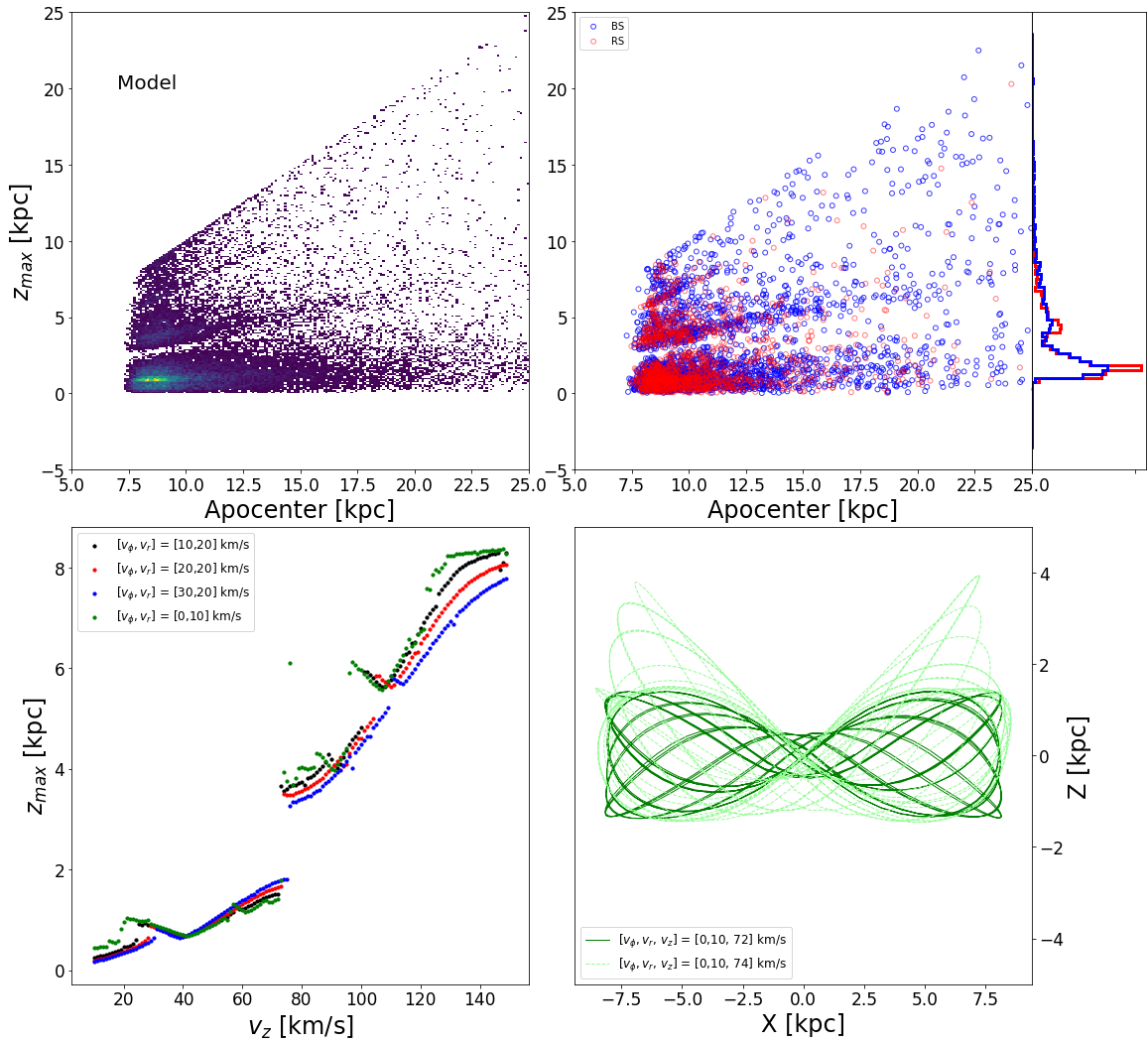
Fig. 2.9 **Top row:** $R_{apo} - z_{max}$ plane for the mock stars from our updated model (left) and *Gaia* sample (right). The *Gaia* stars are colour-coded for the red and blue HRD sequences. The histogram to the right demonstrates that the BS and RS stars span a similar range of z_{max}. **Bottom row:** the left panel shows z_{max} as a function of v_z for *MWPotential2014*, where v_R and v_ϕ have been fixed to the values listed in the legend. The gaps are related to changes in orbital families. This is illustrated in the right panel, where we show two example orbits from either side of the gap at $v_z = 73$ km s^{-1}. Even though the change in v_z for these two orbits is less than 3%, there is a dramatic change in z_{max} as the orbital family changes.

has $\approx 98\%$. This is illustrated in Fig. 2.5, where we have shown that thick disc stars tend to have lower v_t values. Adopting a low cut could produce biased samples and lead to erroneous conclusions regarding the nature of the stellar halo.

2.6.2   On chemistry

By cross-matching the high v_t sample with LAMOST DR5 we have been able to investigate the chemistry of these stars (Section 2.4.1). The [Fe/H] distribution appears bimodal, seemingly composed of a broad metal-poor component with halo-like chemistry and a narrower metal-rich component with thick-disc-like chemistry. Even though a Gaussian distribution may not provide a good representation of the [Fe/H] distribution for a given population, we fit our sample with a two-component Gaussian model and find that around 30% of the stars belong to the latter (thick-disc-like) population.

As expected, the more metal-rich stars populate the RS and, as a consequence, the mean metallicity of the RS is higher than the "canonical" stellar halo. There is some overlap in the [Fe/H] distributions of the two sequences, with the RS/BS having a tail towards the metal-poor/rich side, which is likely due to age effects or scatter from observational errors.

Our analysis has shown that there is a difference between the BS and RS $[\alpha/\text{Fe}]$ distributions, with the latter being consistent with a mix of thick disc and halo populations. This is in line with the findings of Hayes et al. (2018), who detected two distinct populations in a sample of metal-poor APOGEE stars, one with low [Mg/Fe] and one with high [Mg/Fe]. They concluded that the low Mg stars are likely to be an accreted stellar halo population, due to the similarity of their chemistry with nearby dSph stars. On the other hand, the high Mg stars are chemically consistent with the metal poor end of the canonical thick disc, even though some of them have halo-like kinematics (see also Fernández-Trincado et al. 2019). This agrees with Ishigaki et al. (2012), who analysed a metal-poor sample of stars and found a difference in the abundance of α elements between the stellar halo and thick disc (also seen, e.g., in Nissen and Schuster 2010, Hawkins et al. 2015). Finally, Bland-Hawthorn et al. (2019) has also shown that the orbital angular momentum of α-rich stars decreases with [Fe/H] (see their figure 4) indicating a transition between thick-disc and stellar halo.

2.6.3   The metal rich counter-rotating stars

There is clearly a discrepancy in the above estimates for the amount of thick disc contamination in the high v_t sample. The [Fe/H] distribution predicts around 30% of the sample are consistent with the thick disc, while the kinematic decomposition suggests only 13%. In order to further understand this, we can perform the following simple test: if we assume, to first order, that the stellar halo has no net rotation and that the thick disc stars all have prograde motion, we can use the counter-rotating stars as a template for the metallicity distribution of the halo. Given those assumptions, we can obtain the metallicity distribution of the thick

disc by subtracting twice the counter-rotating population from the overall distribution. We present this in Fig. 2.10. There are two interesting points to note: firstly, for the [Fe/H] distribution of the counter-rotating stars there appears to be a secondary peak coinciding with what we previously assumed to be the thick disc population (i.e. [Fe/H] = -0.6); secondly, the subtracted histogram, which we expect to mimic the thick disc contribution, corresponds to $\approx 25\%$ of the data, which is still in disagreement with our kinematic modelling. However, some studies have suggested that the stellar halo has prograde rotation and so we can account for this by multiplying the counter-rotating stars by a larger factor. For example, if we re-scale by 2.2, which would be the factor required to account for a prograde rotation of ≈ 30 $\mathrm{km\,s^{-1}}$ (as seen in Belokurov et al. 2018), then the contribution of the thick disc is $\approx 18\%$. Even though this fraction is now in line with the kinematic modelling, it leaves us with the following curious question - of the stars that are kinematically classified as halo members, why do a non-negligible fraction have thick-disc-like chemistry?

This metal-rich peak in the retrograde distribution suggests that a number of thick-disc stars are, in fact, counter rotating. This is not intuitive, as one would expect that stars formed in a proto-galactic disc should have the same rotation direction. Di Matteo et al. (2019) have already interpreted the presence of metal rich ([Fe/H]≈ -0.5) counter rotating stars as evidence for the heating of the early Milky Way disc by a merging satellite galaxy, such as the one proposed by Belokurov et al. (2018); Helmi et al. (2018). However, it is also possible that some thick disc stars could be scattered onto counter rotating orbits during its formation. For example, Clarke et al. (2019) shows that giant molecular clouds could have significantly heated the early disc, which may produce some counter-rotating stars (see Amarante et al. 2020a for further details). Another possibility is that some of these stars could be members of a different accretion event. For example the Sequoia system (Barbá et al., 2019) has been shown to posses a number of retrograde metal rich globular clusters (such as NGC 3688; Myeong et al. 2019) and hence these stars could be related to this event. We will return to this heated thick-population case in Chapter 3.

Finally, we can test the strength of this result and see how the distance estimate influences the number of retrograde and metal-rich ([Fe/H]>-0.7) stars in our sample. We adopt the parallax bias given by Schönrich et al. (2019) and recalculate our distances and velocities. Although the introduced bias slightly shrinks the distances, we still find that the fraction of the retrograde metal-rich stars is roughly the same: 22.5% (without parallax bias) and 21% (including parallax bias).
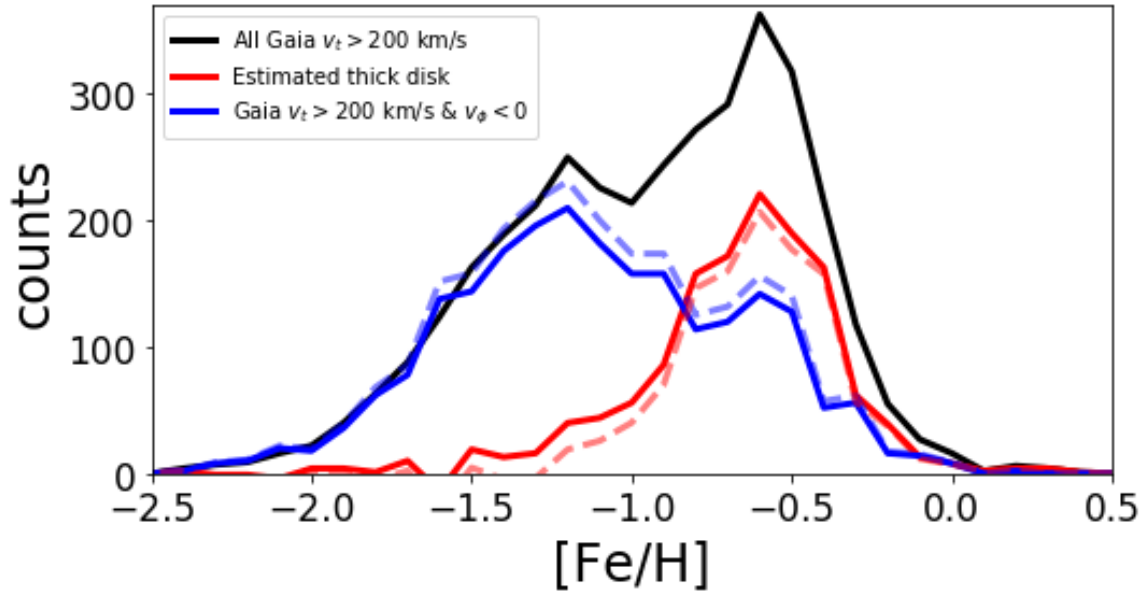
Fig. 2.10 An investigation into the metallicity distribution of the high v_t sample. The black line denotes the [Fe/H] distribution of the entire sample. The blue solid line is the metallicity distribution of all counter rotating stars ($v_\phi < 0$) in the *Gaia* high v_t sample, multiplied by 2. This provides an estimate of the halo distribution under the assumption that (a) the halo has no net rotation and (b) all thick-disc stars have prograde motion. The red solid curve is obtained by subtracting this halo-like (blue) distribution from the overall (black) distribution and should, in principle, mimic the thick disc metallicity distribution. The clear dual peak in the blue distribution indicates that there is a significant number of counter-rotating thick disc stars. The dashed lines uses a multiplication factor of 2.2, which corresponds to the normalisation required to account for a rotation of ~ 30 km s^{-1}.

2.6.4   Nature of the Blue and Red Sequences

We now bring together our findings in an attempt to clarify the nature of the BS and RS.

- The BS is dominated by a halo-like component. Its properties match expectations for the *Gaia*-Sausage/Enceladus (Belokurov et al., 2018; Helmi et al., 2018), being radially anisotropic with little net rotation and having metallicities around $-2 <$[Fe/H]< -1. However, there is a tail of metal rich stars (e.g. 23% have [Fe/H] > -1), indicating that a small amount of chemical thick disc may be present. Our kinematic modelling suggests that all BS stars have halo-like kinematics, which implies these metal rich stars could be part of the aforementioned heated thick disc or the metal-rich tail of accreted material.

- The interpretation of the RS is slightly more complicated. Its chemistry suggests a division of $\sim 20\%$ halo and $\sim 80\%$ thick disc. On the other hand, the v_t fit for this sequence suggests that around 64% have "halo-like" kinematics. These seemingly conflicting results can be resolved if we split this chemical thick disc material approximately evenly between a "canonical" and a "heated/accreted " thick disc, as discussed in the previous subsection. This is reinforced in Fig. 2.10 where we can see that the "canonical" and "heated/accreted" thick discs contribute approximately equally (assuming that the heated/accreted component has small net rotation). The $\sim 20\%$ stars with halo-like chemistry are radially anisotropic, matching expectations for the metal-rich part of the *Gaia*-Sausage/Enceladus (Belokurov et al., 2018; Helmi et al., 2018).

2.6.5   Comparison to previous studies on the same sample

Gallart et al. (2019) estimated the SFH for both sequences using a colour-magnitude diagram fitting technique, focusing on the turn-off region in a slightly larger volume than we have considered here ($\varpi > 0.5$ mas). They found that the RS and BS had similar SFHs (see fig. 2 of their paper) and concluded that the former is made up of stars from the progenitor of the Milky Way and the latter from an accreted satellite galaxy. The pre-existing Milky Way would be more massive, and thus more metal rich, compared to the merging satellite. They estimated a 4:1 mass ratio between the merging satellite and our Galaxy's progenitor. Moreover, the RS (referred by them as in-situ halo) and the Milky Way's thick disc have a common origin. This picture suggests that a pre-existing disc was in place early in our Galaxy, certainly prior to the satellite's accretion. Di Matteo et al. (2019) also supports this scenario by showing that that $\approx 40\%$ of stars with [Fe/H] < -1 have thick disc like kinematics, similar to what we have found here. The study of Sestito et al. (2019) provides further evidence, finding ultra metal-poor stars on thick-disc-like orbits. Since such metal-poor stars must be very old, if they were formed in the Milky Way then this supports the picture that the disc must have formed early (see e.g. Brook et al. 2012; Zolotov et al. 2009). Our findings are similar to those of Haywood et al. (2018). They pointed out that the RS is likely to be made up mostly of thick disc stars and that the BS is likely coming from an accreted population, due to its $[\alpha/\text{Fe}]$ abundances. We come to similar conclusions despite using a different technique, namely fitting of the kinematics, and have quantified the various fractions in each sequence. However, our studies are not in entire agreement, since we disagree with their interpretation of the patterns in the $R_{apo} - z_{max}$ plane. Rather than being a signature

of the accretion event in the early Galaxy, as we have pointed out in Section 2.5, these features naturally occur due to the various orbital families that exist in the Galactic potential. Therefore, even though there is much evidence for such a merger event (e.g. Chiba and Beers 2000, Belokurov et al. 2018 and Helmi et al. 2018), it is not required to explain the observed patterns in the $R_{apo} - z_{max}$ plane.

2.7   Summary and final remarks

Our main findings from our analysis of the high tangential velocity stars ($v_t > 200 \text{ km s}^{-1}$) in *Gaia* DR2 are listed below:

- We estimate the fraction of stellar halo and (kinematic) thick disc within 1 kpc of the Sun to be $f_h = 0.47\%$ and $f_{TD} = 6.52\%$, respectively;

- This high v_t sample has a contamination of 13% stars with thick disc kinematics;

- Using LAMOST chemistry, we estimate that $\approx 30\%$ of high-v_t stars have thick-disc like chemistry;

- There is a metal-rich population of counter-rotating stars, suggesting that a non-negligible number of thick-disc stars have retrograde orbits;

- All of the BS stars have stellar-halo like orbits. This suggests that the metal-rich tail of this sequence with [Fe/H] > -1 (i.e. $\sim$ a quarter of the stars) are likely to be part of the heated thick-disc or the metal-rich tail of accreted material;

- The RS, which contains mostly metal-rich stars, has a similar number of stars with halo and thick-disc kinematics, i.e. it is composed almost equally of both "canonical" and "heated" thick-disc components.

- Our interpretation of the two sequences is in alignment with Haywood et al. (2018) and Gallart et al. (2019), namely the BS is mostly composed of accreted stars, whereas the RS is mostly composed of heated thick-disc material;

- The wedges in the $R_{apo} - z_{max}$ plane, which have been postulated to be a consequence of accretion (Haywood et al., 2018), can be reproduced by a smooth (accretion-free) model such as Galaxia. These wedges are populated by different orbital families which exist in the adopted Galactic potential, i.e. one does not need to invoke accretion to explain their existence.

For a number of years the presence of multiple components in the stellar halo has been debated, but only now, thanks to more extensive observational data, is this picture taking form. It is now known that the density of the stellar halo follows a broken power-law distribution, with a break at $\approx$ 20 kpc (see e.g. Deason et al. 2018 and references therein). Within 20 kpc the stellar halo is dominated by a metal rich component related to the *Gaia*-Sausage/Enceladus event (Chiba and Beers 2000, Belokurov et al. 2018, Helmi et al. 2018), and the apocentres of these stars coincide with this break radius. This merger has also left its imprints in the nearby stars, as we have shown throughout our paper. However, simulations have shown that kinematics alone are not enough to discriminate between accreted stars and those which were born in the main Milky Way progenitor and heated onto halo-like orbits, i.e. the "in-situ" halo, (Zolotov et al. 2009, Rodriguez-Gomez et al. 2016, Qu et al. 2017).

We have shown that our updated fractions for the stellar halo and thick disc provide a good fit to the data, both in terms of the v_t distribution (Fig. 2.1) and the eccentricity distribution (Fig. 2.8). However, if we look in detail we see that the chemical thick disc in the *Gaia* high v_t sample include stars on retrograde orbits. Counter-rotating stars are not expected from standard kinematic models, such as the one we have adopted here (Schönrich and Binney, 2012), and so alternative mechanisms such as additional heating or accretion are required. The properties of these stars are very uncertain and this clearly needs further study, ideally using detailed abundances and ages. Simulations will also be extremely valuable to address the properties of the pre-existing disc and for understanding how this reacts to a significant merger event such as the *Gaia*-Sausage/Enceladus. We will discuss this issue in the next Chapter.

Chapter 3

The kinematically hot thick-disc

In the previous Chapter we quantified the amount of heated thick disc stars observed in the Solar Neighbourhood. Although it has been suggested that these stars were produced by the heating caused during the *Gaia*-Enceladus-Sausage merger event (Di Matteo et al. 2019, Belokurov et al. 2020, Grand et al. 2020), we show in this Chapter that there is an alternative scenario for the formation of this population. For this, we will explore the clumpy formation scenario briefly introduced in Chapter 1. In this scenario a young disc galaxy develops large dense regions of intense star formation and it is these clumps which dynamically heat the disc. We will see that low angular momentum, metal-rich stars are naturally formed in this scenario without the need to invoke a merger.

Cowie et al. (1995) and van den Bergh et al. (1996) were the first authors to observe clumps in high-redshift ($z > 1$) galaxies. The light distribution of clumpy galaxies is dominated by gas rich, giant star-forming clumps, in contrast to the smooth light distribution of disc galaxies in the local Universe. Guo et al. (2015) found that $\sim 55\%$ of intermediate- to high-mass galaxies contain clumps at higher redshifts and this fraction decreases to $\sim 15\%$ at $z \sim 0.5$. The mass and sizes of the clumps are still an open question, due to their dependence on the observational resolution. Nonetheless, recent studies show that, typically, the clumps have masses close to $\approx 10^7 M_\odot$ and linear sizes between $100 - 500$ pc (Cava et al., 2018; Dessauges-Zavadsky et al., 2017).

The origins of clumps in high redshift galaxies have been explored in two scenarios: 1) formation via gravitational instabilities in the proto-disc (e.g. Ceverino et al., 2010; Noguchi, 1999); 2) an ex-situ origin where the clumps were accreted from merging satellites of the observed galaxies (e.g. Mandelker et al., 2014). However, it is unlikely that the observed clumps are caused by multiple mergers that happened simultaneously in the observed galaxies. It is also argued that, in different merger events the individual metallicities of the merging

clumps will depend on the mass and evolution history, thus will likely be very different (Lee et al., 2015). On the other hand, in the fragmented disc scenario, the metallicities are expected to be the same (Immeli et al., 2004). We note, however, that mergers could potentially induce the formation of clumpy, high-density star formation regions as proposed by Perret et al. (2014).

Motivated by the aforementioned clumpy heating scenario, this Chapter will explore the chemical-kinematic trends that arise in a simulated isolated disc galaxy that develops clumps in its first Gyrs, investigating the implications for how we interpret the most recent observations of the Milky Way. Most of the following content was originally published in *Amarante et al. 2020, ApJL, 891, 30.*

3.1 Introduction

Selecting a pure sample of stars in either the stellar halo or in the thick disc in the Solar Neighbourhood is complicated by their significant overlap in both their velocity and metallicity distributions. A common approach for selecting local stellar halo stars uses a kinematic cut to select high transverse velocity stars, as shown in Chapter 2. By selecting stars with $v_t > 200 \ \mathrm{km \, s^{-1}}$, one expects a negligible contamination by thick disc stars. However, with the high quality data provided by *Gaia* (Gaia Collaboration et al., 2018b, 2016), recent studies have shown that such a kinematic cut still leaves a population of stars with thick disc chemistry (Amarante et al., 2020b; Gaia Collaboration et al., 2018a; Haywood et al., 2018). This imprint is also seen when different kinematic criteria are chosen (e.g. Helmi et al. 2018), challenging our understanding of the formation of the Milky Way's thick disc.

Furthermore, Di Matteo et al. (2019) and Amarante et al. (2020b) found that many counter-rotating stars in the Solar Neighbourhood are too metal-rich to be considered part of the accreted halo. In particular, Di Matteo et al. (2019) noted a low angular momentum population with thick disc chemistry (see, e.g., their figure 13) and proposed that the classical Milky Way (MW) inner-halo is actually composed of two stellar populations: *i)* heated stars from the thick disc (referred by them as the "Plume"), where the heating mechanism is associated with a major merger event named the *Gaia*-Sausage/Enceladus[1](Belokurov et al. 2018; Helmi et al. 2018); *ii)* accreted stars from the *Gaia*-Sausage.

Belokurov et al. (2020) (hereafter *B20*), using the Sanders and Das (2018) catalogue, disentangled the aforementioned low angular momentum structure from the canonical thick disc and stellar halo. They suggested that this structure, which they termed the Splash,

---

[1]For short, we will just refer to it as the *Gaia*-Sausage.

is chemically and dynamically distinct from the known stellar populations in our Galaxy. Nonetheless, its formation must be linked to the thick disc as there is a smooth transition between the two populations in the kinematic-metallicity space. Moreover, they found Splash-like structures in hydrodynamical simulations where the host galaxy underwent a major merger. Therefore they concluded the proto-galactic disc of the MW was likely heated during the *Gaia*-Sausage event about 10 Gyr ago, in agreement with other studies (e.g. Di Matteo et al., 2019; Gallart et al., 2019; Mackereth et al., 2019), and thereby formed the Splash. Finally, they argued that the thick disc formation occurred before, during and up to ∼ 2 Gyr after the merger.

On the other hand, Clarke et al. (2019) presented a hydrodynamical simulation of an isolated galaxy that formed a thick disc purely via internal evolution driven by clump formation. These clumps dynamically heat the disc creating two chemically distinct disc components, with an overall double-exponential vertical profile (Beraldo e Silva et al., 2020), similar to the MW's thin and thick discs. They also showed that the model's clumps are similar to those observed in high redshift galaxies. Figure 3.1 shows an example of the striking similarity between the simulation and the Milky Way observations. It shows the radial scale length (h_R) and vertical scale height (h_z) for mono-abundance stellar populations within the simulation's Solar Neighbourhood. The $\alpha-$poor[2] population is associated with larger h_r and lower h_z, in contrast to the $\alpha-$rich population. This reflects the presence of a geometrical and chemical thin and thick disc, similar to what is observed in the Milky Way – note that similarity with Figure 1.3, which shows the results for the Milky Way. Moreover, similar to the Milky Way, the thin disc population is associated with a mixture of mono-abundance populations with a larger spread in [Fe/H] (second panel) and age (third panel) in contrast to the thick disc. The last panel shows the Bayes Factor, which is a metric chosen to compare the fit of a single exponential versus double-exponential models (see Beraldo e Silva et al. 2020 for details). Negative (positive) values favours a single (double) exponential model and are preferred for mono-abundance populations older (younger) than ≈5 Gyrs.

Therefore a question that naturally arises is whether clumps are able to form stars with properties similar to the Splash, or whether the Splash stars uniquely need to form in a major merger event. In the following sections we demonstrate that clumps in the MW progenitor can produce stars with very similar kinematic and chemical properties as the observed Splash stars. This Chapter is organized as follows: Section 3.2 and 3.3 present the details of the

---

[2]In the simulation, [O/Fe] traces the evolution of the α-elements.
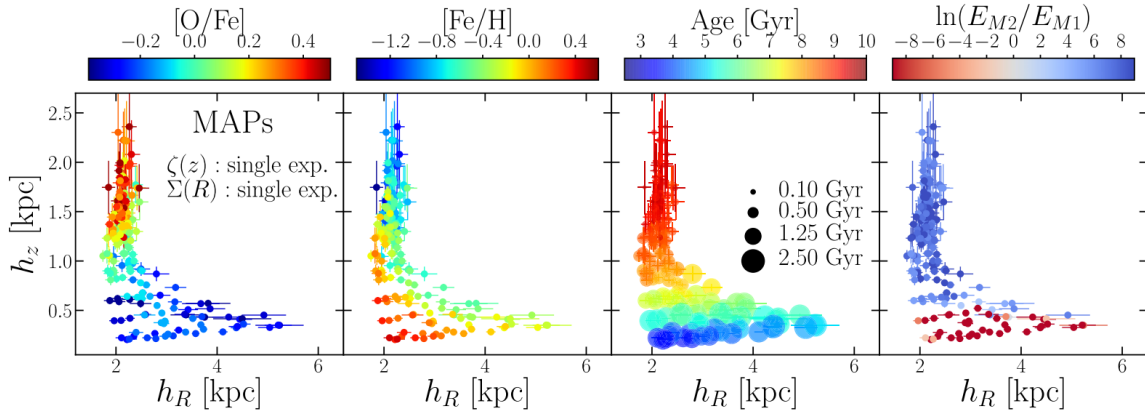
Fig. 3.1 The radial scale length (h_R) versus vertical scale height (h_z) for mono-abundance populations in a clumpy simulation. From left to right the panels are colour-coded by [O/Fe], [Fe/H], age and by the Bayes factor. Similar to the Milky Way, the α-rich stars have larger scale height and are radially concentrated, in contrast to the α-poor population. The former is associated with the thick disc and has the oldest and most metal-poor stars in the disc population. The last panel indicates that a single exponential fit is preferred over a double exponential profile for these mono-abundance stellar populations. [*Reproduced from Beraldo e Silva et al. (2020), figure 3.*]

simulated galaxy and shows its dynamical and chemical features, respectively. Section 3.4 discusses the implications of our results.

3.2   Simulation

The simulation used in this Chapter is described in detail in Clarke et al. (2019). The initial conditions are characterised by a spherical hot gas corona embedded in a dark matter halo with a Navarro-Frenk-White (Navarro et al., 1997) density profile with virial radius $r_{200} \approx 200$ kpc and mass of $10^{12} M_\odot$. The gas has an initial net rotation and cools via metal-line cooling (Shen et al., 2010). It settles into a disc, and stars form wherever the temperature drops below 15,000 K and the density exceeds 1 cm^{-3}. Feedback by supernova explosions follows the blastwave implementation of Stinson et al. (2006), with thermal energy being injected to the interstellar medium with an efficiency of 10%. The feedback of asymptotic giant branch stars is also taken into account. Gas phase diffusion uses the method of Shen et al. (2010).

These initial conditions are self-consistently evolved for 10 Gyrs with the smooth particle hydrodynamics+N-body tree-code GASOLINE (Wadsley et al., 2004). As shown by Clarke et al. (2019), the metal-line cooling results in the formation of clumps during early times of

the simulated galaxy. At the end of the simulation, the galaxy presents a chemical bi-modality and geometric properties very similar to those observed for the MW (as shown by Beraldo e Silva et al., 2020). In particular, a thick disc, composed of old, α-rich stars is formed[3]. This simulation evolves as an isolated galaxy, i.e. without any merger that could produce the metal-poor and high radial velocity dispersion population associated with the *Gaia*-Sausage observed for the MW (see Belokurov et al., 2018; Helmi et al., 2018) or any stellar halo component.

For comparison, we also ran another simulation from the same initial conditions and with the same procedure, except for the supernova feedback efficiency, which was set to 80%. This high feedback efficiency inhibits the formation of clumps and the simulation does not form a chemical or a geometric thick disc (Beraldo e Silva et al., 2020). We refer to this simulation as the non-clumpy simulation. This allows us to study the role of the clumps on the formation of the different populations in the simulation.

3.2.1 Simulated Solar Neighbourhood

In order to reduce contamination from thin disc stars, *B20* selected stars in the region $0.5 < |z|/\mathrm{kpc} < 3$. For reliable comparisons to their results, we apply a similar cut to the simulation data and define our mock Solar Neighbourhood as all star-particles in the region $5 < R/\mathrm{kpc} < 11$ and $|z| < 3$ kpc, where R is the cylindrical radius centered at the simulated galaxy center, and z is the height from the simulated galaxy plane. Unless explicitly mentioned, all our results are based on this geometrical slice. We have tested using the same $|z|$ range as *B20* and the difference is the reduced amount of thin disc star-particles. Nonetheless the trends between the simulated thick disc and Splash region discussed below are the same. Finally, throughout the Chapter the velocities are given in cylindrical coordinates centred on the simulated galaxy centre; v_R, v_ϕ and v_z are positive in the direction of the galaxy centre, galaxy rotation and angular momentum vector, respectively.

3.3 Results

We now compare the kinematics and chemistry of the model to the results of *B20*. As described in Section 3.2, our simulation self-consistently evolves as an isolated galaxy and thus has no accreted stellar halo. Therefore it has a lower fraction of metal-poor and of counter-rotating stars than the MW. For better comparison with the observational results,

---

[3]In the simulation, the $[\alpha/\mathrm{Fe}]$ abundance is tracked by $[\mathrm{O/Fe}]$.
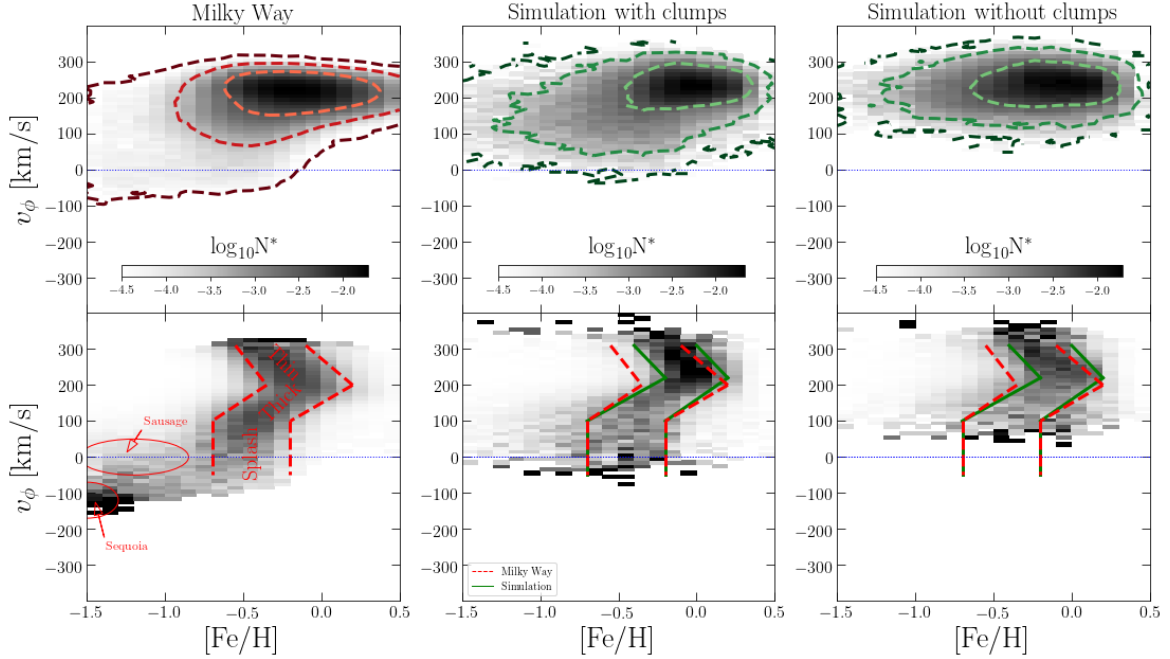
Fig. 3.2 Left column shows the MW stars with $0.5 < |z|/\mathrm{kpc} < 3$ from Sanders and Das (2018). The simulation panels are for stars with $5 < R/\mathrm{kpc} < 11$ and $|z| < 3$ kpc, see details in the text. The middle and right column shows data from the clumpy and non-clumpy simulation, respectively. **Top row:** absolute density plots where each bin is divided by the total number of stars/star-particles following the selection criteria. The dashed-lines are density contours on a logarithmic scale. **Bottom row:** Row-normalised 2D density plot in the [Fe/H]-v_ϕ plane. The dashed red lines indicate the location of the thin disc, thick disc and Splash, as defined by *B20* in the observed data. The solid green lines show the equivalent regions in the clumpy simulation. The Splash region produced by the simulation is similar to that of the MW. Comparison of the central and right panels shows that the clumps are necessary to produce the Splash stars. Moreover the simulation without clumps shows no Splash region in the velocity-metallicity plane. Finally, we also illustrate in the left panel the two known accreted stellar halo structures: *Gaia*-Sausage and Sequoia.

in most of our figures we adopt similar scales and colour schemes as those used by *B20*. Moreover, whenever we use data from Sanders and Das (2018)[4] we select stars with the same spatial selection, small velocity errors ($\sigma_{v_\phi} < 20$ km s^{-1}), low [Fe/H] uncertainty ($\sigma_{[\mathrm{Fe/H}]} < 0.15$) and accurate parallax ($\varpi/\sigma_\varpi > 5$) as in *B20*.

---

[4]http://www.ast.cam.ac.uk/~jls/data/gaia_spectro.hdf5

3.3.1   Chemistry-kinematics features

Fig. 3.2 top row shows the absolute density plot in the [Fe/H]-v_ϕ plane for both the MW (left) and the simulations (center and right). Each bin is divided by the total number of stars/star-particles following the selection criteria in the MW/simulations. As already discussed in *B20*, the MW has a significant amount of metal-rich ([Fe/H]> -1), low angular momentum ($v_\phi < 100$ km s^{-1}) stars (see, e.g., Fernández-Alvar et al. 2019; Nissen and Schuster 2010). The simulation with clumps also has a significant amount of such metal-rich low angular momentum stars, but lacks a significant amount of retrograde stars, mainly due to the absence of accreted stars[5], and has a slight overdensity at [Fe/H]> 0 and $v_\phi < 100$ km s^{-1} compared to MW (but see *B20* figure 1, where, e.g., the left panels clearly shows stars in this region). For comparison, the simulation without clumps, right panel, lacks a significant low angular momentum population.

The bottom row of Fig. 3.2 shows the row-normalised density plot in the [Fe/H]-v_ϕ plane for both the MW (left) and simulations (centre and right). This normalisation has the advantage of enhancing the known velocity-metallicity correlation for both the thin and thick disc, where the former (*latter*) has a negative (*positive*) v_ϕ gradient with [Fe/H] (as discussed in Chapter 1. The red contours in the left panel indicate the different populations in the MW, as identified by *B20*, where the Splash is defined as the over-density seen at the low angular momentum ($v_\phi \leq 80$ km s^{-1}) and relatively metal-rich ($-0.7 <$[Fe/H]< -0.2) region. The two known stellar halo over-densities, *Gaia*-Sausage (Belokurov et al., 2018; Helmi et al., 2018) and Sequoia (Barbá et al., 2019; Myeong et al., 2019), are also indicated. Although the Splash region is defined ad-hoc in this plot, it is significantly different from the accreted stellar halo and the classical thick disc (defined as the α-rich disc, e.g. Bensby et al. 2003; Hayden et al. 2017) regions, as shown in *B20* and later in this work.

The bottom-middle panel of Fig. 3.2 shows the results from the simulated clumpy galaxy. The same trends observed in the MW's thin and thick disc are also observed here. In this panel, the red dashed lines are those defined by *B20* with the MW data, while the green solid lines are defined from the simulation. The narrowness of the bands for the thin and thick discs in the simulation can be understood as being due to the absence of any observational errors. Nonetheless, the Splash region is exactly the same both in the MW and in the simulation. In the right panel, we show the same plot for the non-clumpy simulation. The solid and dashed red lines are the same as in the middle panel. The trends for the thin and thick disc are not as clear now and this galaxy can be described as having only one disc component (Beraldo

---

[5]We note that not all retrograde stars with [Fe/H]>-1 observed in the MW are accreted.
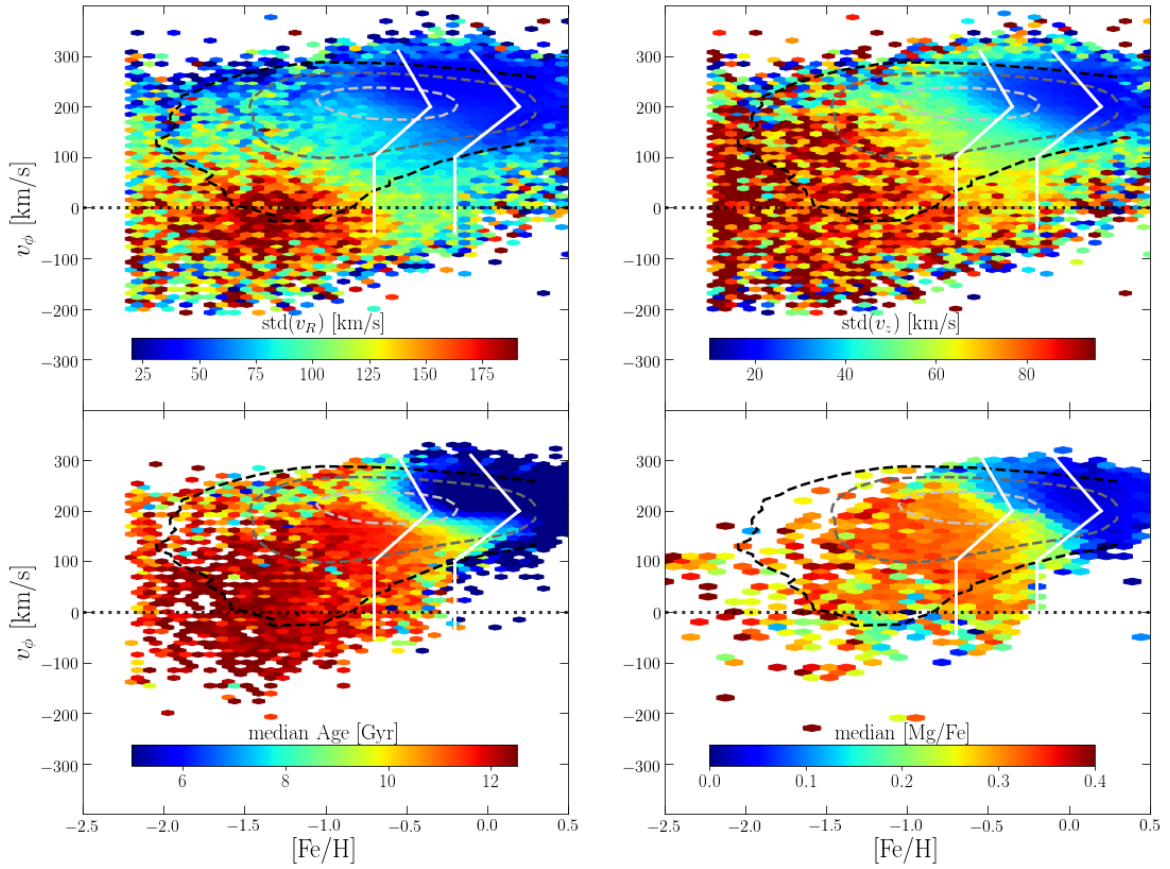
Fig. 3.3 [Fe/H]-$v_\phi-$ plane for Milky Way stars with $0.5 < |z|/\mathrm{kpc} < 3$. Data from Sanders and Das (2018). The dashed lines are the density contours on a logarithmic scale. The solid white lines define the thin disc, thick disc and Splash regions as defined in Belokurov et al. (2020). **Top row:** on the left, colour-coded by radial velocity dispersion, it is possible to see the transition from the thin disc population towards the thick disc going from mild to higher radial velocity dispersion. The Splash region has a higher radial velocity dispersion compared with the thick disc counterpart. A similar trend is observed in the vertical velocity dispersion shown on the right. **Bottom row:** on the left we see the age gradient from the thick-disc to the Splash region. Finally on the right, the smooth [Mg/Fe] transition from the thick region to the Splash region hints at their related origins. *Disclaimer: The original idea of presenting this data in this format is credited to Belokurov et al. (2020).*

e Silva et al., 2020; Clarke et al., 2019). Moreover, it lacks the low angular momentum ($v_\phi \lesssim 50 \ \mathrm{km\,s^{-1}}$) star particles of the Splash region.

In Fig. 3.3, we investigate the [Fe/H]-v_ϕ plane for the MW stars, colour-coded according to different properties. As mentioned previously in Section 3.2.1, we use Sanders and Das (2018) catalogue and follow the same quality cut as mentioned in *B20*. The slanted V-shaped region denoting the thin disc, thick disc and Splash is the same as the one adopted in the plot

of the MW observations (Fig. 3.2). This unconventional, but rather convenient, definition now clearly shows its benefits. The top row show the dispersion in v_R (left) and v_z (right) and how it smoothly increases from the thin disc towards the thick disc. This is the expected result, as the distinct velocity dispersions of the thin and thick disc have been extensively explored in the literature, as summarised in Chapter 1. In contrast to this, at the boundary between the accreted stellar halo ([Fe/H]<-0.7, $v_\phi < 100\,\mathrm{km\,s^{-1}}$) and the Splash (-0.7<[Fe/H]<-0.2, $v_\phi < 100\,\mathrm{km\,s^{-1}}$) there is a sharp drop in the radial velocity dispersion.

The bottom panels of Fig. 3.3 are colour-coded by median age and [Mg/Fe]. Once again, the V-shaped region shows the expected trends for thin and thick discs: the former being younger and $\alpha-$poor, whereas the later is older and $\alpha-$rich (see Chapter 1). It is interesting to note the smooth transition from the thick disc to the Splash region, which is also seen in the velocity dispersion panels, hinting at a common origin for both populations. The Splash stars appear to be, on average, older than the thick disc, but not as old as the accreted halo. We will return to this issue later in this Chapter.

Now, Fig. 3.4 shows the [Fe/H]-v_ϕ plane for the simulated MW analogue colour-coded according to different properties as we have shown for the MW. The top left panel is colour-coded by dispersion in v_R for each bin. As can be noted, the simulated galaxy has the same trends as in the MW: the thin disc has a mild v_R dispersion and it smoothly increases from the thick disc towards the Splash region. As expected, the large v_R dispersion stars observed for [Fe/H] < -0.7, associated with the *Gaia*-Sausage and the Sequoia in the MW, are not present in our simulation as these stars were accreted. As in the MW, a similar trend is also observed for the dispersion in v_z, see top right panel. We stress that not only do trends match between the simulated galaxy and the observed data, but also the velocity dispersion values are very similar.

The bottom panels in Fig. 3.4 show how the median age and [O/Fe] vary in the [Fe/H]-v_ϕ plane. As in the MW, the thin disc region is mostly comprised of young stars and the disc gets older in its thick component. The oldest stars are located in the Splash region. The thin disc region in our simulation is younger compared with the results in *B20*; as mentioned in Section 3.2, the simulation is evolved for only 10 Gyr and thus it will not reflect the same oldest ages as observed in the MW. Nonetheless, the thick disc and Splash region still have similar age gradients compared to the observations. Finally, the trends in [O/Fe] are nicely matched to the [Mg/Fe] trends in the MW, where there is a smooth transition from slightly [O/Fe]-rich for the thick disc to higher values in the Splash region.

Clarke et al. (2019) showed that, in the simulation, a small population of α-poor stars forms at the same time as the α-rich ones (indeed this is one of the key predictions of the
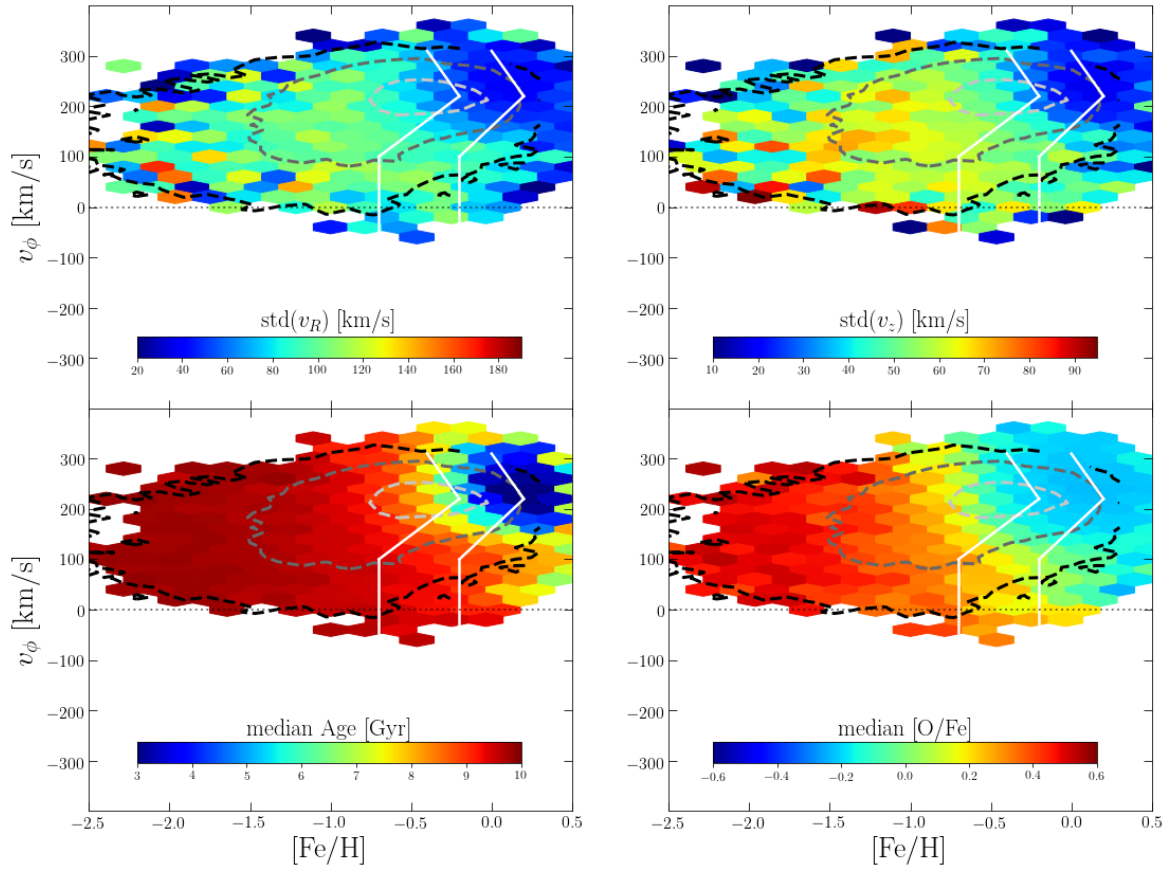
Fig. 3.4 [Fe-H]-v_ϕ plane in the simulated clumpy galaxy, $5 < R/\text{kpc} < 11$ and $|z| < 3$ kpc, which was evolved for only 10 Gyr. The dashed lines are the density contours on a logarithmic scale. The solid white lines define the thin disc, thick disc and Splash regions in the simulation as in Fig. 3.2. **Top row:** on the left, colour-coded by radial velocity dispersion, it is possible to see the transition from the thin disc population towards the thick disc going from mild to higher radial velocity dispersion. The Splash region has a higher radial velocity dispersion compared with the thick disc counterpart. A similar trend is observed in the vertical velocity dispersion shown on the right. **Bottom row:** on the left we see that the Splash region is composed of the oldest stars in the simulation, whereas the thin disc is the youngest and the thick disc has intermediate to old stars. Finally on the right, the smooth [O/Fe] transition from the thick region to the Splash region hints at their related origins.

model). We have verified that the publicly available APOGEE-*Gaia* DR12 catalogue[6] indeed confirms that retrograde Splash stars are found both in the α-rich and α-poor in-situ regions (as defined in Mackereth et al. 2019), supporting our conclusion that scattering by clumps can produce the counter-rotating Splash stars in the MW.

---

[6]https://www.sdss.org/dr12/irspec/spectro_data/

3.3.2 The Splash vertical extension

Belokurov et al. (2020) analysed LAMOST K giants (Luo et al., 2015) in order to verify how far from the plane the Splash stars are detected and to determine where the canonical thick disc transitions to the Splash-dominated region. We reproduce their result in Figure 3.5. In the left panel we can see that the metallicity and velocity ranges they chose for the thin and thick disc, red and orange lines respectively, nicely show how the main disc populations are concentrated near the plane. The black dashed line shows the vertical extension of the low-angular momentum stars that represent the Splash stars. The Splash extends over a wider range in $|z|$ when compared to the disc populations. Their restriction towards the fastest counter-rotating stars avoids a large contamination from the canonical stellar halo, which is represented by the blue dotted line. Finally, on the right panel, they found that at $|z| \sim 5$ kpc there is a sharp gradient in median v_ϕ where the low angular momentum Splash stars dominate for higher $|z|$

Although the stellar density of the disc in our simulated galaxy decreases faster with $|z|$ compared with the MW's disc, we are still able to verify the transition region, if any, in the simulation. The left panel in Fig. 3.6 shows the stellar density in the $R - |z|$ plane for the simulation. The red and orange contours have the same velocity-metallicity intervals as in *B20* and they are a rough representation of the canonical thin and thick discs, respectively. The black dashed contours outline the spatial extent of the Splash stars in our simulation. In order to avoid the tail of the stellar halo distribution, *B20* restricted their velocity range to $-20 < v_\phi < 50$ km s^{-1}. Even though our simulation does not have an accreted halo, we adopt the same range. We note that both in the simulation and in the MW, the Splash stars extend up to $|z| \sim 10$ kpc and are also concentrated within $R \sim 10$ kpc.

The right panel in Fig. 3.6 shows how the median v_ϕ changes in the [Fe/H]-$|z|$ plane. In the Splash metallicity range, defined by the two vertical dashed lines, we note two features similar to those observed in the MW: *i.* the negative gradient of thick disc's median v_ϕ with $|z|$; *ii.* a transition at $|z| \sim 5$ kpc (horizontal dashed line) where the low angular momentum Splash stars start to dominate for larger heights. This reinforces the idea that internal dynamical processes in a clumpy proto-disc can also create Splash stars.

3.3.3 Simulated Splash number fraction

In this subsection, we estimate the Splash-like population in the simulation with clumps and compare with the MW. *B20* estimated that in the range $2 < |z|/\mathrm{kpc} < 3$ and $-0.7 < [\mathrm{Fe/H}] < -0.2$ the Splash population dominates the tail of the v_ϕ distribution, i.e., $v_\phi < 100$ km s^{-1}.
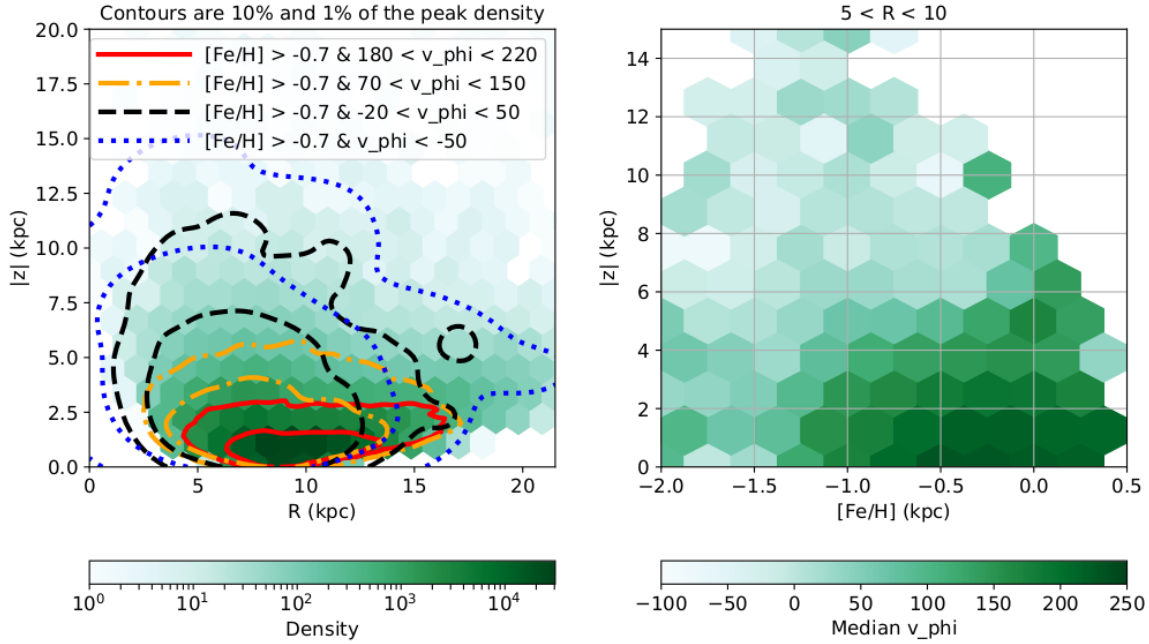
Fig. 3.5 **Left panel:** the distribution of the metal-rich stars for three different velocity ranges. The thin and thick disc-like stars are indicated by the red and orange contours, respectively. The contours denote 10% and 1% of the peak density. The lower angular momentum stars (dashed black contours) are mostly representative of the Splash stars and are concentrated within ≈ 7 kpc, although they do extend up to 10 kpc. The blue dotted contours contain the most retrograde stars and therefore will have more accreted halo material. **Right panel:** the [Fe/H]-$|z|$ plane colour-coded by median v_ϕ. In the Splash metallicity range (-0.7<[Fe/H]<-0.2), there is an apparent transition from the canonical thick-disc (median $v_\phi \gtrsim 150$ km s^{-1}) to the Splash-dominated region (median $v_\phi \lesssim 50$ km s^{-1}), which occurs at $|z| \sim 5$ kpc.[*Reproduced from Belokurov et al. (2020), figure 8.*]

The left panel of Fig. 3.7 shows the cumulative distribution of v_ϕ for the MW (black) and simulation (red) in the aforementioned metallicity and spatial range: approximately 15% of the stars in the MW have $v_\phi < 100$ km s^{-1}, whereas the simulation with clumps has about 25% of star-particles in the same regime. However, if we scale v_ϕ by the median value for each distribution, the simulation with clumps has $\approx 20\%$ of star-particles in the equivalent low angular momentum tail, remarkably similar to the MW.

The right panel of Fig. 3.7 shows the fraction of star-particles with halo kinematics in the simulation chemical thick disc. We used a spatial range similar to that used in Di Matteo et al. (2019). We also followed their criterion for halo kinematics, $\sqrt{(v_\phi - v_{LSR})^2 + v_R^2 + v_z^2} > 180$ km s^{-1}, where $v_{LSR} = 233$ km s^{-1} and it is the velocity at the local standard of rest in the simulation (Clarke et al., 2019). The separation criterion between the thin and thick discs
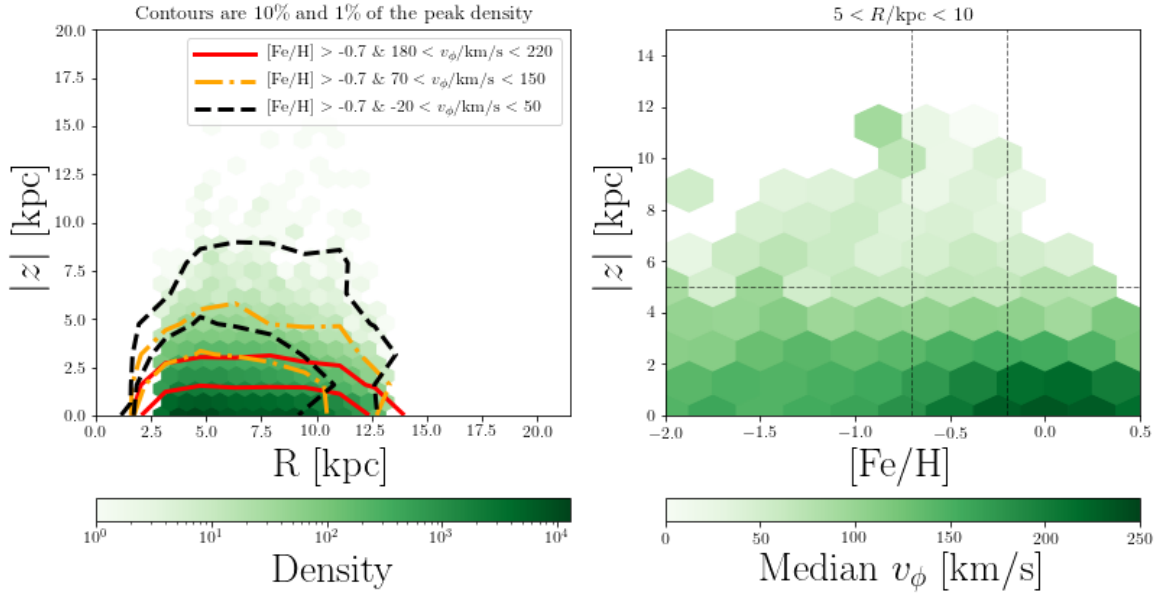
Fig. 3.6 The spatial extent of the Splash stars in the simulation. The left plot shows the distribution of the metal-rich stars for three different velocity ranges. The thin and thick disc-like stars are indicated by the red and orange curves, respectively. The curves are the contours of 10% and 1% of the peak density. The lower angular momentum stars (dashed black curves) represent the Splash stars and have similar $|z|$ extension in comparison to observations. On the right, we show the [Fe/H]-$|z|$ plane colour coded by median v_ϕ. The trends are also remarkably similar to the observations; the transition between the canonical thick-disc to the Splash-dominated region also occurs at $|z| \sim 5$ kpc.

for the simulations follows Clarke et al. (2019). We observe that the simulation follows the same trends as in the MW (see figure 18 in Di Matteo et al. 2019): *i.* the fraction of halo-like kinematics is $\approx 25\%$ in the range where the Splash stars are concentrated; *ii.* this fraction drops quickly as the metallicity increases. The larger fraction of halo-kinematics stars at [Fe/H]>-0.2 in the simulation, compared with the MW, can be due to differences in the details of the later star formation history and/or the selection function of the APOGEE data.

3.3.4   The age of simulated Splash stars

In order to compare the age difference between the accreted halo and the Splash stars, *B20* analysed the age distribution of the counter-rotating stars for two distinct metallicity ranges (see their figure 4). The metal-poor ([Fe/H]<-0.7) region, corresponding to the accreted halo has a peak at $\sim 12.5^7$ Gyr and a sharp drop at ~ 10 Gyr. On the other hand,

---

[7]Their ages are limited to 12.5 Gyr.
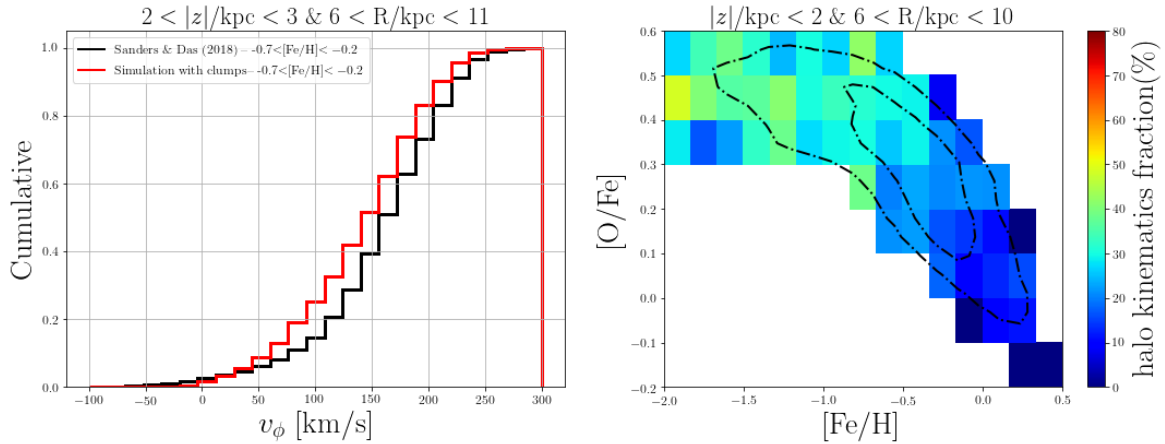
Fig. 3.7 **Left panel:** The cumulative v_ϕ distribution for the MW (black) and simulation with clumps (red) in the Splash metallicity regime, $-0.7 <$[Fe/H]< -0.2. The fractions of stars and star-particles in the tail of the distribution are $\approx 15\%$ and $\approx 25\%$, respectively. **Right panel:** An estimate of the fraction of star-particles with halo like kinematics, $\sqrt{(v_\phi - v_{LSR})^2 + v_R^2 + v_z^2} > 180$ km s^{-1}, following the criteria from Di Matteo et al. (2019) (see their figure 18 for a comparison with the MW). We show the fractions for the chemically defined thick disc in the simulation (Clarke et al., 2019). The black curves are the contours of 50% and 10% of the peak density. The trends in the simulation with clumps are very similar to the MW, see text for details.

the age distribution for the Splash stars, -0.7<[Fe/H]<-0.2, has a slightly younger peak at ~ 11.5 Gyr and also a sharp drop at ~ 10 Gyr ($\sim 30\%$ of these stars are younger than 10 Gyr). They propose that the Splash is made up of stars from the Galaxy's proto-disc whose orbits were heated by to the *Gaia*-Sausage accretion event. Moreover, the star formation for the Splash stars ceased just after the merger, i.e. around 9.5 Gyr ago.

In the left panel of Fig. 3.8, we show the age distribution in our simulation using the same velocity-metallicity interval as in *B20*. As already mentioned, our oldest age is 10 Gyr and the fact there is no shift between the metal-poor (blue) and Splash stars (black) curves merely reflects that our simulation represents an isolated galaxy with no old accreted stellar halo. Nonetheless, it is evident that the counter-rotating stars in the simulation are also old and cease to form after 3 Gyr. This fact is qualitatively similar to what is observed in the MW. The red curve in this panel corresponds to the canonical thin+thick distribution, $v_\phi > 200$ km s^{-1} and [Fe/H]>-0.7. As expected it extends over the full age range in the simulated galaxy in agreement with the observed data. Finally, the green shaded area is the age distribution for the Splash stars defined as in Fig. 3.2, i.e. $v_\phi < 100$ km s^{-1} and $-0.7 <$[Fe/H]< -0.2. Now, the age extends to an extra 1 Gyr, due to the contamination of

thick disc, i.e. α-rich stars. As shown by Clarke et al. (2019), all the star-particles in the simulation thick disc are older than 6 Gyr. Therefore, our result reinforces the connection between the thick disc and the Splash stars, where the latter could naturally exist in galaxies with a disc dichotomy.

Fig. 3.8 right panel shows the cumulative distribution for the MW (dotted lines) and the simulation (solid lines) convolved with the median error from the observational data (median $\sigma_{age} \approx 1.3$ Gyr)[8]. For a better comparison, we divided the age intervals by the maximum age in the simulation (10 Gyr) and observation (12.5 Gyr). For $v_\phi < 0$ and [Fe/H]> -0.7 the MW (black dotted line) has a truncated star formation history characterised by: *i)* approximately 60% of stars are older than $age/max(age) \approx 0.8$, *ii)* an extended tail towards young ages. *B20* associated the truncation with the cessation of the MW's disc heating during the *Gaia*-Sausage merger. Similar to the MW, the simulation also has approximately 60% of stars older than $age/max(age) \approx 0.8$ (black and green solid lines). The lack of young Splash-like stars in the simulation is explained by the fact that the clumps, which are responsible for producing the Splash, stop forming after 4 Gyr. The difference between the simulation and the MW, in terms of the extended tail of ages, only happens after both the clumps and the *Gaia*-Sausage are completed. We also note, by analysing the simulation snapshots, that this old population is already kinematically hot in the first 3 Gyrs of the simulation. Therefore, internal dynamical heating in a MW-like galaxy is enough to heat the primordial disc in its early stages and produce a kinematically hot population with $v_\phi < 100$ km s^{-1}, as shown by the green distribution in Fig. 3.8.

3.4 Conclusions

Di Matteo et al. (2019) suggested that the Splash stars (which they refer to as the "Plume") represent the low angular momentum tail of the thick disc and therefore it is not a distinct component from the MW. On the other hand, *B20* argues on the necessity of three components (thin disc, thick disc and Splash) to explain the v_ϕ distribution for $-0.7 <$[Fe/H]< -0.2 and $2 < |z|/kpc < 3$. Based on their age distribution, they also suggest that the Splash formed only in the early times of the MW, whereas the thick disc had a continuous formation over time.

From *B20*'s work the existence of four distinct stellar populations in the dynamical-chemical space is suggested: thin disc, thick disc, accreted halo and the Splash, the latter sometimes being referred to as the in-situ halo. The origin of the Splash also relates to the

---

[8]We select stars in Sanders and Das (2018) with estimated age error lower than 2 Gyrs.
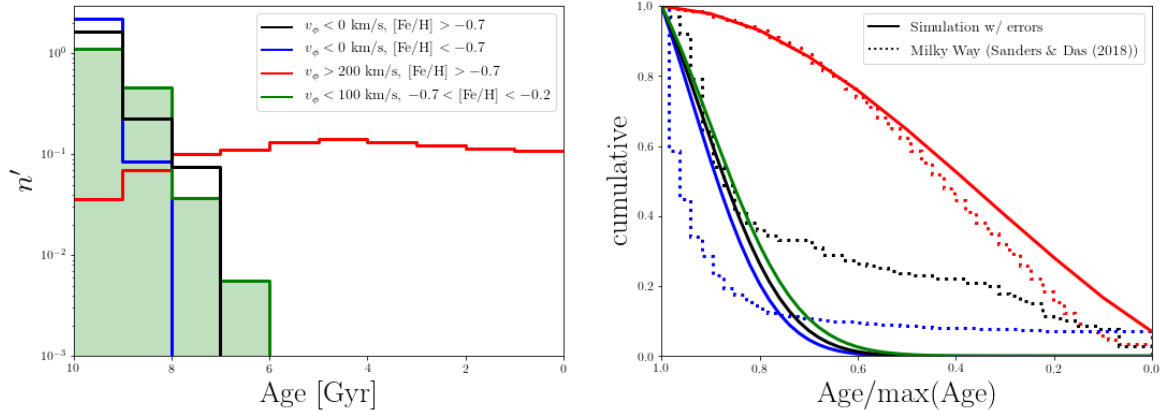
Fig. 3.8 **Left panel:** Error free age distribution for the simulated stars in the simulated clumpy galaxy with $5 < R/\text{kpc} < 11$ and $|z| < 3$ kpc. n' is the probability density function of each 1 Gyr age bin. The black and blue curves show the counter-rotating stars for metal-rich and metal-poor intervals, respectively. All the counter-rotating stars in the simulation are older than 7 Gyr. The absence of the shift in the peak of the age distribution between the two curves, seen by *B20*, reflects the fact that our simulation has no accreted halo. The red curve shows the age distribution of the classical thin+thick disc in the simulation, which was only evolved for 10 Gyr. The green shaded area corresponds to the age distribution of the simulation Splash region defined in Fig. 3.2. As it includes stars with $v_\phi < 100$ km s^{-1}, some thick disc stars are present. **Right panel:** cumulative age distribution for the MW (dotted lines) and simulation (solid lines) convolved with observational errors. The colours correspond to the same velocity and [Fe/H] interval as in the left panel. We divide each age by the maximum age in the MW data (12.5 Gyr) and the simulation (10 Gyr).

thick disc and it possibly contains the first stars in the proto-disc of our Galaxy's progenitor. Besides that, there is clear evidence of a major merger event that occurred in the early stages of the MW (e.g. Belokurov et al. 2018; Di Matteo et al. 2019; Haywood et al. 2018; Helmi 2008b). Di Matteo et al. (2019) and *B20* proposed that this merger event could have excited the proto-disc and given rise to the low angular momentum, high radial velocity dispersion and relatively metal-rich Splash stars.

In this Chapter we analysed an isolated galaxy simulation in order to investigate the formation of Splash stars. We showed that a clumpy MW analogue can naturally form not just the chemical and geometric thin and thick discs (Beraldo e Silva et al., 2020; Clarke et al., 2019), but also the Splash, with distribution, kinematics and chemistry similar to those observed in our Galaxy. This is a new scenario for the formation of the Splash, as in our case there was no accretion event and therefore no accreted stellar halo. Moreover, in this scenario, the formation of the Splash stars occurs in the simulation's first Gyrs. The thick-disc and Splash population have a common origin, where the latter is the low angular momentum tail

of the former, as initially suggested by Di Matteo et al. (2019). This is due to the smooth transition in kinematics, age and [O/Fe] between the thick-disc and Splash region seen in Fig. 3.4. We also show that a similar simulation without clumps fails to reproduce the low rotational velocity patterns of the MW. We verified that the simulated Splash has a similar number fraction (Section 3.3.3) and age trends (Section 3.3.4) as observed in the MW. Our results suggest that a Splash population is expected in any galaxy which underwent a clumpy star-formation episode.

Finally, we note that the two different formation scenarios for the Splash population, i.e., clumpy star formation (this work) or a major merger (Belokurov et al. 2020; Di Matteo et al. 2019), are not mutually exclusive, since clumps can have an ex-situ origin associated to mergers (e.g. Mandelker et al. 2014). The effect of the merger on the disc depends on several parameters, such as the initial gas fraction and orbit (see e.g. Di Matteo et al. 2011). Moreover, the proximity of the satellite's disruption, whether close or far from the disc, also plays an important role on the disc heating (Sellwood et al., 1998), and requires further study for the *Gaia*-Sausage.

Chapter 4

Conclusion and final remarks

In this work we have explored the overlap between the thick disc and the stellar halo in the Solar Neighbourhood. We took advantage of the recent *Gaia* satellite astrometric survey and its synergy with large ground-based spectroscopic surveys, such as LAMOST and APOGEE.

Gaia Collaboration et al. (2018a) demonstrated the level of detail obtained by examining the HR diagrams drawn from *Gaia* photometry: a remarkable double sequence in the HRD is obtained by selecting stars with transverse velocity greater than 200 $km\,s^{-1}$, within 1 kpc of the Sun.

The initial assumption was that these high transverse velocity stars are a probe of the stellar halo, in which case the observed double sequence in the HRD suggests that the local stellar halo is composed of two different populations. Haywood et al. (2018) investigated this sample and concluded that the thick disc was likely to have been heated by a merger, giving rise to the red sequence as seen in that particular HRD. They also linked this merger to the wedges observed in the Apocentre-Zmax plane. Nonetheless, upon closer inspection it became clear that this kinematic cut fails to select a pure stellar halo sample and quantifying the "canonical" thick disc contamination had yet to be done.

Chapter 2 (see also (Amarante et al., 2020b)) has presented an investigation into the contamination of the thick disc in the aforementioned data, developing a new methodology to estimate the thick disc and stellar halo fractions within 1 kpc of the Sun. We updated the popular Galaxia/Besançon model (Sharma et al., 2011), incorporating the latest observational results for the stellar halo (Belokurov et al., 2018). We also adopted a physically motivated v_ϕ probability distribution function (Schönrich and Binney, 2012) for the thick disc. We quantified the contamination of the kinematically defined thick disc in the high-v_t sample to be $\approx 13\%$. Moreover, by combining our new kinematic model with chemistry from LAMOST DR5 (Boeche et al., 2018; Luo et al., 2015) we were able to quantify the amount of

thick disc stars heated to halo like orbits – we found this was $\approx 64\%$. Finally, we explained that the wedges in the Apocentre-Zmax plane, claimed to be caused by the merging satellite in (Haywood et al., 2018), merely reflect a change in the orbital family due to the adopted Galactic potential.

Belokurov et al. (2020) concluded that these metal-rich low-angular-momentum stars are not part of the accreted halo. Instead they linked their formation to the thick disc, suggesting that the *Gaia*-Sausage/Enceladus merger event (e.g. Belokurov et al. 2018 and Helmi et al. 2018, but see also Evans 2020) heated the proto-Galactic disc, giving rise to these stars (which they christened "the Splash") along with the thick disc.

In contrast to this merger scenario, Chapter 3 (see also (Amarante et al., 2020a)) demonstrated that a Splash-like population can be produced via internal dynamical process during our Galaxy's first few Gyrs. We analysed the properties of an isolated galaxy simulation that forms clumps early in the disc. These clumps dynamically heat the disc, giving rise to a geometric and chemical thin/thick disc (Beraldo e Silva et al., 2020; Clarke et al., 2019), similar to the Milky Way. The Splash-like population in the simulation mimics the Milky Way's Splash properties: kinematically hot, vertically extended dominating for $|z| > 5$ kpc, and has the oldest stars in the disc. As the Splash population forms in the first few Gyrs of the simulation, we proposed that it could already be present in the disc when the *Gaia*-Sausage/Enceladus event occured.

We have shown that the study of nearby stars with halo-like kinematics provides evidence for *i)* a major merger and *ii)* a proto-disc formation in the Milky Way's progenitor. However, the detailed consequences of the merger on the proto-disc are yet to be confirmed, as dynamical internal processes in the early stages of the Milky Way can also heat this proto-disc (Amarante et al., 2020a). Specifically, a few important questions are yet to be answered: What are the real effects of a merger on an existing disc? Did the Milky Way experience a clumpy formation in its first Gyrs? Is it possible to disentangle the effects of the merger from an early clumpy phase?

In order to tackle these questions, and as a natural follow up to the present work, we plan to study the effects of mergers using state-of-art clumpy simulations. In the following Section we will preview our current progress and show some promising preliminary results.

4.1 Future work

In Chapter 3, we showed that state-of-the-art N-body + Smoothed Particle Hydrodynamics (SPH) simulations can explore heating mechanisms in Milky Way-like simulated galaxies.

Here we expand our initial conditions, adding a satellite that merges with the main galaxy. Although these simulations are non-cosmological and hence idealised, they can reach higher resolution compared to hydrodynamic cosmological simulations, such as IllustrisTNG galaxies (Springel et al., 2018). Moreover, we can control the initial conditions of the merger (i.e. the velocity and inclination of the impact in the progenitor) and control which physical processes are included, enabling us to understand the influence of each of these components in turn. In these simulations the stellar mass is assembled in a realistic fashion from the gas distribution, using a variety of flexible star formation prescriptions. These prescriptions include: self-consistent chemistry, supernova Ia and II and AGB star feedback, as well as metal and thermal diffusion, and metal-line cooling. These prescriptions have been shown to match a wide range of observational data (Clarke et al. 2019, Beraldo e Silva et al. 2020, Amarante et al. 2020b).

We will now present examples of two merger simulations which, although not intended to reproduce the Milky Way's properties precisely, provide valuable insights into the merger's effect on the disc. In all these simulations the merger is completed by ≈ 3 Gyrs. These simulations, which were run as part of the viability test of this approach, will aid us in fine tuning the best scenario that reproduces the GES merger in our Galaxy. Figure 4.1 shows the [Fe/H]-v_ϕ plane as an example of how the simulations will be compared to the Milky Way. The first two panels reproduce data from the Milky Way and the isolated clumpy galaxy simulation, previously shown in Chapter 3. The third and fourth panels show the same plane for two new simulations where there was a single merger with a 1:10 mass ratio, but with different satellite orbit and supernova feedback. Note that these two examples are again not intended to reproduce the MW's properties. The merger simulation I is a clumpy simulation with a merger and it mimics the smooth transition from the discs to the Splash region. On the other hand, merger simulation II, which does not have a period of early clump formation, does not have a distinct chemical thin/thick disc and Splash transition. This suggests that the merger scenario might not be able to explain the formation of the thick disc (Villalobos and Helmi 2008, Helmi et al. 2018) and the Splash population (Belokurov et al. 2020; Grand et al. 2020). However, it is clear that different orbits and input physics (such as those that allow for early clump formation) are likely to have an effect on the metal-rich low angular momentum stars. Therefore it is crucial to comprehensively study the role that the merger plays in the formation of the thin/thick disc dichotomy and to match these simulations with observations (see, for example, the conclusions in Ciucă et al. 2018).

Groups of stars from the same accretion event will exhibit chemodynamical signatures that will permit us to find substructures in our Galaxy. The z-component of the angular
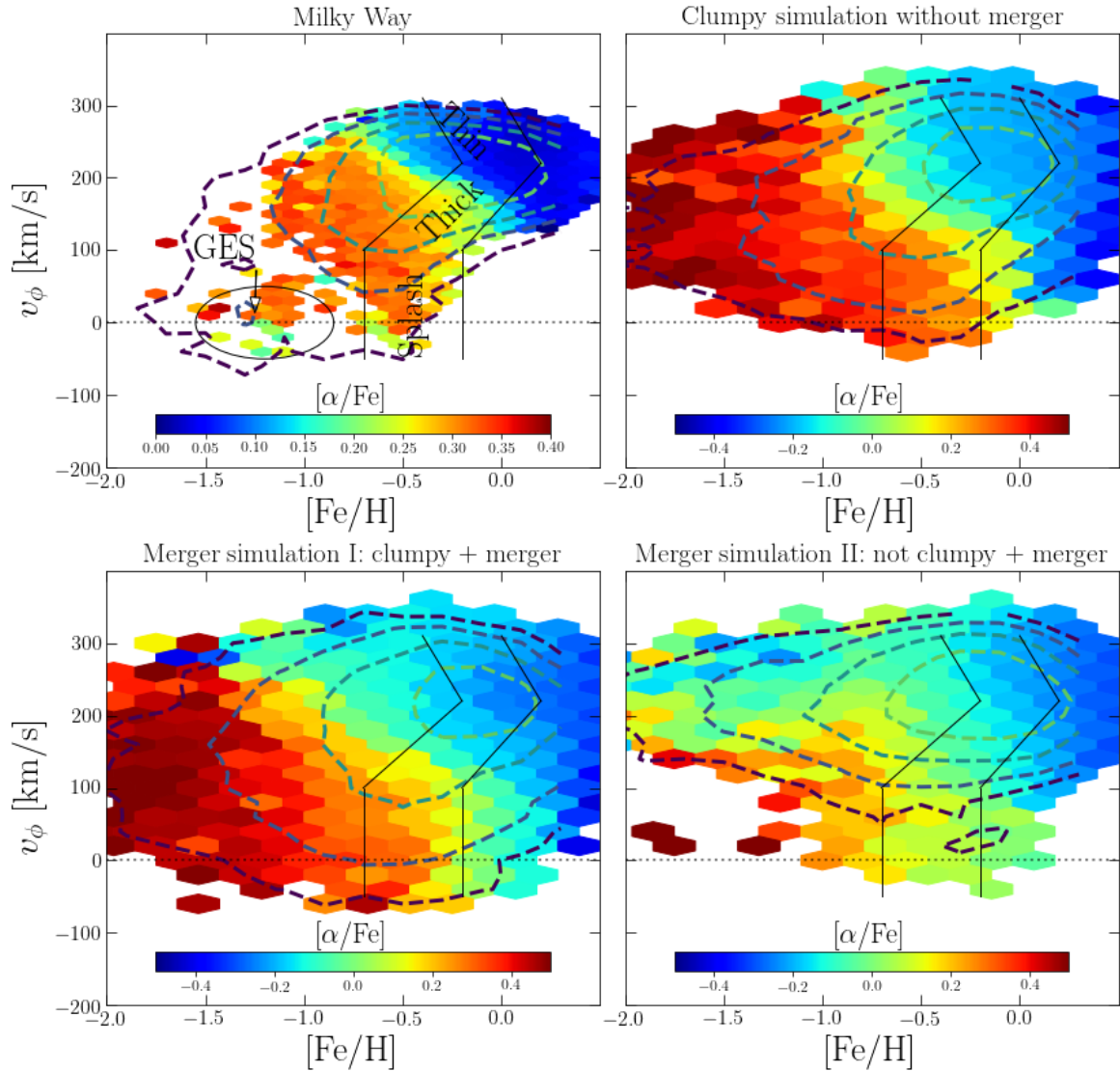
Fig. 4.1 [Fe/H]-v_ϕ plane colour-coded by median [α/Fe]. The thin disc, thick disc, Splash and GES regions are defined according to Belokurov et al. (2020). All the regions, except for GES, are also present in the simulations. The Milky Way data (upper-left panel) is selected from the catalogue of Sanders and Das (2018) and the clumpy simulation (upper-right) is from Chapter 3 (see also (Amarante et al., 2020b)). Two further unpublished simulations are shown in the two lower panels. They both consist of a single merger with a 1:10 mass ratio, but with different orbits and input physics. Although not fine-tuned to reproduce the Milky-Way trends, they provide qualitative insights into the merger's effects on the main proto-galactic disc. The dashed lines are density contours on a logarithmic-scale. The observational and simulation data have different colour-bar scales as they track a different α element. Nonetheless, they are qualitatively equivalent.

momentum (L_z) and total energy are commonly used to search for these structures (e.g. Helmi and de Zeeuw, 2000; Simpson et al., 2019). With larger datasets and high-quality abundance measurements, the number of known substructures is increasingly large. These groups are usually distinguished simply by slicing the chemodynamical space (e.g. Naidu et al., 2020) or applying machine learning techniques (e.g. Koppelman et al., 2019; Yuan et al., 2020). However, several of these substructures either overlap or have smooth transitions in the chemodynamical space, making it unclear whether some of them share a common merger event.

Controlled merger simulations help us to understand how many unique substructures can be identified in the chemodynamic space of simulations with a single merger event. This will enable us to identify in our own Galaxy connections between each substructure. This will be possible with a large suite of medium resolution N-body + SPH simulations, which will improve on the results from pure N-body models such as those of Villalobos and Helmi (2008). As an example of what can be done, Figure 4.2 shows the L_z-Energy plane sliced by [Fe/H] and colour-coded by [α/Fe]. Merger Simulation I and II are the same as those in the two lower panels of Figure 4.1. We selected all of the accreted stars and all of the stars born in the progenitor (in-situ stars) before the merger happened. The blue and red dashed lines are the density-contours for the accreted and in-situ stars, respectively. The orbit of Merger Simulation I is such that it disturbs the disc to lower L_z, creating a large overlap with the accreted stars. On the other hand, the orbit of Merger Simulation II does not disturb the disc sufficiently, and by the end of the simulation it is possible to disentangle the accreted and in-situ stars. The exploration of several orbits, seeing how the resulting signatures in observational space(s) vary, will provide a unique opportunity to explore and understand the origins of substructures in the Milky Way.

A complete exploration of the parameter space for merger simulations will aid the comparison with future large spectroscopic surveys, such as 4MOST (de Jong et al., 2019). 4MOST will expand the legacy of *Gaia* and its first data release, with 7 million stars, is expected to be available by 2023. It will provide accurate radial-velocity measurements for ≈ 25 millions stars down to $V = 20$. This will enable the study of the thick-disc and stellar halo at intermediate heights from the plane ($\approx 5 - 10$ kpc below and above the plane) with unprecedented quality. At these heights we will be able to further investigate the heated thick disc stars, uncovering the role of clumps and mergers during our Galaxy's infancy.
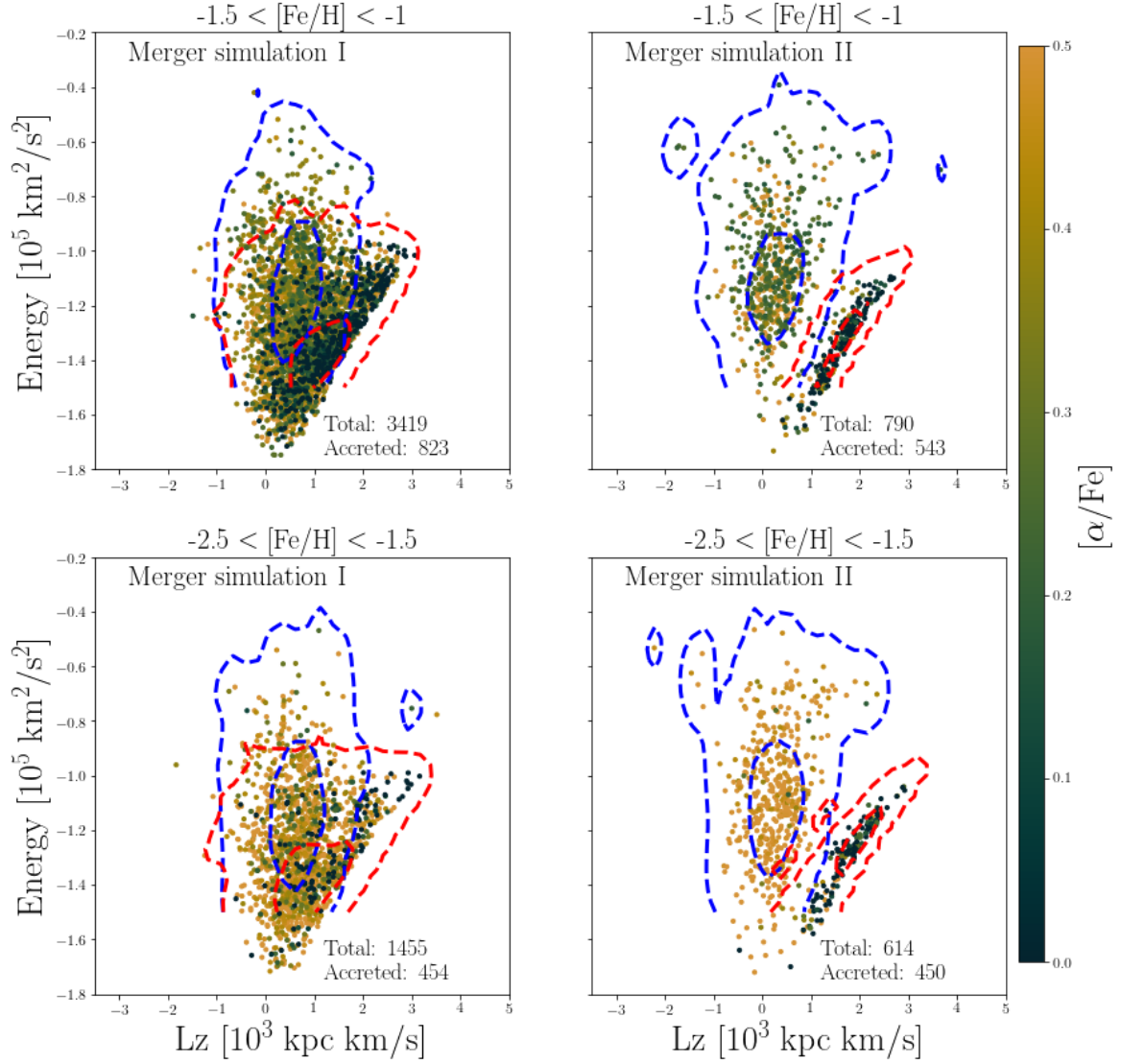
Fig. 4.2 L_z - Energy plane binned in [Fe/H] and colour-coded by [α/Fe]. The density contours for the accreted and in-situ stars are given by the blue and red dashed lines, respectively. Merger simulation I and II have different satellite orbits, creating different signatures in the chemodynamical plane of the simulation. The former has a large overlap between the accreted and in-situ stars, making it harder to disentangle the populations. As a consequence, this may result in the misclassification of some substructures. On the other hand, merger simulation II has a unique signature for the accreted satellite, with almost no overlap between the accreted and in-situ stars.

References

Abazajian, K. N., Adelman-McCarthy, J. K., Agüeros, M. A., Allam, S. S., Allende Prieto, C., An, D., Anderson, K. S. J., Anderson, S. F., Annis, J., Bahcall, N. A., Bailer-Jones, C. A. L., Barentine, J. C., Bassett, B. A., Becker, A. C., Beers, T. C., Bell, E. F., Belokurov, V., Berlind, A. A., Berman, E. F., Bernardi, M., Bickerton, S. J., Bizyaev, D., Blakeslee, J. P., Blanton, M. R., Bochanski, J. J., Boroski, W. N., Brewington, H. J., Brinchmann, J., Brinkmann, J., Brunner, R. J., Budavári, T., Carey, L. N., Carliles, S., Carr, M. A., Castander, F. J., Cinabro, D., Connolly, A. J., Csabai, I., Cunha, C. E., Czarapata, P. C., Davenport, J. R. A., de Haas, E., Dilday, B., Doi, M., Eisenstein, D. J., Evans, M. L., Evans, N. W., Fan, X., Friedman, S. D., Frieman, J. A., Fukugita, M., Gänsicke, B. T., Gates, E., Gillespie, B., Gilmore, G., Gonzalez, B., Gonzalez, C. F., Grebel, E. K., Gunn, J. E., Györy, Z., Hall, P. B., Harding, P., Harris, F. H., Harvanek, M., Hawley, S. L., Hayes, J. J. E., Heckman, T. M., Hendry, J. S., Hennessy, G. S., Hindsley, R. B., Hoblitt, J., Hogan, C. J., Hogg, D. W., Holtzman, J. A., Hyde, J. B., Ichikawa, S.-i., Ichikawa, T., Im, M., Ivezić, Ž., Jester, S., Jiang, L., Johnson, J. A., Jorgensen, A. M., Jurić, M., Kent, S. M., Kessler, R., Kleinman, S. J., Knapp, G. R., Konishi, K., Kron, R. G., Krzesinski, J., Kuropatkin, N., Lampeitl, H., Lebedeva, S., Lee, M. G., Lee, Y. S., French Leger, R., Lépine, S., Li, N., Lima, M., Lin, H., Long, D. C., Loomis, C. P., Loveday, J., Lupton, R. H., Magnier, E., Malanushenko, O., Malanushenko, V., Mand elbaum, R., Margon, B., Marriner, J. P., Martínez-Delgado, D., Matsubara, T., McGehee, P. M., McKay, T. A., Meiksin, A., Morrison, H. L., Mullally, F., Munn, J. A., Murphy, T., Nash, T., Nebot, A., Neilsen, Eric H., J., Newberg, H. J., Newman, P. R., Nichol, R. C., Nicinski, T., Nieto-Santisteban, M., Nitta, A., Okamura, S., Oravetz, D. J., Ostriker, J. P., Owen, R., Padmanabhan, N., Pan, K., Park, C., Pauls, G., Peoples, John, J., Percival, W. J., Pier, J. R., Pope, A. C., Pourbaix, D., Price, P. A., Purger, N., Quinn, T., Raddick, M. J., Re Fiorentin, P., Richards, G. T., Richmond, M. W., Riess, A. G., Rix, H.-W., Rockosi, C. M., Sako, M., Schlegel, D. J., Schneider, D. P., Scholz, R.-D., Schreiber, M. R., Schwope, A. D., Seljak, U., Sesar, B., Sheldon, E., Shimasaku, K., Sibley, V. C., Simmons, A. E., Sivarani, T., Allyn Smith, J., Smith, M. C., Smolčić, V., Snedden, S. A., Stebbins, A., Steinmetz, M., Stoughton, C., Strauss, M. A., SubbaRao, M., Suto, Y., Szalay, A. S., Szapudi, I., Szkody, P., Tanaka, M., Tegmark, M., Teodoro, L. F. A., Thakar, A. R., Tremonti, C. A., Tucker, D. L., Uomoto, A., Vanden Berk, D. E., Vandenberg, J., Vidrih, S., Vogeley, M. S., Voges, W., Vogt, N. P., Wadadekar, Y., Watters, S., Weinberg, D. H., West, A. A., White, S. D. M., Wilhite, B. C., Wonders, A. C., Yanny, B., Yocum, D. R., York, D. G., Zehavi, I., Zibetti, S., and Zucker, D. B. (2009). The Seventh Data Release of the Sloan Digital Sky Survey. *ApJS*, 182(2):543–558.

Amarante, J. A. S., Beraldo e Silva, L., Debattista, V. P., and Smith, M. C. (2020a). The Splash without a Merger. *ApJL*, 891(2):L30.

Amarante, J. A. S., Smith, M. C., and Boeche, C. (2020b). The tale of the tail - disentangling the high transverse velocity stars in Gaia DR2. *MNRAS*, 492(3):3816–3828.

Aoki, M., Aoki, W., and François, P. (2020). Chemical abundance analysis of extremely metal-poor stars in the Sextans dwarf spheroidal galaxy. *A&A*, 636:A111.

Barbá, R. H., Minniti, D., Geisler, D., Alonso-García, J., Hempel, M., Monachesi, A., Arias, J. I., and Gómez, F. A. (2019). A Sequoia in the Garden: FSR 1758—Dwarf Galaxy or Giant Globular Cluster? *ApJL*, 870(2):L24.

Battaglia, G., North, P., Jablonka, P., Shetrone, M., Minniti, D., Díaz, M., Starkenburg, E., and Savoy, M. (2017). What is the Milky Way outer halo made of?. High resolution spectroscopy of distant red giants. *A&A*, 608:A145.

Belokurov, V., Erkal, D., Evans, N. W., Koposov, S. E., and Deason, A. J. (2018). Co-formation of the disc and the stellar halo. *MNRAS*, 478:611–619.

Belokurov, V., Sanders, J. L., Fattahi, A., Smith, M. C., Deason, A. J., Evans, N. W., and Grand , R. J. J. (2020). The biggest splash. *MNRAS*, 494(3):3880–3898.

Bennett, M. and Bovy, J. (2019). Vertical waves in the solar neighbourhood in Gaia DR2. *MNRAS*, 482(1):1417–1425.

Bensby, T., Feltzing, S., and Lundström, I. (2003). Elemental abundance trends in the Galactic thin and thick disks as traced by nearby F and G dwarf stars. *A&A*, 410:527–551.

Beraldo e Silva, L., Debattista, V. P., Khachaturyants, T., and Nidever, D. (2020). Geometric properties of galactic discs with clumpy episodes. *MNRAS*, 492(4):4716–4726.

Binney, J. and Tremaine, S. (2008). *Galactic Dynamics: Second Edition*. Princeton University Press.

Bland-Hawthorn, J. and Gerhard, O. (2016). The Galaxy in Context: Structural, Kinematic, and Integrated Properties. *ARAA*, 54:529–596.

Bland-Hawthorn, J., Sharma, S., Tepper-Garcia, T., Binney, J., Freeman, K. C., Hayden, M. R., Kos, J., De Silva, G. M., Ellis, S., Lewis, G. F., Asplund, M., Buder, S., Casey, A. R., D'Orazi, V., Duong, L., Khanna, S., Lin, J., Lind, K., Martell, S. L., Ness, M. K., Simpson, J. D., Zucker, D. B., Zwitter, T., Kafle, P. R., Quillen, A. C., Ting, Y.-S., and Wyse, R. F. G. (2019). The GALAH survey and Gaia DR2: dissecting the stellar disc's phase space by age, action, chemistry, and location. *MNRAS*, 486(1):1167–1191.

Boeche, C., Smith, M. C., Grebel, E. K., Zhong, J., Hou, J. L., Chen, L., and Stello, D. (2018). LAMOST DR1: Stellar Parameters and Chemical Abundances with SP_Ace. *AJ*, 155:181.

Bournaud, F., Elmegreen, B. G., and Martig, M. (2009). The Thick Disks of Spiral Galaxies as Relics from Gas-rich, Turbulent, Clumpy Disks at High Redshift. *ApJL*, 707(1):L1–L5.

Bovy, J. (2015). galpy: A python Library for Galactic Dynamics. *The Astrophysical Journal Supplement Series*, 216:29.

Bovy, J., Rix, H.-W., Green, G. M., Schlafly, E. F., and Finkbeiner, D. P. (2016). On Galactic Density Modeling in the Presence of Dust Extinction. *ApJ*, 818:130.

Bovy, J., Rix, H.-W., Liu, C., Hogg, D. W., Beers, T. C., and Lee, Y. S. (2012). The Spatial Structure of Mono-abundance Sub-populations of the Milky Way Disk. *ApJ*, 753:148.

Brook, C. B., Kawata, D., Gibson, B. K., and Flynn, C. (2003). Galactic Halo Stars in Phase Space: A Hint of Satellite Accretion? *ApJ*, 585(2):L125–L129.

Brook, C. B., Kawata, D., Gibson, B. K., and Freeman, K. C. (2004). The Emergence of the Thick Disk in a Cold Dark Matter Universe. *ApJ*, 612(2):894–899.

Brook, C. B., Stinson, G. S., Gibson, B. K., Kawata, D., House, E. L., Miranda, M. S., Macciò, A. V., Pilkington, K., Roškar, R., Wadsley, J., and Quinn, T. R. (2012). Thin disc, thick disc and halo in a simulated galaxy. *MNRAS*, 426(1):690–700.

Cava, A., Schaerer, D., Richard, J., Pérez-González, P. G., Dessauges-Zavadsky, M., Mayer, L., and Tamburello, V. (2018). The nature of giant clumps in distant galaxies probed by the anatomy of the cosmic snake. *Nature Astronomy*, 2(1):76–82.

Ceverino, D., Dekel, A., and Bournaud, F. (2010). High-redshift clumpy discs and bulges in cosmological simulations. *MNRAS*, 404(4):2151–2169.

Cheng, J. Y., Rockosi, C. M., Morrison, H. L., Lee, Y. S., Beers, T. C., Bizyaev, D., Harding, P., Malanushenko, E., Malanushenko, V., Oravetz, D., Pan, K., Schlesinger, K. J., Schneider, D. P., Simmons, A., and Weaver, B. A. (2012). A Short Scale Length for the α-enhanced Thick Disk of the Milky Way: Evidence from Low-latitude SEGUE Data. *ApJ*, 752(1):51.

Chiba, M. and Beers, T. C. (2000). Kinematics of Metal-poor Stars in the Galaxy. III. Formation of the Stellar Halo and Thick Disk as Revealed from a Large Sample of Nonkinematically Selected Stars. *AJ*, 119:2843–2865.

Ciucă, I., Kawata, D., Lin, J., Casagrand e, L., Seabroke, G., and Cropper, M. (2018). The vertical metallicity gradients of mono-age stellar populations in the Milky Way with the RAVE and Gaia data. *MNRAS*, 475(1):1203–1212.

Clarke, A. J., Debattista, V. P., Nidever, D. L., Loebman, S. R., Simons, R. C., Kassin, S., Du, M., Ness, M., Fisher, D. B., Quinn, T. R., Wadsley, J., Freeman, K. C., and Popescu, C. C. (2019). The imprint of clump formation at high redshift - I. A disc α-abundance dichotomy. *MNRAS*, 484(3):3476–3490.

Cohen, J. G., Sesar, B., Bahnolzer, S., He, K., Kulkarni, S. R., Prince, T. A., Bellm, E., and Laher, R. R. (2017). The Outer Halo of the Milky Way as Probed by RR Lyr Variables from the Palomar Transient Facility. *ApJ*, 849(2):150.

Coronado, J., Rix, H.-W., and Trick, W. H. (2018). Unbiased TGAS×LAMOST distances and the role of binarity. *MNRAS*, 481:2970–2980.

Cowie, L. L., Hu, E. M., and Songaila, A. (1995). Faintest Galaxy Morphologies From HST WFPC2 Imaging of the Hawaii Survey Fields. *AJ*, 110:1576.

Das, P., Hawkins, K., and Jofré, P. (2020). Ages and kinematics of chemically selected, accreted Milky Way halo stars. *MNRAS*, 493(4):5195–5207.

Das, P., Williams, A., and Binney, J. (2016). Characterizing stellar halo populations II: the age gradient in blue horizontal-branch stars. *MNRAS*, 463(3):3169–3185.

de Boer, T. J. L., Belokurov, V., Beers, T. C., and Lee, Y. S. (2014). The α-element knee of the Sagittarius stream. *MNRAS*, 443(1):658–663.

de Jong, R. S., Agertz, O., Berbel, A. A., and et al. (2019). 4MOST: Project overview and information for the First Call for Proposals. *The Messenger*, 175:3–11.

de La Fuente Marcos, R. (1997). The initial mass function and the dynamical evolution of open clusters. IV. Realistic systems. *A&A*, 322:764–777.

Deason, A. J., Belokurov, V., and Evans, N. W. (2011). The Milky Way stellar halo out to 40 kpc: squashed, broken but smooth. *MNRAS*, 416(4):2903–2915.

Deason, A. J., Belokurov, V., Koposov, S. E., and Lancaster, L. (2018). Apocenter Pile-up: Origin of the Stellar Halo Density Break. *ApJ*, 862(1):L1.

Dessauges-Zavadsky, M., Schaerer, D., Cava, A., Mayer, L., and Tamburello, V. (2017). On the stellar masses of giant clumps in distant star-forming galaxies. *ApJL*, 836(2):L22.

Di Matteo, P., Haywood, M., Lehnert, M. D., Katz, D., Khoperskov, S., Snaith, O. N., Gómez, A., and Robichon, N. (2019). The Milky Way has no in-situ halo other than the heated thick disc. Composition of the stellar halo and age-dating the last significant merger with Gaia DR2 and APOGEE. *A&A*, 632:A4.

Di Matteo, P., Lehnert, M. D., Qu, Y., and van Driel, W. (2011). The formation of a thick disk through the heating of a thin disk: Agreement with orbital eccentricities of stars in the solar neighborhood. *A&A*, 525:L3.

Dotter, A., Chaboyer, B., Jevremović, D., Kostov, V., Baron, E., and Ferguson, J. W. (2008). The Dartmouth Stellar Evolution Database. *ApJs*, 178:89–101.

Eggen, O. J., Lynden-Bell, D., and Sandage, A. R. (1962). Evidence from the motions of old stars that the Galaxy collapsed. *ApJ*, 136:748.

Evans, N. W. (2020). The early merger that made the galaxy's stellar halo. In Valluri, M. and Sellwood, J. A., editors, *IAU Symposium*, volume 353 of *IAU Symposium*, pages 113–120.

Fathi, K., Gatchell, M., Hatziminaoglou, E., and Epinat, B. (2012). Disc scalelengths out to redshift 5.8. *MNRAS*, 423(1):L112–L116.

Fernández-Alvar, E., Fernández-Trincado, J. G., Moreno, E., Schuster, W. J., Carigi, L., Recio-Blanco, A., Beers, T. C., Chiappini, C., Anders, F., Santiago, B. X., Queiroz, A. B. A., Pérez-Villegas, A., Zamora, O., García-Hernández, D. A., and Ortigoza-Urdaneta, M. (2019). The metal-rich halo tail extended in |z|: a characterization with Gaia DR2 and APOGEE. *MNRAS*, 487(1):1462–1479.

Fernández-Trincado, J. G., Beers, T. C., Placco, V. M., Moreno, E., Alves-Brito, A., Minniti, D., Tang, B., Pérez-Villegas, A., Reylé, C., Robin, A. C., and Villanova, S. (2019). Discovery of a New Stellar Subpopulation Residing in the (Inner) Stellar Halo of the Milky Way. *ApJL*, 886(1):L8.

Foreman-Mackey, D., Hogg, D. W., Lang, D., and Goodman, J. (2013). emcee: The MCMC Hammer. *PASP*, 125:306.

Gaia Collaboration, Babusiaux, C., van Leeuwen, F., Barstow, M. A., Jordi, C., Vallenari, A., Bossini, D., Bressan, A., Cantat-Gaudin, T., van Leeuwen, M., and et al. (2018a). Gaia Data Release 2. Observational Hertzsprung-Russell diagrams. *A&A*, 616:A10.

Gaia Collaboration, Brown, A. G. A., Vallenari, A., Prusti, T., de Bruijne, J. H. J., Babusiaux, C., Bailer-Jones, C. A. L., Biermann, M., Evans, D. W., Eyer, L., and et al. (2018b). Gaia Data Release 2. Summary of the contents and survey properties. *A&A*, 616:A1.

Gaia Collaboration, Prusti, T., de Bruijne, J. H. J., Brown, A. G. A., Vallenari, A., Babusiaux, C., Bailer-Jones, C. A. L., Bastian, U., Biermann, M., Evans, D. W., and et al. (2016). The Gaia mission. *A&A*, 595:A1.

Gallart, C., Bernard, E. J., Brook, C. B., Ruiz-Lara, T., Cassisi, S., Hill, V., and Monelli, M. (2019). Uncovering the birth of the Milky Way through accurate stellar ages with Gaia. *Nature Astronomy*, 3:932–939.

Gilmore, G. and Reid, N. (1983). New light on faint stars - III. Galactic structure towards the South Pole and the Galactic thick disc. *MNRAS*, 202:1025–1047.

Gilmore, G., Wyse, R. F. G., and Kuijken, K. (1989). Kinematics, chemistry, and structure of the Galaxy. *ARAA*, 27:555–627.

Gould, A. (2003). Stellar Halo Parameters from 4588 Subdwarfs. *ApJ*, 583(2):765–775.

Gould, A., Flynn, C., and Bahcall, J. N. (1998). Spheroid Luminosity and Mass Functions from Hubble Space Telescope Star Counts. *ApJ*, 503(2):798–808.

Gould, A. and Popowski, P. (1998). Systematics of RR Lyrae Statistical Parallax. III. Apparent Magnitudes and Extinctions. *ApJ*, 508(2):844–853.

Grand, R. J. J., Kawata, D., Belokurov, V., Deason, A. J., Fattahi, A., Fragkoudi, F., Gómez, F. A., Marinacci, F., and Pakmor, R. (2020). The dual origin of the Galactic thick disc and halo from the gas-rich Gaia-Enceladus Sausage merger. *MNRAS*, 497(2):1603–1618.

Grand, R. J. J., Springel, V., Gómez, F. A., Marinacci, F., Pakmor, R., Campbell, D. J. R., and Jenkins, A. (2016). Vertical disc heating in Milky Way-sized galaxies in a cosmological context. *MNRAS*, 459:199–219.

Gravity Collaboration, Abuter, R., Amorim, A., Bauböck, M., Berger, J. P., Bonnet, H., Brand ner, W., Clénet, Y., Coudé Du Foresto, V., de Zeeuw, P. T., Dexter, J., Duvert, G., Eckart, A., Eisenhauer, F., Förster Schreiber, N. M., Garcia, P., Gao, F., Gendron, E., Genzel, R., Gerhard, O., Gillessen, S., Habibi, M., Haubois, X., Henning, T., Hippler, S., Horrobin, M., Jiménez-Rosales, A., Jocou, L., Kervella, P., Lacour, S., Lapeyrère, V., Le Bouquin, J. B., Léna, P., Ott, T., Paumard, T., Perraut, K., Perrin, G., Pfuhl, O., Rabien, S.,

Rodriguez Coira, G., Rousset, G., Scheithauer, S., Sternberg, A., Straub, O., Straubmeier, C., Sturm, E., Tacconi, L. J., Vincent, F., von Fellenberg, S., Waisberg, I., Widmann, F., Wieprecht, E., Wiezorrek, E., Woillez, J., and Yazici, S. (2019). A geometric distance measurement to the Galactic center black hole with 0.3% uncertainty. *A&A*, 625:L10.

Guo, Y., Ferguson, H. C., Bell, E. F., Koo, D. C., Conselice, C. J., Giavalisco, M., Kassin, S., Lu, Y., Lucas, R., Mandelker, N., et al. (2015). Clumpy galaxies in candels. i. the definition of uv clumps and the fraction of clumpy galaxies at 0.5< z< 3. *ApJ*, 800(1):39.

Hawkins, K., Jofré, P., Masseron, T., and Gilmore, G. (2015). Using chemical tagging to redefine the interface of the Galactic disc and halo. *MNRAS*, 453:758–774.

Hayden, M. R., Recio-Blanco, A., de Laverny, P., Mikolaitis, S., and Worley, C. C. (2017). The AMBRE project: The thick thin disk and thin thick disk of the Milky Way. *A&A*, 608:L1.

Hayes, C. R., Majewski, S. R., Shetrone, M., Fernández-Alvar, E., Allende Prieto, C., Schuster, W. J., Carigi, L., Cunha, K., Smith, V. V., Sobeck, J., Almeida, A., Beers, T. C., Carrera, R., Fernández-Trincado, J. G., García-Hernández, D. A., Geisler, D., Lane, R. R., Lucatello, S., Matthews, A. M., Minniti, D., Nitschelm, C., Tang, B., Tissera, P. B., and Zamora, O. (2018). Disentangling the Galactic Halo with APOGEE. I. Chemical and Kinematical Investigation of Distinct Metal-poor Populations. *ApJ*, 852:49.

Haywood, M., Di Matteo, P., Lehnert, M. D., Katz, D., and Gómez, A. (2013). The age structure of stellar populations in the solar vicinity. Clues of a two-phase formation history of the Milky Way disk. *A&A*, 560:A109.

Haywood, M., Di Matteo, P., Lehnert, M. D., Snaith, O., Khoperskov, S., and Gómez, A. (2018). In Disguise or Out of Reach: First Clues about In Situ and Accreted Stars in the Stellar Halo of the Milky Way from Gaia DR2. *ApJ*, 863(2):113.

Helmi, A. (2008a). The stellar halo of the Galaxy. *A&AR*, 15(3):145–188.

Helmi, A. (2008b). The stellar halo of the Galaxy. *Astronomy and Astrophysics Review*, 15:145–188.

Helmi, A. (2020). Streams, substructures and the early history of the Milky Way. *arXiv e-prints*, page arXiv:2002.04340.

Helmi, A., Babusiaux, C., Koppelman, H. H., Massari, D., Veljanoski, J., and Brown, A. G. A. (2018). The merger that led to the formation of the Milky Way's inner stellar halo and thick disk. *Nature*, 563:85–88.

Helmi, A. and de Zeeuw, P. T. (2000). Mapping the substructure in the Galactic halo with the next generation of astrometric satellites. *MNRAS*, 319(3):657–665.

Herschel, W. (1785). On the Construction of the Heavens. *Philosophical Transactions of the Royal Society of London Series I*, 75:213–266.

Immeli, A., Samland, M., Westera, P., and Gerhard, O. (2004). Subgalactic Clumps at High Redshift: A Fragmentation Origin? *ApJ*, 611(1):20–25.

Ishigaki, M. N., Chiba, M., and Aoki, W. (2012). Chemical Abundances of the Milky Way Thick Disk and Stellar Halo. I. Implications of [α/Fe] for Star Formation Histories in Their Progenitors. *ApJ*, 753:64.

Isobe, S. (1974). Space Motion of Subdwarfs and Initial Contraction of the Galaxy. *A&A*, 36(3):333–340.

Ivezić, Ž., Beers, T. C., and Jurić, M. (2012). Galactic Stellar Populations in the Era of the Sloan Digital Sky Survey and Other Large Surveys. *ARAA*, 50:251–304.

Ivezić, Ž., Sesar, B., Jurić, M., Bond, N., Dalcanton, J., Rockosi, C. M., Yanny, B., Newberg, H. J., Beers, T. C., Allende Prieto, C., Wilhelm, R., Lee, Y. S., Sivarani, T., Norris, J. E., Bailer-Jones, C. A. L., Re Fiorentin, P., Schlegel, D., Uomoto, A., Lupton, R. H., Knapp, G. R., Gunn, J. E., Covey, K. R., Allyn Smith, J., Miknaitis, G., Doi, M., Tanaka, M., Fukugita, M., Kent, S., Finkbeiner, D., Munn, J. A., Pier, J. R., Quinn, T., Hawley, S., Anderson, S., Kiuchi, F., Chen, A., Bushong, J., Sohi, H., Haggard, D., Kimball, A., Barentine, J., Brewington, H., Harvanek, M., Kleinman, S., Krzesinski, J., Long, D., Nitta, A., Snedden, S., Lee, B., Harris, H., Brinkmann, J., Schneider, D. P., and York, D. G. (2008). The Milky Way Tomography with SDSS. II. Stellar Metallicity. *ApJ*, 684(1):287–325.

Jean-Baptiste, I., Di Matteo, P., Haywood, M., Gómez, A., Montuori, M., Combes, F., and Semelin, B. (2017). On the kinematic detection of accreted streams in the Gaia era: a cautionary tale. *A&A*, 604:A106.

Jurić, M., Ivezić, Ž., Brooks, A., Lupton, R. H., Schlegel, D., Finkbeiner, D., Padmanabhan, N., Bond, N., Sesar, B., Rockosi, C. M., Knapp, G. R., Gunn, J. E., Sumi, T., Schneider, D. P., Barentine, J. C., Brewington, H. J., Brinkmann, J., Fukugita, M., Harvanek, M., Kleinman, S. J., Krzesinski, J., Long, D., Neilsen, Jr., E. H., Nitta, A., Snedden, S. A., and York, D. G. (2008). The Milky Way Tomography with SDSS. I. Stellar Number Density Distribution. *ApJ*, 673:864–914.

Just, A. and Jahreiß, H. (2010). Towards a fully consistent Milky Way disc model - I. The local model based on kinematic and photometric data. *MNRAS*, 402:461–478.

Kalirai, J. S. and Tosi, M. (2004). Interpreting the colour-magnitude diagrams of open star clusters through numerical simulations. *MNRAS*, 351:649–662.

Kapteyn, J. C. and van Rhijn, P. J. (1920). On the Distribution of the Stars in Space Especially in the High Galactic Latitudes. *ApJ*, 52:23.

Kawata, D., Allende Prieto, C., Brook, C. B., Casagrande, L., Ciucă, I., Gibson, B. K., Grand, R. J. J., Hayden, M. R., and Hunt, J. A. S. (2018). Metallicity gradient of the thick disc progenitor at high redshift. *MNRAS*, 473(1):867–878.

Kawata, D., Grand, R. J. J., Gibson, B. K., Casagrande, L., Hunt, J. A. S., and Brook, C. B. (2017). Impacts of a flaring star-forming disc and stellar radial mixing on the vertical metallicity gradient. *MNRAS*, 464(1):702–712.

Kennicutt, R. C. and Evans, N. J. (2012). Star Formation in the Milky Way and Nearby Galaxies. *ARA&A*, 50:531–608.

Kepley, A. A., Morrison, H. L., Helmi, A., Kinman, T. D., Van Duyne, J., Martin, J. C., Harding, P., Norris, J. E., and Freeman, K. C. (2007). Halo Star Streams in the Solar Neighborhood. *AJ*, 134(4):1579–1595.

Kerber, L. O. and Santiago, B. X. (2005). Physical parameters of rich LMC clusters from modeling of deep HST colour-magnitude diagrams. *A&A*, 435:77–93.

Kirby, E. N., Guhathakurta, P., Simon, J. D., Geha, M. C., Rockosi, C. M., Sneden, C., Cohen, J. G., Sohn, S. T., Majewski, S. R., and Siegel, M. (2010). Multi-element Abundance Measurements from Medium-resolution Spectra. II. Catalog of Stars in Milky Way Dwarf Satellite Galaxies. *ApJS*, 191(2):352–375.

Koppelman, H. H., Helmi, A., Massari, D., Price-Whelan, A. M., and Starkenburg, T. K. (2019). Multiple retrograde substructures in the Galactic halo: A shattered view of Galactic history. *A&A*, 631:L9.

Kordopatis, G., Gilmore, G., Wyse, R. F. G., Steinmetz, M., Siebert, A., Bienaymé, O., McMillan, P. J., Minchev, I., Zwitter, T., Gibson, B. K., Seabroke, G., Grebel, E. K., Bland-Hawthorn, J., Boeche, C., Freeman, K. C., Munari, U., Navarro, J. F., Parker, Q., Reid, W. A., and Siviero, A. (2013). In the thick of it: metal-poor disc stars in RAVE. *MNRAS*, 436:3231–3246.

Krywult, J., Tasca, L. A. M., Pollo, A., Vergani, D., Bolzonella, M., Davidzon, I., Iovino, A., Gargiulo, A., Haines, C. P., Scodeggio, M., Guzzo, L., Zamorani, G., Garilli, B., Granett, B. R., de la Torre, S., Abbas, U., Adami, C., Bottini, D., Cappi, A., Cucciati, O., Franzetti, P., Fritz, A., Le Brun, V., Le Fèvre, O., Maccagni, D., Małek, K., Marulli, F., Polletta, M., Tojeiro, R., Zanichelli, A., Arnouts, S., Bel, J., Branchini, E., Coupon, J., De Lucia, G., Ilbert, O., McCracken, H. J., Moscardini, L., and Takeuchi, T. T. (2017). The VIMOS Public Extragalactic Redshift Survey (VIPERS). The coevolution of galaxy morphology and colour to z 1. *A&A*, 598:A120.

Lee, D. M., Johnston, K. V., Sen, B., and Jessop, W. (2015). Reconstructing the Accretion History of the Galactic Stellar Halo from Chemical Abundance Ratio Distributions. *ApJ*, 802(1):48.

Li, Z.-Z., Qian, Y.-Z., Han, J., Li, T. S., Wang, W., and Jing, Y. P. (2020). Constraining the Milky Way Mass Profile with Phase-space Distribution of Satellite Galaxies. *ApJ*, 894(1):10.

Lockman, F. J. (2002). H I and Galactic Structure. In Taylor, A. R., Landecker, T. L., and Willis, A. G., editors, *Seeing Through the Dust: The Detection of HI and the Exploration of the ISM in Galaxies*, volume 276 of *Astronomical Society of the Pacific Conference Series*, page 107.

Loebman, S. R., Roškar, R., Debattista, V. P., Ivezić, Ž., Quinn, T. R., and Wadsley, J. (2011). The Genesis of the Milky Way's Thick Disk Via Stellar Migration. *ApJ*, 737(1):8.

Luo, A. L., Zhao, Y.-H., Zhao, G., Deng, L.-C., Liu, X.-W., Jing, Y.-P., Wang, G., Zhang, H.-T., Shi, J.-R., Cui, X.-Q., Chu, Y.-Q., Li, G.-P., Bai, Z.-R., Wu, Y., Cai, Y., Cao, S.-Y., Cao, Z.-H., Carlin, J. L., Chen, H.-Y., Chen, J.-J., Chen, K.-X., Chen, L., Chen, X.-L., Chen, X.-Y., Chen, Y., Christlieb, N., Chu, J.-R., Cui, C.-Z., Dong, Y.-Q., Du, B., Fan,

D.-W., Feng, L., Fu, J.-N., Gao, P., Gong, X.-F., Gu, B.-Z., Guo, Y.-X., Han, Z.-W., He, B.-L., Hou, J.-L., Hou, Y.-H., Hou, W., Hu, H.-Z., Hu, N.-S., Hu, Z.-W., Huo, Z.-Y., Jia, L., Jiang, F.-H., Jiang, X., Jiang, Z.-B., Jin, G., Kong, X., Kong, X., Lei, Y.-J., Li, A.-H., Li, C.-H., Li, G.-W., Li, H.-N., Li, J., Li, Q., Li, S., Li, S.-S., Li, X.-N., Li, Y., Li, Y.-B., Li, Y.-P., Liang, Y., Lin, C.-C., Liu, C., Liu, G.-R., Liu, G.-Q., Liu, Z.-G., Lu, W.-Z., Luo, Y., Mao, Y.-D., Newberg, H., Ni, J.-J., Qi, Z.-X., Qi, Y.-J., Shen, S.-Y., Shi, H.-M., Song, J., Song, Y.-H., Su, D.-Q., Su, H.-J., Tang, Z.-H., Tao, Q.-S., Tian, Y., Wang, D., Wang, D.-Q., Wang, F.-F., Wang, G.-M., Wang, H., Wang, H.-C., Wang, J., Wang, J.-N., Wang, J.-L., Wang, J.-P., Wang, J.-X., Wang, L., Wang, M.-X., Wang, S.-G., Wang, S.-Q., Wang, X., Wang, Y.-N., Wang, Y., Wang, Y.-F., Wang, Y.-F., Wei, P., Wei, M.-Z., Wu, H., Wu, K.-F., Wu, X.-B., Wu, Y.-Z., Xing, X.-Z., Xu, L.-Z., Xu, X.-Q., Xu, Y., Yan, T.-S., Yang, D.-H., Yang, H.-F., Yang, H.-Q., Yang, M., Yao, Z.-Q., Yu, Y., Yuan, H., Yuan, H.-B., Yuan, H.-L., Yuan, W.-M., Zhai, C., Zhang, E.-P., Zhang, H.-W., Zhang, J.-N., Zhang, L.-P., Zhang, W., Zhang, Y., Zhang, Y.-X., Zhang, Z.-C., Zhao, M., Zhou, F., Zhou, X., Zhu, J., Zhu, Y.-T., Zou, S.-C., and Zuo, F. (2015). The first data release (DR1) of the LAMOST regular survey. *Research in Astronomy and Astrophysics*, 15(8):1095.

Mackereth, J. T., Schiavon, R. P., Pfeffer, J., Hayes, C. R., Bovy, J., Anguiano, B., Allende Prieto, C., Hasselquist, S., Holtzman, J., and Johnson, J. A. (2019). The origin of accreted stellar halo populations in the Milky Way using APOGEE, Gaia, and the EAGLE simulations. *MNRAS*, 482(3):3426–3442.

Majewski, S. R., Schiavon, R. P., Frinchaboy, P. M., Allende Prieto, C., Barkhouser, R., Bizyaev, D., Blank, B., Brunner, S., Burton, A., Carrera, R., Chojnowski, S. D., Cunha, K., Epstein, C., Fitzgerald, G., García Pérez, A. E., Hearty, F. R., Henderson, C., Holtzman, J. A., Johnson, J. A., Lam, C. R., Lawler, J. E., Maseman, P., Mészáros, S., Nelson, M., Nguyen, D. C., Nidever, D. L., Pinsonneault, M., Shetrone, M., Smee, S., Smith, V. V., Stolberg, T., Skrutskie, M. F., Walker, E., Wilson, J. C., Zasowski, G., Anders, F., Basu, S., Beland, S., Blanton, M. R., Bovy, J., Brownstein, J. R., Carlberg, J., Chaplin, W., Chiappini, C., Eisenstein, D. J., Elsworth, Y., Feuillet, D., Fleming, S. W., Galbraith-Frew, J., García, R. A., García-Hernández, D. A., Gillespie, B. A., Girardi, L., Gunn, J. E., Hasselquist, S., Hayden, M. R., Hekker, S., Ivans, I., Kinemuchi, K., Klaene, M., Mahadevan, S., Mathur, S., Mosser, B., Muna, D., Munn, J. A., Nichol, R. C., O'Connell, R. W., Parejko, J. K., Robin, A. C., Rocha-Pinto, H., Schultheis, M., Serenelli, A. M., Shane, N., Silva Aguirre, V., Sobeck, J. S., Thompson, B., Troup, N. W., Weinberg, D. H., and Zamora, O. (2017). The Apache Point Observatory Galactic Evolution Experiment (APOGEE). *AJ*, 154(3):94.

Mandelker, N., Dekel, A., Ceverino, D., Tweed, D., Moody, C. E., and Primack, J. (2014). The population of giant clumps in simulated high-z galaxies: in situ and ex situ migration and survival. *MNRAS*, 443(4):3675–3702.

Meylan, G. and Heggie, D. C. (1997). Internal dynamics of globular clusters. *A&Ar*, 8:1–143.

Minchev, I., Martig, M., Streich, D., Scannapieco, C., de Jong, R. S., and Steinmetz, M. (2015). On the Formation of Galactic Thick Disks. *ApJL*, 804(1):L9.

Moreno, E., Pichardo, B., and Schuster, W. J. (2015). Resonant trapping in the galactic disc and halo and its relation with moving groups. *MNRAS*, 451:705–723.

Myeong, G. C., Vasiliev, E., Iorio, G., Evans, N. W., and Belokurov, V. (2019). Evidence for two early accretion events that built the Milky Way stellar halo. *MNRAS*, 488(1):1235–1247.

Naidu, R. P., Conroy, C., Bonaca, A., Johnson, B. D., Ting, Y.-S., Caldwell, N., Zaritsky, D., and Cargile, P. A. (2020). Evidence from the H3 Survey That the Stellar Halo Is Entirely Comprised of Substructure. *ApJ*, 901(1):48.

Navarro, J. F., Frenk, C. S., and White, S. D. M. (1997). A Universal Density Profile from Hierarchical Clustering. *ApJ*, 490(2):493–508.

Nissen, P. E. and Schuster, W. J. (2010). Two distinct halo populations in the solar neighborhood. Evidence from stellar abundance ratios and kinematics. *A&A*, 511:L10.

Noguchi, M. (1999). Early evolution of disk galaxies: formation of bulges in clumpy young galactic disks. *ApJ*, 514(1):77.

Norris, J. (1986). Population Studies. II. Kinematics as a Function of Abundance and Galactocentric Position for [Fe/H]<=-0.6. *ApJS*, 61:667.

Oort, J. H. and Rougoor, G. W. (1960). The position of the galactic centre. *MNRAS*, 121:171.

Perek, L. (1951). Motions of RR LYR variables. *Bulletin of the Astronomical Institutes of Czechoslovakia*, 2:57.

Perret, V., Renaud, F., Epinat, B., Amram, P., Bournaud, F., Contini, T., Teyssier, R., and Lambert, J. C. (2014). Evolution of the mass, size, and star formation rate in high redshift merging galaxies. MIRAGE - A new sample of simulations with detailed stellar feedback. *A&A*, 562:A1.

Perryman, M. A. C., Lindegren, L., Kovalevsky, J., Hog, E., Bastian, U., Bernacca, P. L., Creze, M., Donati, F., Grenon, M., Grewing, M., van Leeuwen, F., van der Marel, H., Mignard, F., Murray, C. A., Le Poole, R. S., Schrijver, H., Turon, C., Arenou, F., Froeschle, M., and Petersen, C. S. (1997). The Hipparcos Catalogue. *A&A*, 500:501–504.

Posti, L., Helmi, A., Veljanoski, J., and Breddels, M. A. (2018). The dynamically selected stellar halo of the Galaxy with Gaia and the tilt of the velocity ellipsoid. *A&A*, 615:A70.

Qu, Y., Helly, J. C., Bower, R. G., Theuns, T., Crain, R. A., Frenk, C. S., Furlong, M., McAlpine, S., Schaller, M., and Schaye, J. (2017). A chronicle of galaxy mass assembly in the EAGLE simulation. *MNRAS*, 464(2):1659–1675.

Quinn, P. J., Hernquist, L., and Fullagar, D. P. (1993). Heating of Galactic Disks by Mergers. *ApJ*, 403:74.

Rix, H.-W. and Bovy, J. (2013). The Milky Way's stellar disk. Mapping and modeling the Galactic disk. *A&AR*, 21:61.

Robin, A. C., Reylé, C., Derrière, S., and Picaud, S. (2003). A synthetic view on structure and evolution of the Milky Way. *A&A*, 409:523–540.

Robin, A. C., Reylé, C., Fliri, J., Czekaj, M., Robert, C. P., and Martins, A. M. M. (2014). Constraining the thick disc formation scenario of the Milky Way. *A&A*, 569:A13.

Rodriguez-Gomez, V., Pillepich, A., Sales, L. V., Genel, S., Vogelsberger, M., Zhu, Q., Wellons, S., Nelson, D., Torrey, P., and Springel, V. (2016). The stellar mass assembly of galaxies in the Illustris simulation: growth by mergers and the spatial distribution of accreted stars. *MNRAS*, 458(3):2371–2390.

Roman, N. G. (1954). A group of high velocity F-type stars. *AJ*, 59:307–312.

Rybizki, J., Demleitner, M., Fouesneau, M., Bailer-Jones, C., Rix, H.-W., and Andrae, R. (2018). A Gaia DR2 Mock Stellar Catalog. *PASP*, 130(7):074101.

Sahlholdt, C. L., Casagrande, L., and Feltzing, S. (2019). Characteristics of the two sequences seen in the high-velocity Hertzsprung-Russell diagram in Gaia DR2. *arXiv e-prints*, page arXiv:1907.05652.

Saio, H. and Yoshii, Y. (1979). Three-dimensional motion of dwarf stars and RR Lyrae variables. *PASP*, 91:553–570.

Sandage, A. (1990). On the formation and age of the galaxy. *JRASC*, 84:70.

Sanders, J. L. and Das, P. (2018). Isochrone ages for 3 million stars with the second Gaia data release. *MNRAS*, 481(3):4093–4110.

Schönrich, R. (2012). Galactic rotation and solar motion from stellar kinematics. *MNRAS*, 427:274–287.

Schönrich, R. and Binney, J. (2009). Chemical evolution with radial mixing. *MNRAS*, 396(1):203–222.

Schönrich, R. and Binney, J. (2012). A new formula for disc kinematics. *MNRAS*, 419(2):1546–1556.

Schönrich, R., Binney, J., and Dehnen, W. (2010). Local kinematics and the local standard of rest. *MNRAS*, 403:1829–1833.

Schönrich, R., McMillan, P., and Eyer, L. (2019). Distances and parallax bias in Gaia DR2. *MNRAS*, 487(3):3568–3580.

Schuster, W. J., Moreno, E., Nissen, P. E., and Pichardo, B. (2012). Two distinct halo populations in the solar neighborhood. III. Evidence from stellar ages and orbital parameters. *A&A*, 538:A21.

Searle, L. and Zinn, R. (1978). Composition of halo clusters and the formation of the galactic halo. *ApJ*, 225:357–379.

Sellwood, J. A., Nelson, R. W., and Tremaine, S. (1998). Resonant Thickening of Disks by Small Satellite Galaxies. *ApJ*, 506(2):590–599.

Sestito, F., Longeard, N., Martin, N. F., Starkenburg, E., Fouesneau, M., González Hernández, J. I., Arentsen, A., Ibata, R., Aguado, D. S., and Carlberg, R. G. (2019). Tracing the formation of the Milky Way through ultra metal-poor stars. *MNRAS*, 484(2):2166–2180.

Sharma, S., Bland-Hawthorn, J., Johnston, K. V., and Binney, J. (2011). Galaxia: A Code to Generate a Synthetic Survey of the Milky Way. *ApJ*, 730:3.

Shen, S., Wadsley, J., and Stinson, G. (2010). The enrichment of the intergalactic medium with adiabatic feedback - I. Metal cooling and metal diffusion. *MNRAS*, 407(3):1581–1596.

Simpson, C. M., Gargiulo, I., Gómez, F. A., Grand, R. J. J., Maffione, N., Cooper, A. P., Deason, A. J., Frenk, C., Helly, J., Marinacci, F., and Pakmor, R. (2019). Simulating cosmological substructure in the solar neighbourhood. *MNRAS*, 490(1):L32–L37.

Smith, M. C., Evans, N. W., Belokurov, V., Hewett, P. C., Bramich, D. M., Gilmore, G., Irwin, M. J., Vidrih, S., and Zucker, D. B. (2009). Kinematics of SDSS subdwarfs: structure and substructure of the Milky Way halo. *MNRAS*, 399(3):1223–1237.

Springel, V., Pakmor, R., Pillepich, A., Weinberger, R., Nelson, D., Hernquist, L., Vogelsberger, M., Genel, S., Torrey, P., Marinacci, F., and Naiman, J. (2018). First results from the IllustrisTNG simulations: matter and galaxy clustering. *MNRAS*, 475(1):676–698.

Stinson, G., Seth, A., Katz, N., Wadsley, J., Governato, F., and Quinn, T. (2006). Star formation and feedback in smoothed particle hydrodynamic simulations - I. Isolated galaxies. *MNRAS*, 373(3):1074–1090.

van den Bergh, S., Abraham, R. G., Ellis, R. S., Tanvir, N. R., Santiago, B. X., and Glazebrook, K. G. (1996). A morphological catalog of galaxies in the hubble deep field. *ApJ*, 112:359.

Villalobos, Á. and Helmi, A. (2008). Simulations of minor mergers - I. General properties of thick discs. *MNRAS*, 391(4):1806–1827.

Wadsley, J., Stadel, J., and Quinn, T. (2004). Gasoline: a flexible, parallel implementation of treesph. *New Astronomy*, 9(2):137 – 158.

Wegg, C., Gerhard, O., and Bieth, M. (2019). The gravitational force field of the Galaxy measured from the kinematics of RR Lyrae in Gaia. *MNRAS*, 485(3):3296–3316.

Woolley, R. (1978). The velocity ellipsoid of RR Lyrae variable stars. *MNRAS*, 184:311–317.

Yao, J. M., Manchester, R. N., and Wang, N. (2017). Determination of the Sun's offset from the Galactic plane using pulsars. *MNRAS*, 468(3):3289–3294.

Yoshii, Y. (1982). Density distribution of faint stars in the direction of the north galactic pole. *PASPJ*, 34:365–379.

Yoshii, Y., Ishida, K., and Stobie, R. S. (1987). Galactic Structure Towards the North Galactic Pole Based on an Analysis of UBV Star-Count Data. *AJ*, 93:323.

Yoshii, Y. and Saio, H. (1979). Kinematics of the Old Stars and Initial Contraction of the Galaxy. *PASPJ*, 31:339–368.

Yuan, Z., Myeong, G. C., Beers, T. C., Evans, N. W., Lee, Y. S., Banerjee, P., Gudin, D., Hattori, K., Li, H., Matsuno, T., Placco, V. M., Smith, M. C., Whitten, D. D., and Zhao, G. (2020). Dynamical Relics of the Ancient Galactic Halo. *ApJ*, 891(1):39.

Zasowski, G., Johnson, J. A., Frinchaboy, P. M., Majewski, S. R., Nidever, D. L., Rocha Pinto, H. J., Girardi, L., Andrews, B., Chojnowski, S. D., Cudworth, K. M., Jackson, K., Munn, J., Skrutskie, M. F., Beaton, R. L., Blake, C. H., Covey, K., Deshpande, R., Epstein, C., Fabbian, D., Fleming, S. W., Garcia Hernandez, D. A., Herrero, A., Mahadevan, S., Mészáros, S., Schultheis, M., Sellgren, K., Terrien, R., van Saders, J., Allende Prieto, C., Bizyaev, D., Burton, A., Cunha, K., da Costa, L. N., Hasselquist, S., Hearty, F., Holtzman, J., García Pérez, A. E., Maia, M. A. G., O'Connell, R. W., O'Donnell, C., Pinsonneault, M., Santiago, B. X., Schiavon, R. P., Shetrone, M., Smith, V., and Wilson, J. C. (2013). Target Selection for the Apache Point Observatory Galactic Evolution Experiment (APOGEE). *AJ*, 146(4):81.

Zolotov, A., Willman, B., Brooks, A. M., Governato, F., Brook, C. B., Hogg, D. W., Quinn, T., and Stinson, G. (2009). The Dual Origin of Stellar Halos. *ApJ*, 702:1058–1067.

Appendix A

ADQL query

The Gaia DR2 high velocity stars sample that we have used in Chapter 2 can be obtained with the following ADQL query.

```
SELECT * FROM gaiadr2.gaia_source
WHERE parallax_over_error > 10
AND parallax > 1
AND phot_g_mean_mag < 17
AND phot_g_mean_flux_over_error > 50
AND phot_rp_mean_flux_over_error > 20
AND phot_bp_mean_flux_over_error > 20
AND (sqrt(power(pmra,2) + power(pmdec,2)) * 4.74/parallax)
    >200
AND phot_bp_rp_excess_factor > 1. +0.015*power(bp_rp,2)
AND phot_bp_rp_excess_factor < 1.3 +0.06**power(bp_rp,2)
AND visibility_periods_used > 8
AND astrometric_chi2_al/astrometric_n_good_obs_al − 5 <
    1.44*max(1, exp(−0.4*phot_g_mean_mag −19.5))
```

Appendix B

Standard deviation of the epoch radial velocities

In Chapter 2 we mentioned on the possibility of the observed double sequence observed in the CMD of high transverse velocity stars in *Gaia*, Figure 2.6, to be an artefact caused by unresolved binaries. It is known that unresolved equal mass binary systems can be identified as a single star with the same colour as the bluer sequence, but brighter by a factor of $2.5 \log 2$. This creates a second sequence in the HRD and we note that this difference in brightness is within the range difference between BS and RS. Moreover, such effect is observed for example in many globular and open clusters. The binary fraction can vary from 4 to 40% in globular clusters(see, e.g., the review of Meylan and Heggie, 1997), and reach up to 30% in open clusters (e.g. de La Fuente Marcos 1997 and Kalirai and Tosi 2004).

We note that, it has also been pointed out that depending on the CMD modelling technique, the exact value of binary fraction may not affect the CMD fitting (see, e.g, Kerber and Santiago, 2005). Nonetheless, we decided to verify any binarity signal that could potentially have not been flagged in *Gaia* pipeline. Firstly, we analysed the error distribution of the line-of-sight velocity (v_{los}) error distribution for both sequences. A high fraction of stars with large v_{los} error could potentially indicate the effect of a binary system. Figure B.1 left panel shows that both sequences have a low fraction of stars with relative error in v_{los} greater than 20%.

Secondly, we calculated the standard deviation of the epoch radial velocities, $\sigma(v_{rad}^t)$, given by equation:

$$\sigma(v_{rad}^t) = \sqrt{\frac{2}{\pi}} \frac{\sqrt{rv\_e + 0.11^2}}{\sqrt{rv\_nb\_transits}} \tag{B.1}$$
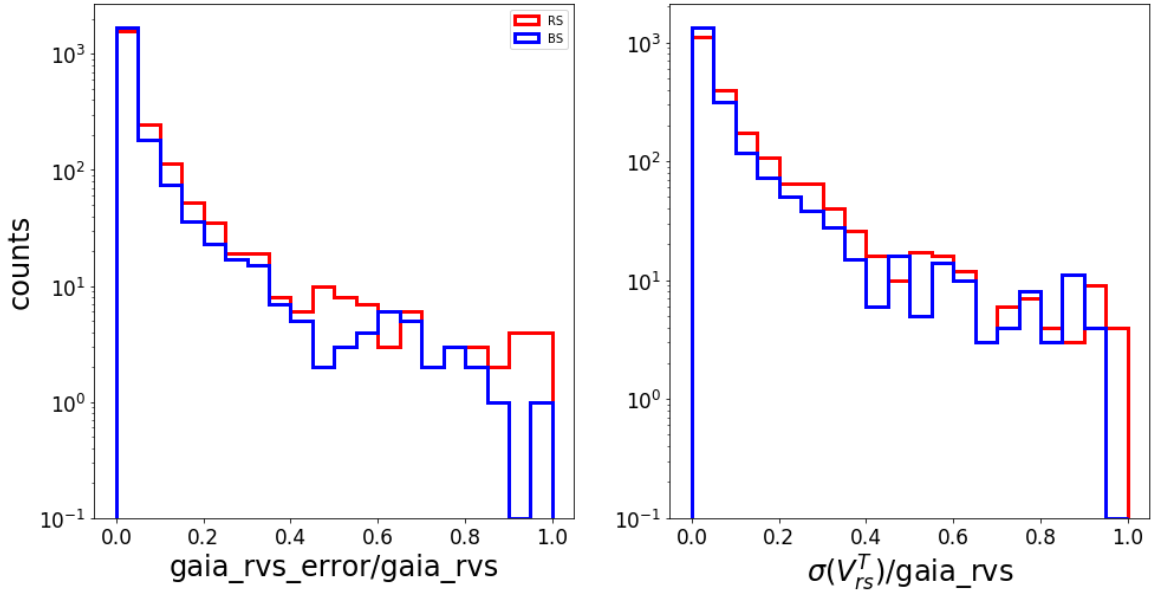
Fig. B.1 The relative line-of-sight velocity error distribution (left) and the standard deviation of the epoch radial velocities (right) for *Gaia* high transverse velocity stars. The colours represent the distribution of the observed Blue and Red Sequences defined in Chapter 2. Both panels show no significant difference between the observed sequences. Moreover, the vast majority of the stars have relative errors lower than 20% in both measurements. This rule out the possibility of binary contamination in this sample.

where, *rv_nb_transits* is the number of transits used to compute radial velocity, and *rv_e* is the given radial velocity error in Gaia data. Figure B.1 right panel shows that less than 0.5% of the stars have $\frac{\sigma(v_{rad}^t)}{rvs} > 0.3$, where *rvs* is the given radial velocity value in *Gaia*, and that the distribution for both sequences is very similar. As this ratio is comparable for the Blue and Red Sequence, the former can not be simply explained by a population with unresolved binaries. Should also be noted that the calculated ratio is biased towards the brighter end of our sample, however there is no reason to expect that it should be considerably larger towards the fainter end of the sample.

João Antônio Silveira do Amarante
Curriculum Vitae

Professional Address

Shanghai Astronomical Observatory

Nandan Road 80, Xujiahui

Shanghai, China

Phone: + 55 48 988619870

Phone: +86 13916274984

Email: joaoant@gmail.com

Education

- P.hD Astrophysics, Shanghai Astronomical Observatory, 2016-present

    - *Ph.D. Thesis Topic:* The structure of the Milky Way stellar halo as seen from Gaia-*LAMOST Advisor:* Martin C. Smith
      CAS-TWAS Fellowship

- B.Sc. Electrical Engineering, Universidade Federal do Rio de Janeiro, 2013-2014

    - *Interrupted*

- M.Sc. Astrophysics, Universidade Federal do Rio de Janeiro, 2010-2012

    - *Master Thesis:* Statistical Proprieties of Planetary Systems
      Advisor: Helio J. Rocha Pinto
      CNPq scholarship (08/2010 - 08/2012)

- B.Sc. Astronomy, Universidade Federal do Rio de Janeiro, 2006-2010

    - *Senior Thesis:* A Statistical Study of Planeatry Systems
      Advisor: Helio J. Rocha Pinto
      CNPq scholarship (06/2007 - 06/2010)

Summer/Winter Schools

- **Summer School on Galactic Dynamics 2019**, Shanghai, China, 2019

- **Heildelberg Summer School 2018: Gaia Data & Science**, Heildeberg, Germany, 2018

- XVI Special Courses of the Observatório Nacional, Rio de Janeiro/Brazil, 2011

- Second Iberoamerican School of Astrobiology, Montevideo/Uruguay, 2009

    - *Poster:* Angular Momentum Distribution on Extrasolar Planetary Systems

- W.E. Heraeus Physics School on The Early Phase of Planet Formation, Bad Honnef/Germany, 2008

    - *Poster:* Angular Momentum Distribution on Extrasolar Planetary Systems

Conferences, Workshops & Contributed talks

- **Talk (online): The effects of clumps in disc galaxies: Implications to the Milky Way**; *Galaxy Coffee - informal seminar of the Galaxies & Cosmology department - MPIA*, September, 2020

- **IAUS 353: Galactic Dynamics in the Era of Large Surveys**, Shanghai, China, 2019

    - *Poster: The high transverse velocity stars in Gaia-LAMOST*

- **The life and times of the Milky Way - the symbiosis between Gaia and ground based spectroscopic surveys**, Shanghai, China, 2018

    - *Talk: The high transverse velocity stars in Gaia-LAMOST*

- **European Week of Astronomy and Space Science**, Liverpool, UK, 2018

    - *Talk: Probing the stellar halo in TGAS-LAMOST*

- XXXVI Annual Meeting of the Brazilian Astronomical Society, Águas de Lindóia/Brazil, 2011

    - *Poster:* Including Metallicity Gradient on TRILEGAL

- III Astronomy's Graduate Week, Observatório do Valongo, UFRJ, Rio de Janeiro/Brazil, 2011

    - *Talk:* New constrains on Milky Way's formation using TRILEGAL

- ESF Conference - Putting the Solar System in Context, Obergurgl/Austria, 2010

- Scientific Initiation Journey, Observatório do Valongo - UFRJ, Rio de Janeiro/Brazil, 2007-2010

    - *Talk:* Planetary Populations according to the Orbital Angular Momentum, 2010
    - *Talk:* Chromospheric Age Correction with Metallicity, 2009
    - *Talk:* Distiguishing Planetary Populations according to the Orbital Angular Momentum, 2008
    - *Talk:* Angular Momentum Distribution of Extrasolar Planetary Systems, 2007

- XXVII IAU General Assembly, Rio de Janeiro/Brazil, 2009

    - *Poster:* Planetary populations according to the orbital angular momentum

- XXXIV Annual Meeting of the Brazilian Astronomical Society, Passa Quatro/Brazil, 2008

    - *Poster:* Angular Momentum Distribution on Extrasolar Planetary Systems

- XXXIII Annual Meeting of the Brazilian Astronomical Society, Passa Quatro/Brazil, 2007

    - *Poster:* Angular Momentum Distribution on Extrasolar Planetary Systems

Honors and Awards

- Best Undergraduate Project in Astronomy, 2010, Universidade Federal do Rio de Janeiro

- Best Undergraduate Project in Astronomy, 2008, Universidade Federal do Rio de Janeiro

Publications

Refereed Publications

- **Amarante, J. A. S.**, Smith, M., Boeche, C., The tale of the tail - disentangling the high transverse velocity stars in Gaia DR2, Monthly Notices of the Royal Astronomical Society, Volume 492, Issue 3, p.3816-3828. **# citations: 16**

- **Amarante, J. A. S.**, Beraldo e Silva, L., Debattista, V., Smith, M., The Splash without a merger, The Astrophysical Journal Letters, Volume 891, Issue 2, id.L30, 7 pp. (2020). **# citations: 11**

Submitted Papers

- Beraldo e Silva, L., Debattista, V., Nidever, D., **Amarante, J. A. S.**, Garver, B., Co-formation of the thin and thick discs revealed by APOGEE-DR16 and Gaia-DR2 arXiv:2009.03346 (2020)

Popular Scientific Publications

- **Amarante, J. A. S.**, Notícias de outros mundos, *Ciência Hoje das Crianças*, Brazil, 2008

Proceedings

- **Amarante, J. A. S.**, Rocha-Pinto, Helio, J., Planetary populations according to the orbital angular momentum. *Proceeding of the International Astronomical Union*, IAU Symposium, Volume 265, 2009, v.265 p.420-421

- **Amarante, J.A.S.**, Smith, M., Boeche, C., The high transverse velocity stars in *Gaia*-LAMOST, *Proceedings of the International Astronomical Union*, IAU Symposium, Volume 353, 2020, pp. 59-60

Peer reviews

- The Astronomical Journal (AJ): since 2020.

Addition Research Experience

- Science Visit: Jeremiah Horrocks Institute, University of Central Lancashire, United Kingdom, 09/2019 – 03/2020. The scope of the visit was to join Professor Victor P. Debattista's group on a project comparing their suite of state-of-art chemo-dynamical simulations of the Milky Way to data from *Gaia* satellite. The visit resulted in a published paper and continued scientific collaboration in future projects.

- Science Visit: Royal Observatory Edinburgh, Edinburgh, United Kingdom, 03/03/2020 – 05/03/2020. I was hosted by Dr. Jorge Penarrubia. During the visit I showed my work during the institute's Wednesday's "Theory Lunch" and had science conversations with Dr. Penarrubia and colleagues.

- Science Visit: California Institute of Technology, California, USA, 24/09/2018 – 27/09/2018. I was hosted by Professor Evan Kirby. During the visit I joined Professor Kirby's group meeting and discussed my current work at his group meeting.

- Science Visit: Oxford University, Oxford, United Kingdom, 09/04/2018 – 12/04/2018. I was hosted by Dr. Ralph Schoenrich. During the visit, Dr. Schoenrich and I had fruitful discussions about my work and he gave important advice to improve the quality of my analysis which was part of the paper Amarante et al., MNRAS, 2020, 492, 3816

Membership in Scientific Societies

- Sociedade Astronômica Brasileira (Brazilian Astronomical Society)

Teach Experience

- *Tutoring:* Undergraduate Physics for Engineering students and basic Math and Physics for Primary and High School students, 2011-2016

Work Experience

- Artificial Intelligence Laboratory, 2013-2014.
    - Study of Simultaneous Localization and Mapping problem
    - CNP-q Fellowship

- Interinstitutional Laboratory of e-Astronomy, 2011.

    – Worked to Sloan Digital Sky Survey III / Braziliam Participation Group

Observational Experience

- Palomar Observatory – USA, 2018 (3 nights)

    – 5.1m telescope: Double Spectrograph (DBSP)

Outreach Experience

- Faculty of Nuclear Sciences and Physical Engineering, Czech Technical University, Prague/Czech Republic, 2008

    – One Lecture about Exoplanets to second year Nuclear Engineering students

Organization of Events

- Shanghai, China, 2018

    – *Shanghai Hack-a-thon:* three-day event to build up collaborations and hands on activities on Gaia data analysis

- Observatório do Valongo, Universidade Federal do Rio de Janeiro, 2011

    – *Folhetim Astronômico:* Biweekly seminars to discuss graduate students projects

Other Considerations

- Computer skills

    – Operational System: Linux

    – Languages: Python, LaTeX

- Languages

    – Native: Portuguese

- Advanced: English

- Basic: Spanish